Development of New Photocatalytic Systems for Sustainable Applications

Von der Fakultät für Naturwissenschaften genehmigte

Dissertation

zur Erlangung des akademischen Grades

Doktor der Naturwissenschaften

(Dr. rer. nat.)

von

Dagny D. Konieczna

geboren am 10.05.1988 in Lüneburg

Paderborn

The experimental part of this work was carried out between October 2013 and September 2016 at the University of Paderborn, Institute of Organic Chemistry under the supervision of Prof. Dr. René Wilhelm. Between January 2015 and October 2015 a research project was performed at the University of Regensburg, Institute of Organic Chemistry under the supervision of Prof. Dr. Burkhard König.

The dissertation was submitted on: 15.11.2016

Date of the colloquium: 09.12.2016

Board of examiners:

Prof. Dr. René Wilhelm   (1st referee)

Prof. Dr. Jan Paradies   (2nd referee)

Prof. Dr. Wolfgang Bremser   (examiner)

Prof. Dr. Sabine Fechner   (chairman)

Für meine Eltern

„Träume dir dein Leben schön und mach aus diesen Träumen eine Realität."

Marie Curie

Abstract

This dissertation deals with sustainable approaches and applications in photocatalytic processes. The chapter "*Photocatalysis*" explains the principles of photocatalytic reactions that involve the absorption of light in the presence of participating substances (catalysts) without being consumed.

In the second chapter "*Photocatalytic Reduction by Cadmium Sulfide*", the semiconductor cadmium sulfide was applied in photocatalytic reactions, which are contributed to sustainability: 1) Generation of hydrogen considered as future energy by water splitting. The semiconductor exhibited a higher photocatalytic activity and stability against photocorrosion by modification of CdS with $Co^{III}(dmgH)_2pyCl$ (dmg = dimethylglyoxime, py = pyridine). The H_2 evolution occurs under strongly basic conditions, which offers the possibility to potentially combine it with water oxidation catalysts. Furthermore, water acts as the only proton source, in contrast to the most established photocatalytic systems, generating hydrogen from protic solutions. 2) High selective release of carbon monoxide from formic acid or formate under simple and ambient conditions. This offers the possibility to generate on-site CO that is used in several industrial processes, whereby transportation routes of the high toxic gas could be reduced. 3) Detoxification of chlorinated organic compounds and generation of methane as sustainable energy storage from polluting chlorinated halomethanes.

The third chapter "*Task Specific Ionic Liquids as New Organic Photosensitizers*" comprised the synthesis and characterization of new organic dyes as potential photosensitizer in photocatalytic H_2 evolution. These dyes are consisting of Donor-π-Acceptor (D-π-A) structures that are usually used in organic solar cells. The acceptor is based on a cationic moiety, which would allow to specify the photosensitizer as task specific ionic liquid. Further a complex was synthesized, in which a D-π-A photosensitizer is linked as ligand to cobaloxime as the proton reduction catalyst for enabling a fast intramolecular electron transfer. The resulted complex showed high stability and potential in photocatalytic H_2 evolution.

Due to their ionic character ionic liquids have an impact on the excited photocatalytic components and the subsequent electron transfer, which was investigated and discussed in the last

chapter "*Ionic Liquids in Photocatalysis*" based on the photocatalytic hydrogen evolution but also in reduction of CO_2 into hydrocarbons on TiO_2. The application of ionic liquids led to a reduced photoactivity in H_2 evolution. The electrostatic attraction between the photoexcited photocatalyst and the cation of the ionic liquid impeded the access for the protons and the re-generation by the sacrificial electron donor. In case of CO_2 reduction, the ionic liquid has a major role as CO_2-absorbing material in the photocatalytic conversion of carbon dioxide, whereby a reduction can be facilitated. Various physical and chemical properties can be used by variation of the ions. An exchange of a hydrophobic cation or anion could support the selectivity towards the formation of higher hydrocarbons, since a combination of the carbon-based radicals could be favorable in case of a lower water concentration. Higher hydrocarbons have a higher volumetric energy density and can be directly used as fuels.

Zusammenfassung

Die vorliegende Dissertation beschäftigt sich mit nachhaltigen Lösungsansätzen und Anwendungen in photokatalytischen Prozessen. Im ersten Kapitel "*Photocatalysis"* werden die Grundlagen photokatalytischer Reaktionen erläutert, die unter Einfluss von Licht in Gegenwart von Substanzen (Katalysatoren) stattfinden, die aus der Reaktion unverbraucht hervorgehen.

In dem zweiten Kapitel "*Photocatalytic Reduction by Cadmium Sulfide*" wird Cadmium Sulfid in drei photokatalytischen Prozessen angewendet, die der Nachhaltigkeit beitragen: 1) Erzeugung von Wasserstoff als Energiequelle der Zukunft durch Wasserspaltung. Durch die Modifizierung mit dem Cobalt-Komplex ($Co^{III}(dmgH)_2pyCl$) (dmg = Dimethylglyoxim, py = Pyridin) wies CdS eine höhere photokatalytische Aktivität und Stabilität gegenüber Photokorossion auf. Die Wasserstofferzeugung findet unter stark basischen Bedingungen statt, womit eine potentielle Kombination mit einem Oxidationskatalysator gegeben ist. Des Weiteren ist hervorzuheben, dass Wasser als alleinige Protonenquelle vorliegt. Viele der bisher etablierten Systeme erzeugen nur H_2 aus protischen Lösungen. 2) Hochselektive Freisetzung von CO aus Ameisensäure oder Formiat unter einfachen und milden Bedingungen. Dieses bietet die Möglichkeit, Kohlenstoffmonoxid vor Ort zu gewinnen, welches in zahlreichen industriellen Prozessen Verwendung findet, wodurch Transportwege des hochgiftigen Gases reduziert werden können. 3) Detoxifizierung organisch chlorierter Verbindungen und die Entwicklung von Methan als Energiespeicher aus umweltbelastenden chlorierten Halogenmethanen.

Das dritte Kapitel "*Task Specific Ionic Liquids as New Organic Photosensitizer"* beinhaltet die Synthese und Charakterisierung neuer organischer Farbstoffe als potentielle Photosensibilisatoren in der photokatalytischen Entwicklung von Wasserstoff. Diese bestehen aus einer Donor-π-Akzeptor (D-π-A) Struktur, welche gewöhnlich Verwendung in organischen Solarzellen finden. Der Akzeptor basiert dabei auf einem Kation, wodurch die Möglichkeit gegeben ist, den Photosensibilisator als aufgabenspezifische ionische Flüssigkeit (engl. task specific ionic liquid) auszulegen. Des Weiteren wurde ein Komplex synthetisiert, in dem ein D-π-A-Farbstoff als Ligand an einem Protonen-Reduktionskatalysator gebunden ist, wodurch eine schnelle intramolekulare Elektronenübertragung ermöglicht werden soll. Dieser zeigte hohe Stabilität und Potential in der photokatalytischen Erzeugung von Wasserstoff.

Zusammenfassung

Im letzten Kapitel "*Ionic Liquids in Photocatalysis*" wird der Einfluss von ionischen Flüssig-keiten in der Photokatalyse anhand der Entwicklung von Wasserstoff und der Reduktion von Kohlenstoffdioxid zu Kohlenwasserstoffen an TiO_2 untersucht und diskutiert. Angeregte Zu-stände photokatalytischer Komponenten können von ionischen Flüssigkeiten aufgrund ihres Salzcharakters stabilisiert werden, wodurch eine Ladungsrekombination gehemmt wird und eine darauffolgende Elektronenübertragung unterstützt werden kann. Der Einsatz von ionischen Flüssigkeiten in der photokatalytischen Entwicklung von H_2 führte zu einer Minderung der Pho-toaktivität. Die elektrostatische Anziehung zwischen dem angeregten Photokatalysator und dem Kation der ionischen Flüssigkeit erschwert den Zugang der Protonen und die Regeneration durch Elektronendonoren. Bei der photokatalytischen Umwandlung von Kohlenstoffdioxid spielte die ionische Flüssigkeit eine entscheidende Rolle als CO_2-absorbierendes Mittel, wodurch eine Reduktion erleichtert werden kann. Durch Variation der Ionen können unter-schiedliche physikalische und chemische Eigenschaften genutzt werden. So kann z. B. durch den Austausch eines hydrophoben Kations oder Anions die Selektivität der Bildung von höheren Kohlenwasserstoffen unterstützt werden, da die Kombination von kohlenstoffhaltigen Radika-len möglicherweise bevorzugt stattfinden kann. Höhere Kohlenwasserstoffe besitzen eine hö-here volumetrische Energiedichte und können direkt als Kraftstoff eingesetzt werden.

Abbreviations

AQY	Apparent quantum yield
bpy	2,2'-bipyridyl
c	Speed of light
cat	Catalyst
calcd.	Calculated
CB	Conduction band
CV	Cyclic voltammetry
C_2mim	3-Ethyl-1-methyl imidazolium
C_4mim	3-Butyl-1-methyl imidazolium
C_8mim	3-Octyl-1-methyl imidazolium
d	Day(s)
DFT	Density functional theory
DMSO	Dimethyl sulfoxide
DSSC	Dye sensitized solar cell
DLS	Dynamic light scattering
dmg	Dimethylglyoxime
D-π-A	Donor-π-Acceptor
EA	Elemental analysis
EDTA	Ethylenediaminetetraacetic acid
EDX	Energy-dispersive X-ray spectroscopy
eq	Equivalent(s)
eq.	Equation
eV	Electron volt
Fc	Ferrocene
h	Planck constant

Abbreviations

HOMO	Highest occupied molecular orbital
IL	Ionic Liquid
λ	Wavelength
LUMO	Lowest unoccupied molecular orbital
M. p.	Melting point
NBS	*N*-Bromosuccinimide
NMR	Nuclear magnetic resonance
ν	Frequency
NHE	Normal hydrogen electrode
NTf$_2$	Tris(trifluoromethylsulfonyl)amid
OTf	Trifluoromethanesulfonate
ppm	Parts per milion
PS	Photosensitizer
rt	Room temperature
SED	Sacrifical electron donor
SEM	Scanning electron microscopy
TEA	Triethylamine
TEOA	Triethanolamine
THF	Tetrahydrofurane
TLC	Thin layer chromatography
TON	Turnover number
VB	Valence band
XRD	X-ray diffraction

Table of Contents

1. Photocatalysis

1.1. Principles

Photochemistry deals with chemical reactions, which are initiated by absorption of energy in form of electromagnetic radiation, commonly known as light. Electromagnetic radiation is caused by acceleration of electric charge, which is affected in oscillating electric and magnetic fields traveling in a quantum of energy called a photon. The resulting electromagnetic wave travels at the speed of light (c = 299792458 m s^{-1} in vacuum) and can be described by their frequency and wavelength, which are mathematically related according to eq. (1). The transferred energy (E) of a photon can be expressed in electron volt [eV] by calculation of eq. (2) with h = 4.135667662(25) 10^{-15} eVs known as Planck constant.[1]

$$\nu = \frac{c}{\lambda} \tag{1}$$

$$E = h \cdot \nu \tag{2}$$

The electromagnetic spectrum that is shown in Figure 1.1 provides a continuum of all photons in accordance to their frequency and wavelengths, which are summarized into seven ranges assigned with descriptive names. Human eyes are only sensitive for a narrow range of the electromagnetic spectrum which is assigned as visible light. It ranges from violet to red with corresponding wavelengths from $400 - 750$ nm and linked frequencies of $7.5 - 4.0 \cdot 10^{14}$ Hz. Solar radiation from the sun reaching the earth's surface, which represents the most abundant renewable energy source, is extended across the ultraviolet, visible and near infrared ranges whereby ultraviolet radiation makes up only a minor part of almost 8%. 49.4% are covered by infrared and 42.3% by visible radiation. However, the highest intensity of solar radiation is provided in the visible range.[2] The light absorption of molecules causes a transient excited state providing chemical and physical properties which differ from the original ground state. Many processes in natures utilize photochemical reactions.

The most known example is the photosynthesis by plants, in which solar energy is absorbed by chlorophyll and channeled into chemical energy by conversion of carbon dioxide and water into glucose under release of oxygen. Further example is the formation of vitamin D from 7-dehydrocholesterol in skin of humans and animals by exposure to sun's ultraviolet radiation.[3]
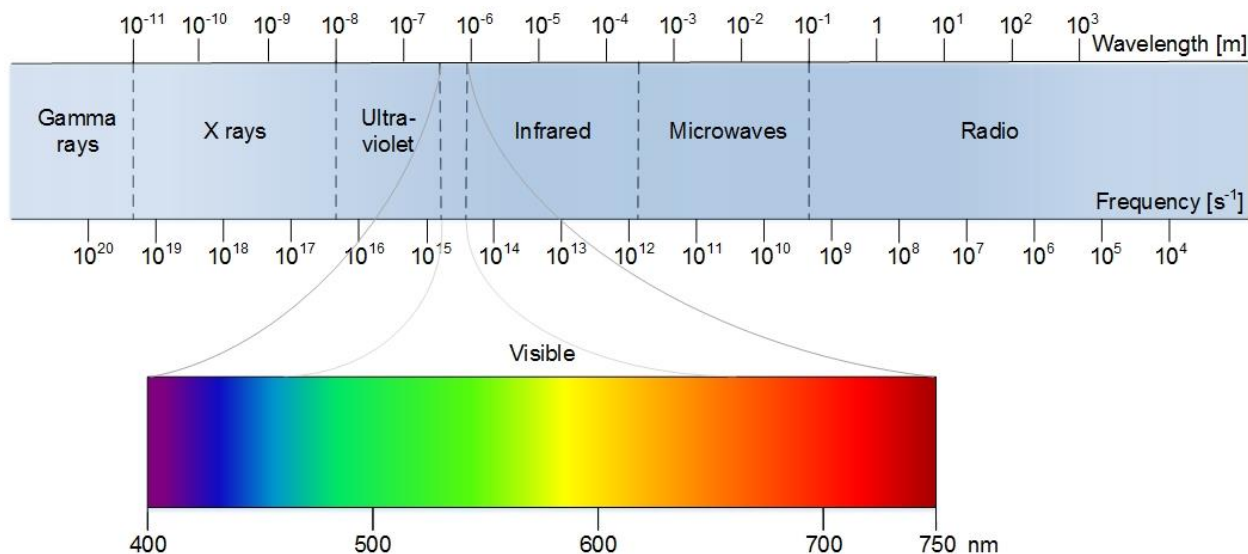

Figure 1.1 *Electromagnetic spectrum.*

The change in electronic configuration by light absorption is defined by the Franck-Condon principle.[4] The electron transition from the ground state in the excited state is vertical even when the geometry of the excited state is not the energy minimum due to the assumption that the heavy atom nuclei virtually do not move. A spin conversion of the excited electron is forbidden during the photoexcitation. The excited state in the molecule can undergo the following physical pathways: (1) Vibronic relaxation of the electronic excited state into vibrational levels of the excited state with a lower energetically location. The energy is released to the environment. (2) Radiationless transition by the return of the excited state in the ground state under release of thermal energy. (3) Radiative transition by the return into the ground state (luminescence, phosphorescence, fluorescence). (4) Intersystem crossing whereby the singlet excited state is converted to the lowest energy triplet state by spin inversion. (5) Transfer of energy from singlet or triplet state to another molecule.[5]

The excited energy-rich states of the reactant may facilitate product formation which occurs only under highly endothermic conditions. Further, new reaction opportunities are opens up due to the photo-induced occupation of antibonding orbitals and triplet states, which is not possible under thermal conditions.

The concept of photochemistry was extended by employing light-absorbing molecules, which activate while in the excited state the reaction participants. Since the light-absorbing molecules are acting as catalyst but not being consumed in the reaction themselves that they can be excited again, which is called photocatalysis. This approach might be helpful in case of not reaching an excited state of the reactant due to spectroscopic properties.

In the past several decades photocatalysis was explored in the conversion of solar energy into electricity (photovoltaic) and chemical fuels.[6] Moreover photocatalytic approaches are found in the synthesis of organic compounds, where the term photoredox catalysis is applied.[7]

So far transition metal complexes were studied in synthetic photocatalysis but also solar energy conversion whereby the most are based on ruthenium and iridium. The light-induced activation includes modes which are explained in the following on basis of $Ru(bpy)_3^{2+}$ (**1**) representing the most well studied transition metal complex in photocatalysis (Figure 1.2). In the excited state the $Ru(bpy)_3^{2+}$ complex shows a stronger redox ability than in the ground state. By one-electron transfer $Ru^*(bpy)_3^{2+}$ can undergo both reductive and oxidative pathways which yield strongly reducing or oxidizing substrates (S) as radical ions which are involved as key reactive intermediates in photocatalytic reactions. A further pathway is the direct transfer of physical energy by transfer of the excited electron from $Ru^*(bpy)_3^{2+}$ to the substrate, called as photosensitization. Regeneration of the photocatalyst occurs by interaction with sacrificial electron donor (D) or acceptor (A) for ensuring a catalytic cycle.[8]

Photocatalysis including the photosensitization can be performed under homogenous conditions and heterogeneous conditions. Beside transition metal complexes further used homogeneous visible light absorbing photocatalysts are organic Photosensitizers (PS), such as Eosin Y, Rose Bengal, Nile Red or Rhodamine B. Typical heterogeneous photocatalysts refers to organic and inorganic semiconductors. The first application of heterogeneous photocatalysts were mainly in the degradation of organic pollutants or dyes in waste water or in the photocatalytic generation

of H_2 and O_2 from water. Only recently heterogeneous photocatalysis was more widely applied to the synthesis of organic compounds.[3, 9-10]
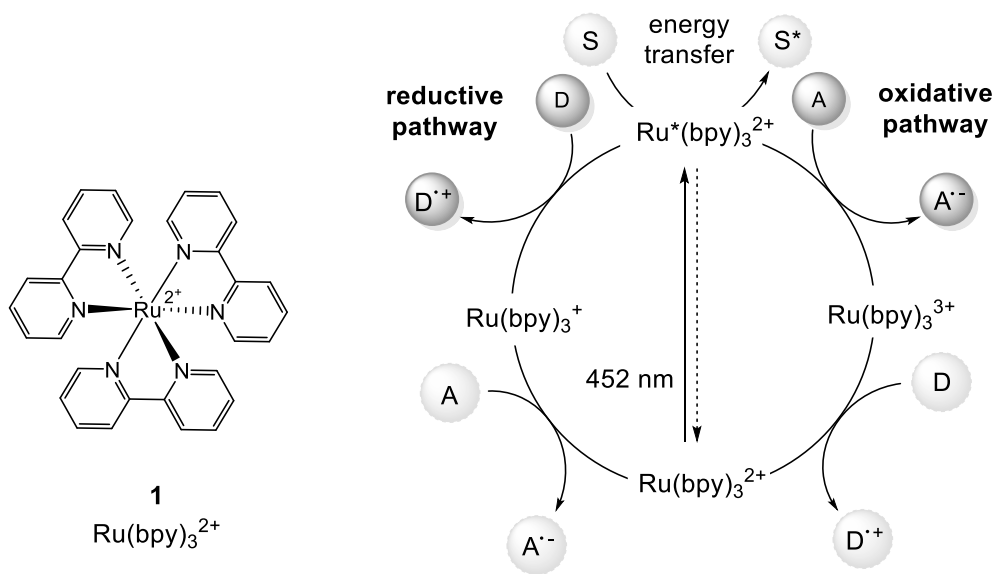

Figure 1.2   *Structure of Ru(bpy)$_3^{2+}$ and its various photocatalytic ability for chemical transformations. S = substrate, D = donor, A= acceptor.[8]*

Semiconductors exhibit an energy band structure in which the valence band (VB) is fully occupied with electrons while the conduction band (CB) remains empty at T = 0 K. The bands are separated from each other with a band gap within electronic states are forbidden. The absorption of a photon with energy equal to or greater than the bandgap energy cause an electron transfer from VB to the CB.[1] This provides an unoccupied state, which is called hole. The resulting electron/hole pair (e^-/h^+) forms the basic building block (eq. (3)). The stabilization of the charge-separated state, which has only a short lifetime of a few nanoseconds, is necessary for the photoreaction.[11]

$$\text{Photocatalyst} \xrightarrow{h\nu} e^- + h^+ \tag{3}$$

Figure 1.3 shows a photoexcitation of an electron from the VB to the CB, which is initiated by photon absorption. The competing charge recombination is prevented by suitable donor or acceptor species adsorbed on the semiconductor surface. The electron can be donated to an adsorbed acceptor or the hole can combine with electrons from a donator species. However, the

generated charges can also recombine either at the surface (surface recombination) or in the particle of the semiconductor (volume recombination).[12]
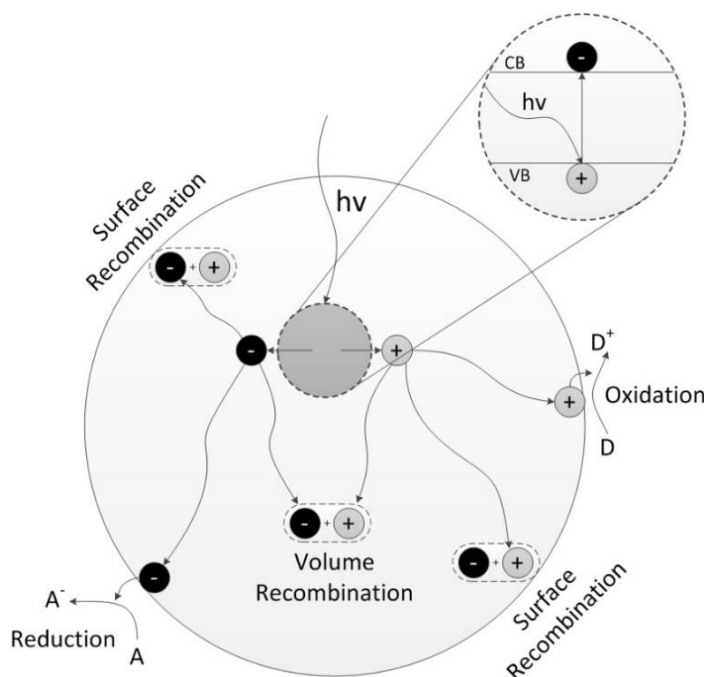

Figure 1.3   *Photoinduced generation of electron/hole (e^-/h^+) pair in a semiconductor with possible pathways.[12]*

An efficient semiconductor photocatalyst should provide a small bandgap to absorb as much solar energy as possible. However, the most semiconductors, which exhibit high oxidizing and reducing power and show less tendency toward photocorrosion, such as WO_3 (2.8 eV), ZnO (3.2 eV) and TiO_2 (3.0 eV in rutile and 3.2 eV in anatase), can absorb only a minor part of solar energy owing to their wide band gaps. In contrast, small band gap semiconductors such as Fe_2O_3 (2.2 ev), CdSe (1.7 ev) and CdS (2.4 eV) provide a higher visible light harvesting ability but tend to decompose under light irradiation.[13]
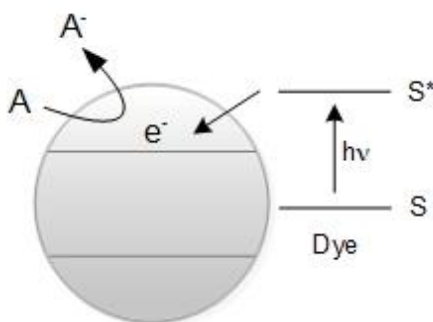
Figure 1.4   *Scheme of photocatalytic process in photosensitized semiconductor.[14]*

Many efforts have been made to develop new or modified semiconductor photocatalysts for improving their visible light response among doping and deposition with metallic and non-metallic elements of the semiconductor. Further, sensitization with organic photosensitizers (PSs) transferring the photoexcited electron to the semiconductor might enhance the efficiency due to effective separation of the charges (Figure 1.4).[14] A sacrificial electron is required for regeneration of the PS that can be again excited. This approach is widely exploited in the field of dye-sensitized solar cells (DSSC), in which solar energy is converted into electrical power. However, it has to be noted, that the LUMO of the dye has to be higher in energy than the CV of TiO_2, otherwise there cannot occur an electron transfer.

1.2. References

1. P. A. Tippler, *Physics for Scientists and Engineers*, 6 edn., Freeman, San Francisco, **2008**.

2. J. Gibson, *UVB radiation: Definition and Characteristics*, http://uvb. nrel. colostate. edu, **2003**.

3. H. Kisch, *Semiconductor Photocatalysis: Principles and Applications*, John Wiley & Sons, **2014**.

4. J. Franck and E. G. Dymond, *Trans. Faraday Soc.*, **1926**, *21*, 536-542.

5. P. W. Atkins and R. S. Friedman, *Molecular Quantum Mechanics*, Oxford University Press, **2011**.

6. U. Gaya, *Heterogeneous Photocatalysis using Inorganic Semiconductor Solids*, Springer Science & Business Media, **2013**.

7. M. H. Shaw, J. Twilton and D. W. C. MacMillan, *J. Org. Chem.*, **2016**, *81*, 6898-6926.

8. T. P. Yoon, M. A. Ischay and J. Du, *Nat. Chem.*, **2010**, *2*, 527-532.

9. B. König, *Chemical Photocatalysis*, Walter de Gruyter, **2013**.

10. M. A. Fox and M. T. Dulay, *Chem. Rev.*, **1993**, *93*, 341-357.

11. J. Bussi, M. Ohanian, M. Vazquez and D. A. Dalchiele, *J. Environ. Eng.*, **2002**, *128*, 733.

12. L. Schmidt-Mende, J. K. Stolarczyk and S. N. Habisreutinger, *Angew. Chem. Int. Ed.*, **2013**, *52*, 7372-7408.

13. A. Kudo and Y. Miseki, *Chem. Soc. Rev.*, **2009**, *38*, 253-278.

14. J. Schneider, D. Bahnemann, J. Ye, G. L. Puma and D. D. Dionysiou, *Photocatalysis: Fundamentals and Perspectives*, Royal Society of Chemistry, **2016**.

2.   Photocatalytic Reduction by Cadmium Sulfide

2.1.   Reduction of Water

2.1.1.   Introduction

Photocatalytic hydrogen evolution from water is currently an active field of research, due to an increasing interest in sustainable energy supplies. In 1972, semiconductors were used for the first time in photoelectrocatalytic hydrogen evolution by Fujishima and Honda *et al*.[1] Since then, these materials have attracted considerable attention resulting in various reports.[2] Semiconductors based on metal oxides, such as the widely-used TiO_2, fulfill the thermodynamic requirements for water splitting and are known for their high stability. However, the use of organic PSs is essential to allow the use of visible light, since these metal oxide semiconductors only absorb UV light. In contrast, metal sulfides like CdS show visible light responses due to their narrow band gap and are more stable than organic dyes.[3]

CdS has proved as an efficient photocatalyst with suitable band positions for reducing H_2O to H_2. The disadvantages of CdS are toxicity and photocorrosion, which results in an anodic dissolution caused by photogenerated holes.[4] An improved stability and enhanced photoactivity of CdS for H_2 evolution has been achieved by the hybridization with other semiconductors and modification by noble metals or inorganic cocatalysts and inorganic or organic molecular catalysts.[5] The inhibition of photocorrosion is also suppressed by the addition of sulfide and sulfite as sacrificial electron donor (SED). S^{2-} and SO_3^{2-} accumulate in huge amounts as extraction products from fossil fuels. Furthermore, they are industrial side products in hydrogenation and desulfurization processes, which makes the use of them as SED additionally attractive.[6] The photocatalytic activity for hydrogen evolution of CdS increases dramatically in the presence of noble metals, whereby Pt is the most efficient cocatalyst so far.[7]

In view of industrial production non-noble metal cocatalysts (e. g. Mo, Ni and Co) are intensively investigated as low-cost and abundantly available alternatives for H_2 evolution. The development of molecular cocatalysts based on earth-abundant elements possess the opportunity of adjusting suitable physicochemical and redox properties. [8]

The cobalt complex (Co^{III}(dmgH)$_2$(py)Cl) **2** with dimethylglyoxime ligands belongs to the class called cobaloxime showing high tolerance to oxygen and is titled as the most promising earth-abundant catalyst for the reduction of protons.[9] Cobaloximes are well suited as efficient catalyst in homogenous systems containing PSs either with noble metals but also organic PSs and a SED which is in the most cases triethanolamine (TEOA) for regeneration the oxidized PS. In most cases it is also serving as proton source to give H$_2$. The H$_2$ evolution takes place via a Co(III) hydride complex, formed by reduction and subsequent protonation of the initial cobaloxime catalyst. The detailed mechanism of H$_2$ evolution by cobaloxime is given in chapter 3.2.1.
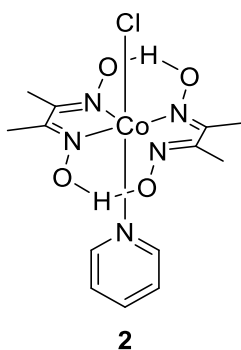

2

Figure 2.1   *Structure of the cobalt catalyst (CoIII(dmgH)$_2$(py)Cl) called as cobaloxime.*

There are various reports of cobaloxime in modified systems with semiconductors in visible-light driven photocatalytic hydrogen evolution.[10] They have been combined with CdS[11] via physical interactions with different axial pyridine ligands or covalent linked to TiO$_2$[12-14] and CdSe/ZnS core/shell quantum dots (QDs)[15] by an anchor group.

However, most reported visible light driven photocatalysts based on cadmium sulfide and earth-abundant metals require proton sources and low pH values. So far, the highest value in H$_2$ production ever reported on CdS photocatalytic systems with earth-abundant metals, was recently achieved using a cobalt phosphide/CdS hybrid system that generated 254 mmol H$_2$ g^{-1} h^{-1} during 4.5 h of sunlight irradiation.[16] Nevertheless, it is only progressing in presence of lactic acid. The need of a sacrificial electron donor like triethanolamine or lactic acid providing at the same time protons does not represents strictly speaking pure water splitting.

From a thermodynamic point of view the reduction of protons is more favorable under a neutral to acidic medium.[17] A system efficiently evolving H$_2$ under basic reaction conditions offer the

possibility to establish a potential for the combination of reduction and water oxidation catalysts. There are reports based on heterogeneous photocatalytic systems evolving H_2 under basic conditions, but consist of noble-metals such as Pt[18] and Ru[19] particles. Photocatalytic heterogeneous systems based on earth-abundant materials working in basic aqueous solution are rare. Lu *et al.* published Cu_2O decorated CdS evolving hydrogen with a rate of 4.76 mmol g^{-1} h^{-1}.[20] Other reported systems are CdS nanorods[21] hybridized with NiS generating hydrogen with a rate of 1.13 mmol g^{-1} h^{-1} and CdS/carbon nanotubes[22] loaded with NiS giving H_2 with a rate of 12.13 mmol g^{-1} h^{-1}.

This chapter presents a photocatalytic system, which exhibits a high photocatalytic activity and stability against photocorrosion by modification of CdS with the cobaloxime catalyst ($Co^{III}(dmgH)_2pyCl$). The reaction occurs in a mixture of MeCN and an aqueous solution of Na_2S and Na_2SO_3, which serves as the sacrificial electron donor but also induces the cobaloxime CdS interaction. It is remarkable, that the H_2 evolution occurs under strongly basic conditions, which offers the possibility to potentially combine it with water oxidation catalysts. Furthermore, water acts as the only proton source, in contrast to most established photocatalytic systems generating H_2 from protic solutions.

2.1.2. Results and Discussion

CdS powder was prepared from Na_2S and an aqueous NH_3 solution of cadmium sulfate. The resulting CdS according to this synthesis procedure was already studied in photocatalytic reactions for example in the photoaddition of olefins and enol/allyl ethers to *N*-phenylbenzophenone.[23-24]

The structure of CdS powder was analysed by X-ray diffraction. XRD pattern of CdS illustrated in Figure 2.2 is identified as face centered cubic structure of CdS with peaks corresponding to the reflections at 2θ values of 27.0, 44.2, 51.9 and 71.3 fitting with the (111), (220), (311) and (331) planes of the face centered cubic structure of CdS (ICDD PDF 89-0440). The average crystallite size of CdS is 3 nm and the average particle size is 245 nm.
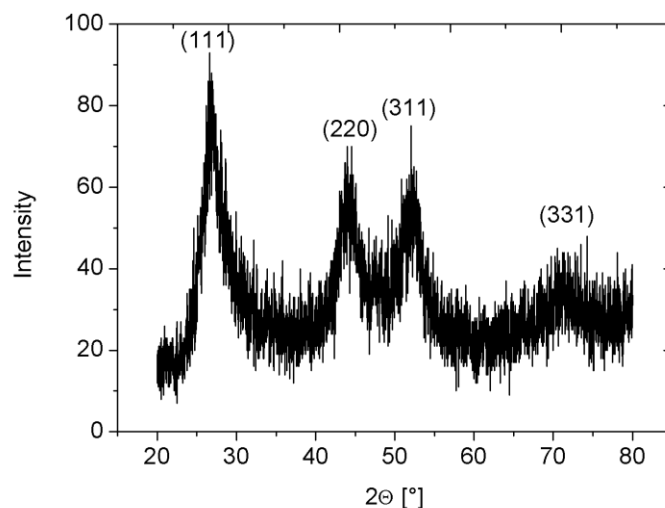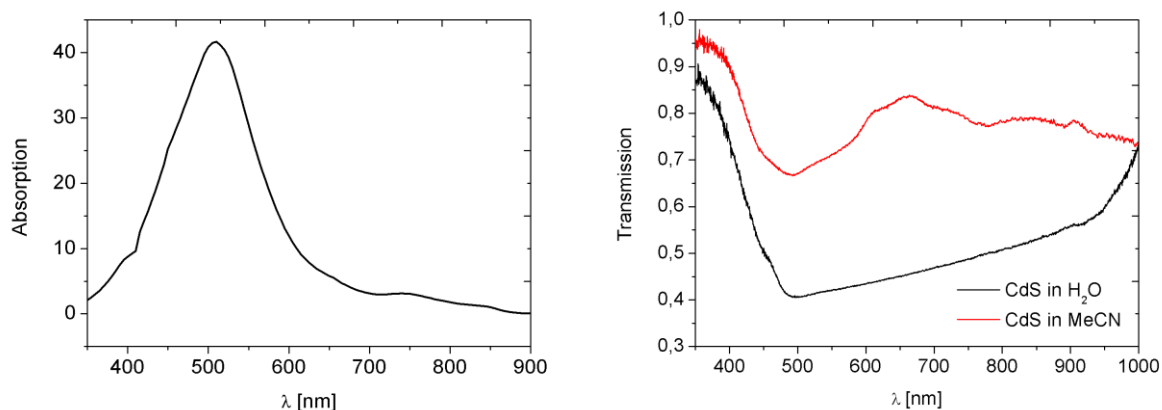
Figure 2.2 *P-XRD pattern of CdS powder.*

Figure 2.3 *Diffuse reflectance spectra (DRS) of CdS powder (left) and transmission spectra of CdS powder (right) suspended in H₂O (black line) and MeCN (red line).*

A band gap of 2.18 eV was determined by diffuse reflectance spectroscopy (DRS) using the Kubelka-Munk function.[25] The corresponding spectra in Figure 2.3 (left) showed a broad absorption band in visible light range with a maximum at 510 nm. In view of the photocatalytic application of suspended CdS, transmission spectra in water and MeCN were acquired. The spectrum, presented in Figure 2.3 (right), demonstrated that CdS suspended in protic medium show a more efficient use of light compared to aprotic medium due to the lower percentage of transmission in the visible light range. CdS suspended in water showed in UV range almost

transmission of light, which is continually decreased from visible light range. The highest light absorption can be concluded at 492 nm, according the lowest light transmission of 40.5%. Since then the longer the wavelength, the more the transmission is increased. In comparison, the light transmission of CdS suspended in MeCN is around 66 – 83% in visible range, which concludes that the amount of aprotic solvent should be minimized in photocatalytic applications with visible light for achieving higher efficiency.
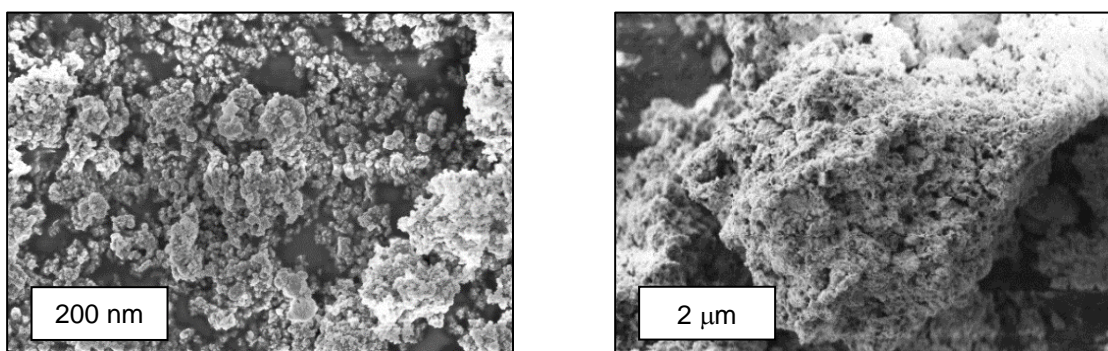

Figure 2.4   *SEM images of CdS powder.*
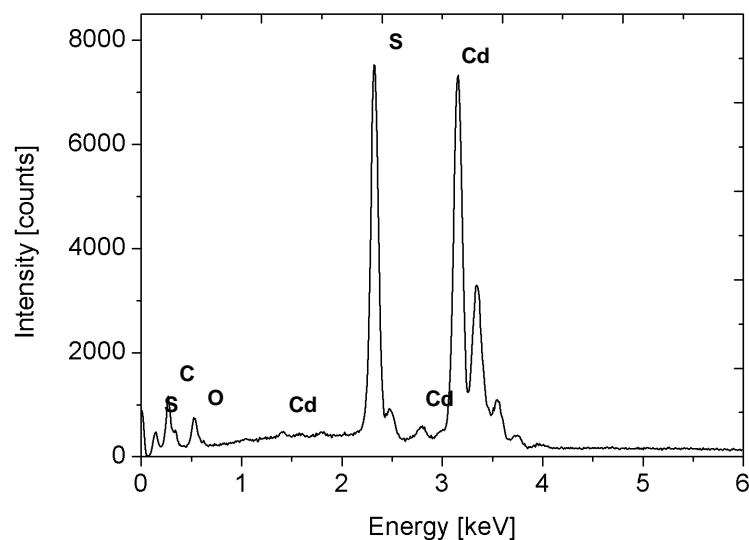
Figure 2.5   *EDX spectra of CdS powder.*

The morphology of CdS was studied by scanning electron microscopy (SEM). The images in Figure 2.4 show irregular shaped particles by aggregation with the dimensions in a broad range of 50 nm – 100 μm. A specific surface area of 129.972 m^2 g^{-1} was determined by N_2 physio

sorption. Elemental composition and its purity has been verified using EDX shown in Figure 2.5. The low percentage of carbon is due to coal used as carrier material for the CdS sample.

The photocatalytic evolution of H_2 was performed with in situ formed species of CdS and the cobaloxime catalyst **2** under visible light irradiation ($\lambda = 455$ nm). A mixture of an aqueous solution of Na_2SO_3/Na_2S and MeCN as solvent for **2** in a 9:1 ratio was used as reaction medium with a pH of 13. The salts Na_2SO_3 and Na_2S served as SEDs and stabilized the CdS. The S^{2-} ion is known to prevent efficiently the photocorrosion of sulfide semiconductors by trapping the photogenerated holes.[26] According to eq. (4) this oxidation results in the formation of yellow disulfide acting as an optical filter. Added SO_3^{2-} ions convert it to thiosulfate (eq. (5)) which does not compete with the light absorption of CdS anymore.

$$2S^{2-} + 2h^+ \rightarrow S_2^{2-} \tag{4}$$

$$S_2^{2-} + SO_3^{2-} \rightarrow S_2O_3^{2-} + S^{2-} \tag{5}$$

A small amount of organic solvent like MeCN is needed to dissolve the cobaloxime. After the addition of the aqueous solution of the SED, the cobaloxime is extracted from the organic into the aqueous phase. This is indicated by an orange coloration of the aqueous phase while the organic phase becomes decolorized. Although MeCN is usually water-miscible, in this case two separate phases formed, due to the high concentration of SEDs in the aqueous solution. The extraction of **2** into the aqueous phase of the SED is shown in Figure 2.6 by UV-Vis spectroscopy, which is indicated by the appearance of an absorption band in the visual spectral range. The extraction of **2** might be explained by undergoing a ligand exchange through the SED. A clear structural characterization is not given, since the formed species based on cobaloxime is only short-term stable under this conditions and is then decomposed. This is indicated by the fact, that the aqueous solution is decolorized with suspended dark solids.
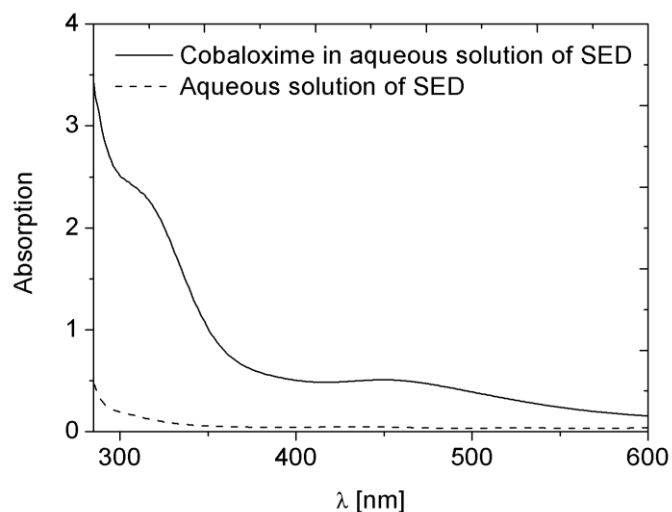
Figure 2.6 *UV-Vis spectra of H_2O with Na_2S and Na_2SO_3 (0.35 and 0.25 mol L^{-1}) (dash line) and of **2** extracted from MeCN ($1.26·10^{-4}$ mol L^{-1}) into the aqueous phase containing Na_2S/Na_2SO_3 (straight line).*

The elemental composition of modified CdS after 24 h irradiation was obtained by EDX measurement under the SEM and is visualized in Figure 2.7. After the irradiation the reaction sample was filtered and washed and the residue was dried under high vacuum. The low percentage of carbon is due to coal used as carrier material for the CdS sample. Further, the presence of sodium is considered as impurity caused by skin contact. In contrast to non-irradiated CdS (EDX is shown in Figure 2.5), the normalized wt% of oxygen is increased from 2.6 to 7.51 after irradiation, which concludes a marginal oxidation of CdS during the reaction and underlines the high robustness of CdS. The EDX measurement shows that CdS is doped with Co from cobaloxime. No significant difference is seen in SEM images between non-irradiated and irradiated CdS (see Figure 2.4).
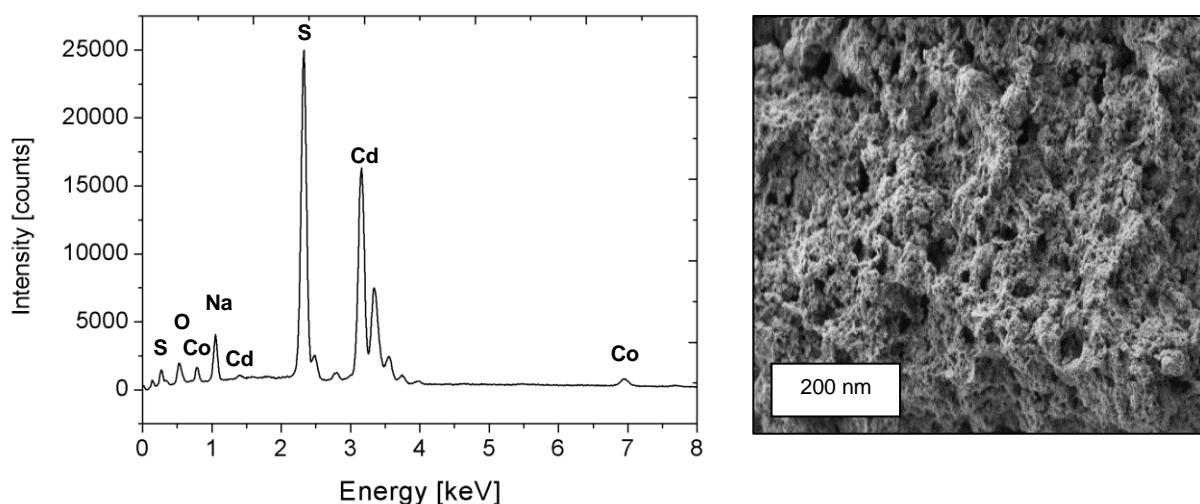
Figure 2.7   *EDX spectra and SEM image of modified CdS after photocatalytic hydrogen evolution of 24 h irradiation.*

The modification had a positive influence on the stability of CdS. Figure 2.8 shows reaction samples with modified CdS (A) and the pristine CdS (B) after 3 h of irradiation. The yellow color of the pristine CdS sample A originated from sulfur, which is generated by photocorrosion of CdS. In contrast, sample B with modified cobaloxime did not evolve any yellow color which indicated the inhibition of photocorrosion. Sample A also evolved more hydrogen, as quantified by gas chromatography.
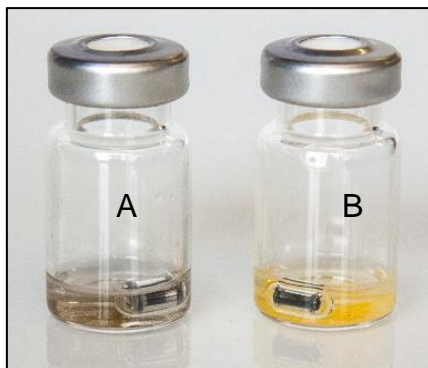
Figure 2.8   *Reaction samples of modified CdS (A) and pristine CdS (B) after irradiation of 3 h.*

The photocatalytic activity of pristine CdS and modified CdS in terms of hydrogen generation is shown in Figure 2.9. Both pristine CdS and the modified system show activity for H_2 evolution over 48 h. In contrast to pristine CdS evolving 116 mmol H_2 g_{cat}^{-1} with a rate of 2.39 mmol H_2 g_{cat}^{-1} h^{-1} after 48 h irradiation, the modified system of CdS/cobaloxime generated hydrogen of 377 mmol H_2 g_{cat}^{-1} with a rate of 14.3 mmol H_2 g_{cat}^{-1} h^{-1} during the initial 10 h and 8.0 mmol H_2 g_{cat}^{-1} h^{-1} over the whole time course of 48 h light irradiation. After 48 h of irradiation, no significant hydrogen evolution was observed, probably due to the consumption of the SED. The consumption is caused by the trapping of the photogenerated holes and the reaction of SO_3^{2-} and S^{2-} to thiosulfate.[6]

Without CdS, no hydrogen evolution was observed. The apparent quantum yield (AQY) was estimated under the same reaction conditions and calculated according to eq. (32) described in the experimental part (chapter 2.4.1). The system with pristine CdS results in an AQY of 0.4% at 455 nm. By the addition of cobaloxime, the AQY increased up to 3.5%.
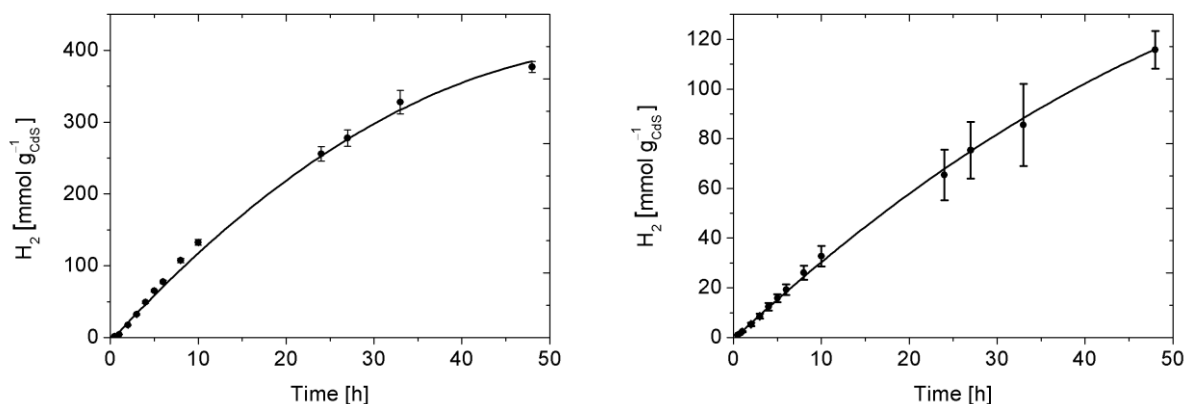

Figure 2.9 *Photocatalytic activity of modified CdS (left) and pristine CdS (right). [λ = 455 nm, 0.5 mg CdS, 1.26·10⁻⁴ mol L⁻¹ CoIII(dmgH)₂(py)Cl, 1.0 mL mixture of MeCN (0.1 mL) and H₂O (0.9 mL) solution of 0.35 mol L⁻¹ Na₂S and 0.25 mol L⁻¹ Na₂SO₃].*

In view of the recorded EDX spectra, which shows a deposition of cobalt on CdS, the reaction was also done with cobalt chloride instead of cobaloxime. After 24 h irradiation the photoactiv-

ity of the system with cobalt chloride is about a factor of 36 lower than the system with cobalox-ime. This implies that cobaloxime not only affect the increased photoactivity of CdS as cobalt source.

The photocatalyst was recycled by centrifugation removing the consumed sacrificial electron donor solution. The addition of a fresh mixture of an aqueous solution of Na_2S and Na_2SO_3 lead to renewed evolution of hydrogen, which indicated the previous consumption of the SED after 48 h irradiation. The easily recycled system produced hydrogen of 257 mmol H_2 g_{cat}^{-1} during 48 h, which represents 74% of its original activity. The separation of the reaction residue confirms that the species based on cobaloxime was accumulated on the CdS surface. Pristine CdS retained the same photoactivity in the second run finally evolving hydrogen of 116 mmol H_2 g_{cat}^{-1} (Figure 2.10).
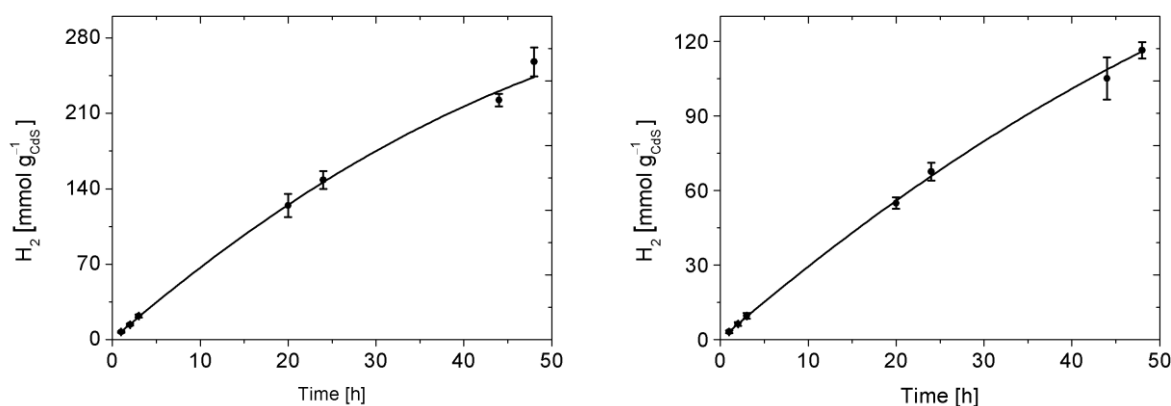

Figure 2.10 *Photocatalytic activity of modified CdS (left) and pristine CdS (right) after sec-ond recycling process. [λ = 455 nm, 0.5 mg CdS, 1.26·10^{-4} mol L^{-1} CoIII(dmgH)$_2$(py)Cl, 1.0 mL H$_2$O of 0.35 mol L^{-1} Na$_2$S and 0.25 mol L^{-1} Na$_2$SO$_3$].*

Both the modified system and pristine CdS could be recycled a second time with an almost constant photoactivity of 251 mmol H_2 g_{cat}^{-1} and 121 mmol H_2 g_{cat}^{-1} during 48 h light irradiation, shown in Figure 2.11. A further recycling could not be performed anymore, since the separation of the catalytic residue could not be completely achieved due to the fine dispersion of the residue which is probably caused due to the mechanically impact by stirring during the reaction time.
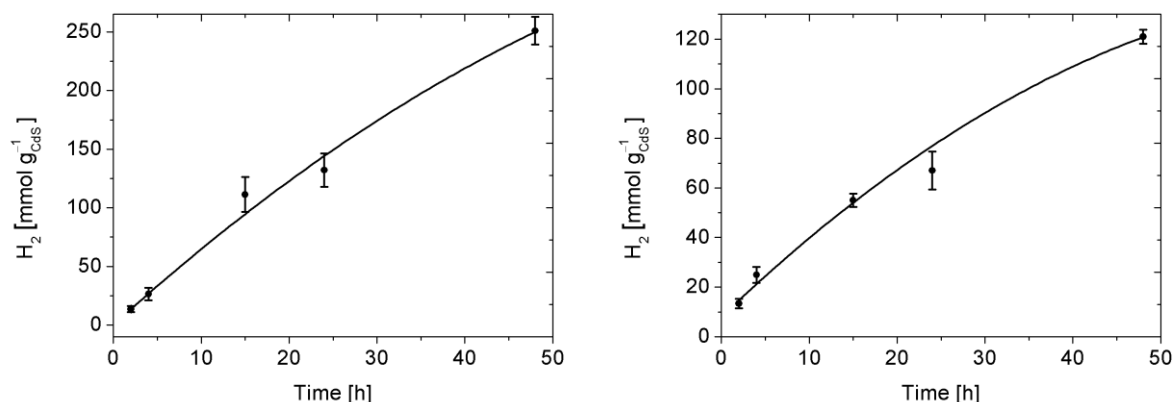
Figure 2.11   *Photocatalytic activity of modified CdS (left) and pristine CdS (right) after third recycling process. [λ = 455 nm, 0.5 mg CdS, 1.26·10^{-4} mol L^{-1} CoIII(dmgH)$_2$(py)Cl, 1.0 mL H$_2$O of 0.35 mol L^{-1} Na$_2$S and 0.25 mol L^{-1} Na$_2$SO$_3$].*

2.1.3.   Conclusion

Cobaloxime (Co^{III}(dmgH)$_2$pyCl, **2**) and CdS form in the presence of Na$_2$S/Na$_2$SO$_3$ an active modified species with increased photoactivity and stability for visible light driven photocatalytic H$_2$ evolution. The resulting photocatalytic system generating H$_2$ from water molecules under highly basic conditions (pH of 13) caused by added Na$_2$S/Na$_2$SO$_3$, which may facilitate its combination with water oxidation catalysts. After 48 h of visible light irradiation (λ = 455 nm) the system finally generated 377 mmol H$_2$ g$_{cat}$$^{-1}$ with a rate of 14.3 mmol H$_2$ g$_{cat}$$^{-1}$ h^{-1} during the initial 10 h and 8 mmol H$_2$ g$_{cat}$$^{-1}$ h^{-1} during the whole irradiation time. The H$_2$ evolution rate of our system ranks with literature-known photocatalytic water splitting systems based on CdS and earth-abundant co-catalysts generating H$_2$ in the absence of a proton source.[20-22] An ability of recycling could be demonstrated by separation of the catalyst residue from consumed reaction solution and renewed H$_2$ evolution by addition of fresh water containing SED. A clear structural confirmation of the modified species based on cobalt and CdS would provide more hints in the molecular design for CdS surface improving H$_2$ evolution.

18

2.2.   Reduction of Sodium Formate

2.2.1.   Introduction

Formic acid is known to undergo two pathways of decomposition to give either H_2 by decarboxylation (eq. (6)) or CO by decarbonylation (eq. (7)). The release of H_2 via catalytic dehydrogenation has received considerable attention due to the increased interest of H_2 as future energy carrier. To ensure sustainability the photocatalytic decomposition enabling generation of H_2 under mild conditions, which has been recently perceived as an alternative. Photocatalysts for H_2 generation from formic acid are based on noble metals such as Pd[27-29], Pt[30], Rh[31] and Ru[32] but also on noble metal free catalysts such as CdS quantum dots, recently published.[33] Reports about catalytic decarbonylation of formic acid to give CO and H_2O according to eq. (7) are rare and typically requires high temperatures[34]

$$HCOOH \rightarrow H_2 + CO_2 \tag{6}$$

$$HCOOH \rightarrow CO + H_2O \tag{7}$$

CO is an important carbonyl synthon used in various industrial chemical processes with a high economic impact, e.g. in hydroformylation[35] to give aldehydes and in Monsanto and Cativa acetic acid production.[36] Due to the fact that CO gas is highly toxic and flammable, a simple and inexpensive possibility of generating CO on-site linked to industrial applications could reduce transportation routes achieving more safety handling.

In the recently published work of Reisner *et al.*[33] a photocatalytic system was reported, which consisted mercaptopropionic acid (MPA)-capped CdS quantum dots promoting selective H_2 conversion from $NaHCO_2$ in formic acid. By investigations to tune the reaction pathway towards dehydration, high selective CO evolution was achieved with ligand-stripped CdS quantum dots charge-stabilized by BF_4^- ions in aqueous solution evolving CO in a basic aqueous environment containing sodium formate (4 mol L^{-1}) and $KOH/K_2CO_2/CO_2$ as buffer. The CO evolution was performed with 96% selectivity with a rate of 102 mmol CO g_{cat}^{-1} h^{-1} in the first reaction hour and finally generating 14 mol CO g_{cat}^{-1} after one week irradiation. This represents so far the first example of a selective photocatalytic generation of CO from sodium formate. We present

selective photocatalytic CO evolution from $NaHCO_2$ with CdS powder, which surpasses the report of Reisner et al.[33] in activity and selectivity towards CO.

2.2.2. Results and Discussion

CdS powder in aqueous $NaHCO_2$ (pH 8.3) showed activity for CO evolution over a time of 7 days, shown in Figure 2.12. The photocatalytic system generated CO at an initial rate of 278 mmol CO g_{cat}^{-1} h^{-1} which is almost constant during the first day irradiation and then gradually halved per day. After 7 days irradiation almost 19.6 mol CO g_{cat}^{-1} are generated. Furthermore, 66 mmol H_2 g_{cat}^{-1} are formed, which results in a selectivity towards CO of 99.7%. An apparent quantum yield (AQY) of 4% was determined. Without CdS, no gas evolution was observed. Furthermore, no gas is evolved in pure H_2O in the absence of $NaHCO_2$ which indicated that it simultaneously served as sacrificial electron donor. The yield of CO was 26.5%. Taking into consideration, that $NaHCO_2$ is also consumed by oxidation of VB holes from CdS, the yield could only be assumed as apparent value. The photocorrosion of CdS seemed to be inhibited since no sulfur is formed, which originated from the decomposition of CdS.

For indicating the permanent need of photons, the irradiation was stopped after 24 h and the reaction was stirred again for another day in the dark. With no irradiation no further gas evolution was observed, which precluded a light-driven formation of a catalytic species promoting the reduction. The irradiation could be repeatedly stopped without having any influence on the gases turnover.

In comparison to the work of Reisner et al.[33] our photocatalytic system is simpler in terms of the number of reactants and synthesis of the photocatalyst and even showed enhanced activity and selectivity, summarized in Table 2.1 (entry 1 and 2).
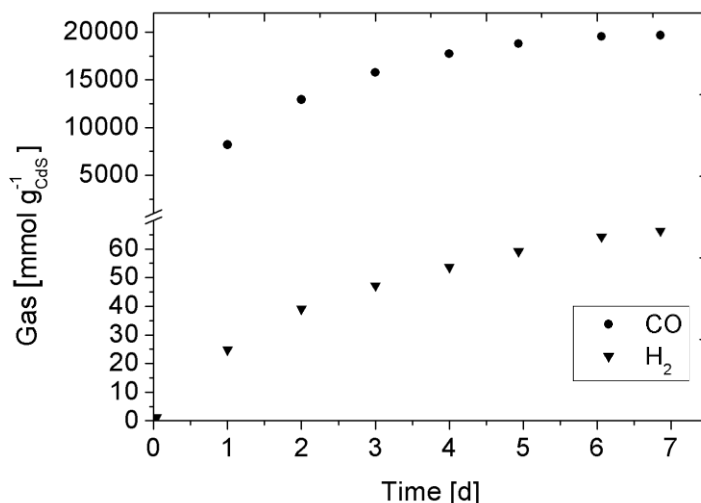
Figure 2.12 *Time course of photocatalytic CO and H$_2$ evolution over 7 d of irradiation.*

[λ = 455 nm, 0.1 mg CdS in aqueous solution containing 4.0 mol L^{-1} NaHCO$_2$].

Table 2.1 *Comparison of CdS based photocatalysts promoting selective photoreduction of*

aqueous NaHCO$_2$ to CO after 7 d irradiation.

Entry	Catalyst	Medium	Activity [mmol g$_{cat}$$^{-1}$ h^{-1}]	CO[c] [mmol g$_{cat}$$^{-1}$]	Sel.[d] [%]	Ref.
1[a]	CdS powder	NaHCO$_2$/H$_2$O	278	19596	99.7	this work
2[b]	QD-BF$_4$	NaHCO$_2$/H$_2$O	102	14000	96.3	[33]
3[c]	CdS powder	HCOOH/Na-HCO$_2$	15	4336	87.6	this work

[a] λ = 455 nm, 0.1 mg CdS, 4.0 mol L^{-1} NaHCO$_2$ in water at pH 8.3 [b] λ > 420 nm, 0.1

mg CdS, 4.0 mol L^{-1} NaHCO$_2$ in aqueous KHCO$_3$/K$_2$CO$_2$/CO$_2$ buffer at pH 9.7. [c] λ

= 455 nm, 0.1 mg CdS, 4.0 mol L^{-1} NaHCO$_2$ in HCOOH at pH 0.7.

[d] Selectivity = 100% · nCO/(nCO + nH$_2$).

CdS powder was also studied under aqueous-free conditions in formic acid containing $NaHCO_2$. An initial rate of 15 mmol CO g_{cat}^{-1} h^{-1} and 247 mmol H_2 g_{cat}^{-1} h^{-1} were achieved. The gas evolution proceeded over the course of one week, finally generating 4336 mmol CO g_{cat}^{-1} and 614 mmol H_2 g_{cat}^{-1} with a decomposition selectivity of formic acid to CO of 87.6% (Figure 2.13). The reason for increased H_2 evolution is obvious due to the higher concentration of protons by formic acid compared to the weak basic conditions in the aqueous medium. Nevertheless, the pathway of decarbonylation is favored and presents the first example of high selectivity towards CO generation under acidic conditions with formic acid.

Figure 2.13 *Time course of photocatalytic CO and H_2 evolution over 7 d of irradiation. [λ=455 nm, 0.1 mg CdS in HCOOH containing 4.0 mol L^{-1} $NaHCO_2$].*

The mechanism of the decomposition of formate in aqueous suspension of CdS powder under irradiation was discussed for the first time at the end of the 1980s.[37-39] Based on this works the mechanism for CdS powder was subsequently revised and extended.[40] The decomposition either by dehydrogenation to CO and H_2O or dehydration to H_2 or CO_2 is based on the oxidation of formate by photogenerated holes from CdS (eq. (8)). This step results to $\cdot CO_2^-$ anion radicals capable to reduce CdS in solution to Cd(0), shown by pulse radiolysis experiments.[41-42] The photoformation of Cd(0) from CdS in the presence of formate was proved experimentally and is also probably taking place in this work since the yellow CdS powder adopts a grey tint during

the irradiation concluding that the powder is coated by elementary cadmium. The proposed formation of Cd(0) is performed by a trapped electron of the conduction band and the subsequent interaction with $\cdot CO_2^-$ anion radicals, according to eq. (9) and (10).

$$HCOO_2^- + h^+ \rightarrow \cdot CO_2^- + H^+ \tag{8}$$

$$CdS + e^- \rightarrow (Cd^{2+} + e^- + S^{2-}) \tag{9}$$

$$\left(Cd^{2+} + e^- + S^{2-}\right) + \cdot CO_2^- \rightarrow Cd + S^{2-} + CO_2 \tag{10}$$

The photoformation of Cd(0) is proposed as the catalytic surface for H_2 production, since the H_2 evolutions took place even after the CdS became accumulated with the metal. Two mechanisms of the formation of H_2 are proposed: The resulted $\cdot CO_2^-$ may be oxidized with the photogenerated hole to give CO_2 (eq. (11)) and two electrons are required to form hydrogen (eq. (12)). But it may also be possible that $\cdot CO_2^-$ is reacting with a proton (eq. (13)) so that only one electron is still required to produce hydrogen molecules (eq. (14)).

The decarbonylation pathway of formate to CO is proposed on the interaction of $\cdot CO_2^-$ anion radical with a proton and an electron of the conduction band (eq. (15)). In our experiment the pH is increasing during the irradiation from 8.3 to 12 suggesting the formation of hydroxide. A summarized visualization of the reaction pathways are given in Figure 2.14.

$$HCO_2^- + h^+ \rightarrow \cdot CO_2^- + H^+ \tag{8}$$

$$\cdot CO_2^- + h^+ \rightarrow CO_2 \tag{11}$$

$$2H^+ + 2e^- \rightarrow H_2 \tag{12}$$

$$\cdot CO_2^- + H^+ \rightarrow CO_2 + \frac{1}{2}H_2 \tag{13}$$

$$H^+ + 2e^- \rightarrow \frac{1}{2}H_2 \tag{14}$$

$$\cdot CO_2^- + H^+ + e^- \rightarrow CO + OH^- \tag{15}$$

Figure 2.14 *Visualization of reactions occurring during formate photodecomposition with CdS powder.[40]*
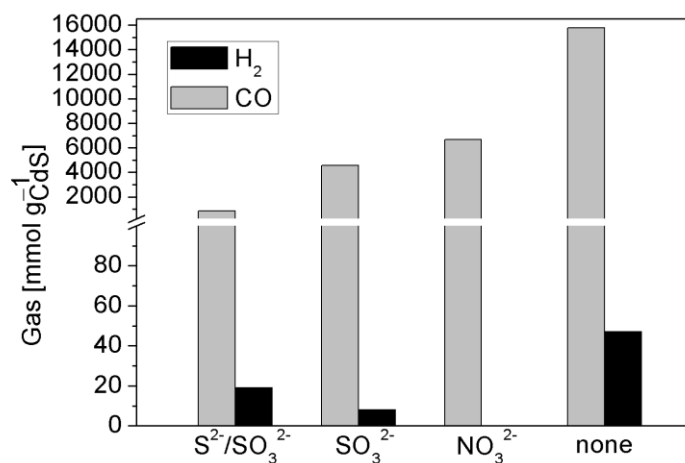

Figure 2.15 *Effect of different salts (0.1 mol L^{-1}) on CO (grey) and H_2 (black) evolution after 2 d irradiation [λ=455 nm, 0.1 mg CdS in aqueous solution containing 4.0 mol L^{-1} Na-HCO$_2$,].*

The addition of Na_2S and Na_2SO_3, commonly used as sacrificial electron donor in photocatalytic water splitting with CdS, has a negative impact on the CO but also H_2 evolution observed by the much lower amount of evolved gases compared to none addition. A direct comparison is given in Figure 2.15. A decrease in catalytic activity by addition of Na_2S was already observed. They hypothesized that the Cd ions form the catalytic active side and is probably blocked through the S^{2-} ions. A further explanation could be also that both S^{2-} and SO_3^{2-} ions are acted

as hole acceptors consuming the required holes for formate oxidation to give the key intermediate $\cdot CO_2^-$ (eq. (8)). Addition of only SO_3^{2-} ions is also inhibiting the photocatalytic activity, but in a lesser extent which is probably due to the fact that S^{2-} is more efficiently trapping holes compared to SO_3^{2-}. No hydrogen evolution is observed by addition of NO_3^{2-} as electron acceptor which is explained by scavenging the electrons required for H_2 formation according to eq. (12) and (14). However, this affected also negatively the CO evolution decreased by a factor of nearly 2.4 compared to conditions without additive. This seems obviously due to the less available electrons required for CO formation (eq. (15)).

2.2.3. Conclusion

The here presented selective photocatalytic CO evolution is based on simple and ambient conditions by using only aqueous solution of $NaHCO_2$ with suspended CdS powder. The photocatalytic system generated CO at an initial rate of 278 mmol CO g_{cat}^{-1} h^{-1}. After 7 days irradiation almost 19.6 mol CO g_{cat}^{-1} are generated. Furthermore, 66 mmol H_2 g_{cat}^{-1} are formed, which results in a selectivity towards CO of 99.7%. An AQY of 4% was determined.

This simple conditions, in which CdS shows remarkably robustness under this simple conditions and do not require further additive for inhibiting the photocorrosion, might facilitates an in situ production of CO that is widely used in industrial applications. Transportation routes of highly toxic CO might be reduced, which is considered as desirable in regards to economic and safety aspects. To the best of knowledge, this described system exhibits the highest activity and selectivity towards CO in photocatalytic decarbonylation of $NaHCO_2$.
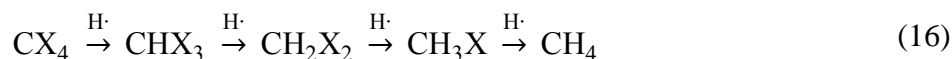
Furthermore, this system show high selectivity towards photocatalytic CO production in formic acid, which is a typical condition for H_2 release by decarboxylation. An initial rate of 15 mmol CO g_{cat}^{-1} h^{-1} and 247 mmol H_2 g_{cat}^{-1} h^{-1} were achieved. The gas evolution proceeded over the course of one week, finally generating 4336 mmol CO g_{cat}^{-1} and 614 mmol H_2 g_{cat}^{-1} with a decomposition selectivity of formic acid to CO of 87.6%.

2.3.   Reductive Dehalogenation

2.3.1.   Introduction

Chlorinated halomethanes are widely used in industrial applications, especially as solvents due to their high solubility, such in metal cleaning and degreasing.[43] However they are representing the most frequent chemical contaminant in the ecosystem by accumulation in the ground water. They are considered as harmful and suspected to be carcinogen for human.[44] Degradation of halomethanes by photocatalytic dehalogenation was investigated on illuminated TiO_2 suspensions, whereby the formation of various products such as CO_2, CO, MeOH, HCOOH and HCHO was observed.[45-49] The respective product formation depends on aerobic or anaerobic conditions and the presence of electron donors.[50]

A degradation pathway of halomethanes towards CH_4 formation was only described in the late 1980s by using conditions of a water photolysis system, which induced in situ hydrogen radicals during H_2 generation, that act as reducing agent for hydrogenolysis according to eq. (16).[51-52]

$$CX_4 \xrightarrow{H\cdot} CHX_3 \xrightarrow{H\cdot} CH_2X_2 \xrightarrow{H\cdot} CH_3X \xrightarrow{H\cdot} CH_4 \tag{16}$$

H_2 generation was performed by visible-light excitation of $Ru(bpy)_3^{2+}$ transferring an electron to methyl viologen as electron relay mediator, which is then reacting on Pt colloids surface with water to give the reducing agent H_2. EDTA was used as SED for regeneration of the oxidized PS (Figure 2.16).

Figure 2.16   *Water-photolysis system evolving H_2.[52]*

However the synthesis of the future energy carrier CH_4 from toxic industrial waste seems to be attractive, no further studies were reported about CH_4 generation by decomposition of chloromethanes. Herein, our photocatalytic system based on CdS powder showed potential in the CH_4 generation by reduction of chlorinated halomethanes in aqueous solution of $NaHCO_2$ as SED.

2.3.2. Results and Discussion

We observed that CdS powder suspended in aqueous solution of $NaHCO_2$ promoted the reductive dehalogenation of chloroform to CH_4 by a photocatalytic reaction. The required protons originated from in situ generated H_2 by CdS. An appropriate amount of chloroform was added into the water and the two-phase system was irradiated for a defined time. The addition of 50 μL $CHCl_3$ led to CH_4 evolution of 169 mmol g_{CdS}^{-1} after 2 d irradiation. The yield of CH_4 was 3.3% (Table 2.2, entry 1). CO and H_2 evolution took also place as competitive reactions. While the produced amount of H_2 is almost the same and independent if $CHCl_3$ is added or not, the yield of CO was 13% which is halved compared to the conditions in the absence of chloroform (see chapter 2.2). Without $NaHCO_2$ no gases are evolved, which indicated its acting as SED.

By an increased amount of $CHCl_3$, the yield of CO as byproduct is continuously decreased and is then almost constant from addition of 100 μL $CHCl_3$. However, the highest yield of CH_4 was achieved with 50 μL $CHCl_3$, which is then decreased by increasing amount of $CHCl_3$ and then remained consistent (Figure 2.17). H_2 is not explored in the bar graph, since chloroform has no influence on the production of H_2.

A further addition of 50 μL $CHCl_3$ to the reaction sample after no more gas evolution was overserved, finally 127 mmol CH_4 g_{CdS}^{-1} were again produced after 17 h irradiation, which corresponds to a yield of 2.5% (entry 2). The fact that the gas evolution already stopped after 17 h could be due to the previous consumption of $NaHCO_2$ during the reaction. A lower concentration of the sacrificial electron donor $NaHCO_2$, which was expected to lead to less competitive CO evolution, did not lead to a higher CH_4 evolution (entry 3). The dehalogenation of $CHBr_3$ compared to $CHCl_3$ is much slower and after almost 2.7 d light irradiation only traces of methane were achieved (entry 4). The reduction potential of a halide depends on the halogen and is

shifted from iodide to fluorine towards cathodic values, whereby ·CHBr$_2$ radical is more desta-bilized that the respective chloride radical.[53]
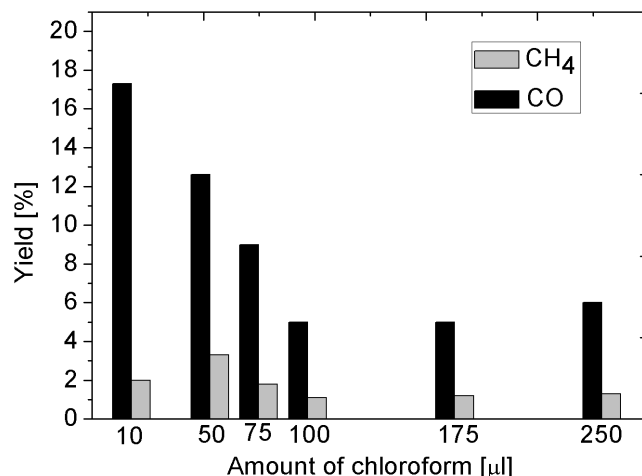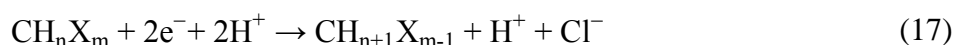

Figure 2.17 *Photocatalytic conversion of CO from NaHCO$_2$ (4.0 mol L^{-1}) and CH$_4$ from chloroform by CdS suspended in 2.0 mL water depended on different amounts of CHCl$_3$.*

As already mentioned, only two reports from one group are given in the late 1980s about CH$_4$ formation from halomethanes (CCl$_4$, CHCl$_3$, CHBr$_3$, CHCl$_2$Br and CHClBr$_2$) by a stepwise re-duction according eq. (17).[51-52]

$$CH_nX_m + 2e^- + 2H^+ \rightarrow CH_{n+1}X_{m-1} + H^+ + Cl^-$$ (17)

CCl$_4$ and CHCl$_2$ were also explored in our photocatalytic system. CCl$_4$ showed the highest ac-tivity towards CH$_4$ formation of 242 mmol CH$_4$ g$_{CdS}^{-1}$ (entry 5). On the basis of CCl$_4$ a stepwise reductive dehalogenation involves the radical formation of ·CCl$_3$ (eq. (18)) and the ensuing re-action with a proton to generate CHCl$_3$, which is then undergoing the same reaction steps until a complete reduction to CH$_4$ is achieved. The use of the less substituted CH$_2$Cl$_2$ showed the lowest activity (entry 6) compared to higher substituted chloromethanes. The yield of CH$_4$ is decreased in the series of CCl$_4$, CHCl$_3$ and CH$_2$Cl$_2$, which is probably due to the higher stability of the carbon radical the more substituted the carbon atom is. Further, the higher the oxidation state of the carbon atom is, the less it is exposed to oxidative reactions in aqueous medium.[49] Considering a stepwise hydrogenation it should be expected that the less substituted the carbon

28

atom the less reduction steps are required, which should result in the same or higher yields. This justified question could be explained by the proposal that the stepwise reduction starting with an electron transfer occurs so fast while the in situ formed chloromethane is still in a higher vibrational energy state and is more reactive than in its initial state.

$$CCl_4 + e^- \rightarrow \cdot CCl_3 + Cl^- \tag{18}$$

Table 2.2 *Photocatalytic activity of CdS powder suspended in aqueous solution with halogenated compound.[a]*

Entry	Starting material	CH$_4$ [mmol g$_{CdS}^{-1}$]	Yield [%]	Time [h]
1	CHCl$_3$	169	3.3	48
2[b]	CHCl$_3$	127	2.5	17
3[c]	CHCl$_3$	40	0.7	41
4	CHBr$_3$	1.6	0.02	67
5	CCl$_4$	242	5.5	48
6	CH$_2$Cl$_2$	9	0.1	48

[a] Reaction conditions: $\lambda = 455$ nm, 0.1 mg CdS, 2.0 mL aqueous solution of 4 mol L^{-1} NaHCO$_2$ and 50 μL of halogenated compound. [b] Addition of further 50 μL CHCl$_3$ after no more CH$_4$ production was detected. [c] Addition of 0.7 mol L^{-1} NaHCO$_2$.

For investigating the scope of the reaction, halogenated arylenes were tested in the photocatalytic dehalogenation according eq. (19).

$$PhCH_2Hal + e^-(CdS) \rightarrow Ph \cdot CH_2 + Hal^- \tag{19}$$
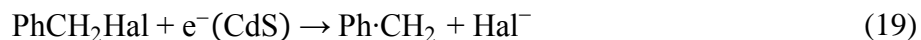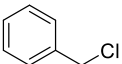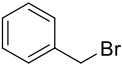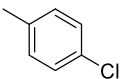
By addition of 50 µl of benzyl chloride to the aqueous suspension of CdS containing NaHCO$_2$, the yield of benzyl chloride to toluene was 21.5% after 24 h irradiation and finally reached 41% after 48 h irradiation (Table 2.3, entry 1). The corresponding NMR in Figure 2.18 indicates a high selective conversion to toluene, since no side products are formed. The use of benzyl bromide resulted in a low yield of 3% (entry 2). Compared to the C-Cl (bond energy = 327 kJ, bond length = 1.76 Å) the C-Br (bond energy = 285 kJ, bond length = 1.91 Å) is a better leaving group[54] so that benzyl formate was also formed as side product by a SN2 reaction. The NMR spectra is shown in Figure 2.19. Dehalogenation of *p*-chlorotoluene to toluene was not observed (entry 3), which is explained by the less stability of phenyl radicals.[55]

Table 2.3   *Yield of toluene by reduction of various halogenated arylenes after 48 h light irradiation.[a]*

Entry	Starting material	Product	Yield [%][b]
1	(benzyl chloride, C₆H₅CH₂Cl)	(toluene)	41
2	(benzyl bromide, C₆H₅CH₂Br)	(toluene)	3
3	(p-chlorotoluene)	(toluene)	0

[a] Reaction conditions: λ = 455 nm, 0.1 mg CdS, 2.0 mL aqueous solution of 4.0 mol L^{-1} NaHCO$_2$ and 50 µL of halogenated starting material. [b] The yield was determined by ^{1}H-NMR integration.
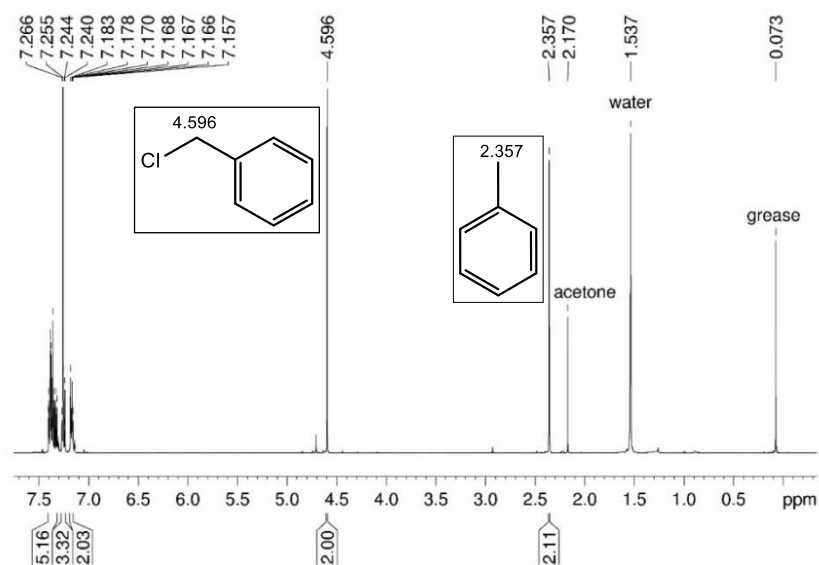
Figure 2.18 *^{1}H NMR spectra reductive dehalogenation of benzyl chloride after 48 h irradiation. Solvent: CDCl$_3$.*
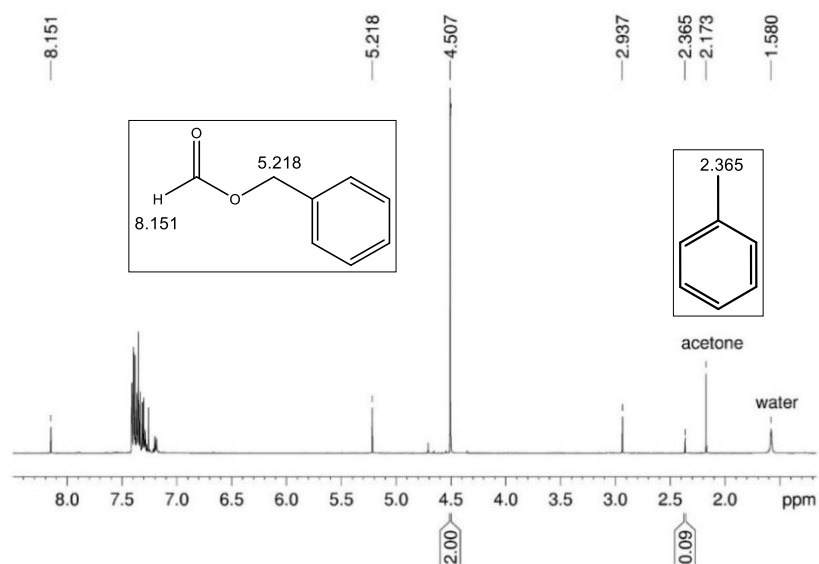
Figure 2.19 *^{1}H NMR spectra of reductive dehalogenation of benzyl bromide after 48 h irradiation. Solvent: CDCl$_3$.*

2.3.3. Conclusion

During the study focusing on photocatalytic CO evolution from aqueous solution of $NaHCO_2$ by CdS powder (chapter 2.2), we coincidentally noticed the release of CH_4 in the presence of chlorinated halomethanes under these reaction conditions. This observation picks up a promising approach to generate CH_4 as future carrier from halomethanes by dehalogenation. In view of ecological aspects the use of chlorinated halomethanes as CH_4 should be preferentially considered since they accumulate in huge amounts of industrial waste contaminants. Nevertheless, the last study in this field was discussed in the late 1980s.

The here presented system based on simplicity and earth-abundant photocatalyst showed already potential in the formation of CH_4 and should continue to be pursuit. The highest evolution of CH_4 was obtained by the addition of 50 μL CCl_4 to the reaction sample, which resulted in 242 mmol CH_4 g_{CdS}^{-1} after 2 d irradiation. For improving the photocatalytic activity further studies should be performed by exploring an alternative SED instead of $NaHCO_2$ for suppressing its competitive reduction to CO, which could increase the conversion rate of halomethanes into CH_4.

2.4.   References

1.   A. Fujishima and K. Honda, *Nature*, **1972**, *238*, 37-38.

2.   K. Maeda and K. Domen, *J. Phys. Chem. Lett.*, **2010**, *1*, 2655-2661.

3.   K. Zhang and L. Guo, *Catal. Sci. Tech.*, **2013**, *3*, 1672-1690.

4.   M. C. Liu, Y. C. Du, L. J. Ma, D. W. Jing and L. J. Guo, *Int. J. Hydrogen Energy*, **2012**, *37*, 730-736.

5.   S. Huang, L. Y., J.-H. Yang and Y. Yu, *ACS Symp. Ser.*, **2013**, *1140*, 219-241.

6.   N. Bao, L. Shen, T. Takata and K. Domen, *Chem. Mater.*, **2008**, *20*, 110-117.

7.   J. Yu, Q. Li, S. Liu and M. Jaroniec, *Chem. Eur. J.*, **2013**, *19*, 2433-2441.

8.   M. Wang, K. Han, S. Zhang and L. Sun, *Coord. Chem. Rev.*, **2015**, *287*, 1-14.

9.   J. Niklas, K. L. Mardis, R. R. Rakhimov, K. L. Mulfort, D. M. Tiede and O. G. Poluektov, *J. Phys. Chem. B*, **2012**, *116*, 2943-2957.

10.   F. Niu, S. Shen, N. Zhang, J. Chen and L. Guo, *Appl. Catal. B*, **2016**, *199*, 134-141.

11.   F. Wen, J. Yang, X. Zong, B. Ma, D. Wang and C. Li, *J. Catal.*, **2011**, *281*, 318-324.

12.   F. Lakadamyaliy, A. Reynal, M. Kato, J. R. Durrant and E. Reisner, *Chem. Eur. J.*, **2012**, *18*, 15464-15475.

13.   F. Lakadamyaliy and E. Reisner, *Chem. Commun.*, **2011**, *47*, 1697-1697.

14.   F. Lakadamyaliy, M. Kato and E. Reisner, *Faraday Discuss.*, **2012**, *155*, 191-205.

15.   J. Huang, K. L. Mulfort, P. Du and C. L. X., *J. Am. Chem. Soc.*, **2012**, *134*, 16472-16475.

16.   S. Cao, Y. Chen, C.-J. Wang, X.-J. Lv and W.-F. Fu, *Chem. Commun.*, **2015**, *51*, 8708-8711.

17.   E. Amouyal and P. Koffi, *J. Photochem.*, **1985**, *29*, 227-242.

18.   M. Grätzel and J. Moser, *J. Proc. Natl. Acad. Sci. U.S.A.*, **1983**, *80*, 3129-3132.

19.   Y. Yamada, T. Miyahigashi, H. Kotani, K. Ohkubo and S. Fukuzumi, *J. Am. Chem. Soc.*, **2011**, *133*, 16136-16145.

20.   W.-Y. Cheng, T.-H. Yu, K.-J. Chao and S.-Y. Lu, *Int. J. Hydrogen Energy*, **2013**, *38*, 9665-9672.

21.   J. Zhang, S. Z. Qiao, L. Qi and J. Yu, *Phys. Chem. Chem. Phys.*, **2013**, *15*, 12088-12094.

22.   X. Wang, M. Liu, Q. Chen, K. Zhang, J. Chen, M. Wang, P. Guo and L. Guo, *Int. J. Hydrogen Energy*, **2013**, *38*, 13091-13096.

23. A. Reinheimer, R. van Eldik and H. Kisch, *J. Phys. Chem. B*, **2000**, *104*, 1014-1024.

24. H. Keck, W. Schindler, F. Knoch and H. Kisch, *Chem. Eur. J.*, **1997**, *3*, 1638-1645.

25. H. Kisch, *Angew. Chem. Int. Ed.*, **2013**, *52*, 812-847.

26. J.-F. Reber and M. Rusek, *J. Phys. Chem.*, **1985**, *90*, 824-834.

27. K. Tsutsumi, N. Kashimura and K. Tabata, *Silicon*, **2015**, *7*, 43-48.

28. Y.-Y. Cai, X.-H. Li, Y.-N. Zhang, X. Wei, K.-X. Wang and J.-S. Chen, *Angew. Chem. Int. Ed.*, **2013**, *52*, 11822-11825.

29. G. Halasi, G. Schubert and F. Solymosi, *J. Phys. Chem. C*, **2012**, *116*, 15396-15405.

30. T. Chen, G. Wu, Z. Feng, G. Hu, W. Su, P. Ying and C. Li, *Chin J. Catal.*, **2008**, *29*, 105-107.

31. G. Halasi, G. Schubert and F. Solymosi, *Catal. Lett.*, **2012**, *142*, 218-223.

32. B. Loges, A. Boddien, H. Junge, J. R. Noyes, W. Baumann and M. Beller, *Chem. Commun.*, **2009**, *45*, 4185-4187.

33. M. F. Kuehnel, D. W. Wakerley, K. L. Orchard and E. Reisner, *Angew. Chem. Int. Ed.* , **2015**, *54*, 9627-9631.

34. E. G. Graeber and D. S. Cryder, *Ind. Eng. Chem. Res.*, **1935**, *27*, 828-831.

35. R. Franke, D. Selent and A. Börner, *Chem. Rev.*, **2012**, *112*, 5675-5732.

36. M. Beller and W. X.-F., *In Transition Metal Catalyzed Carbonylation Reactions*, Springer, Berlin/Heidelberg, **2013**.

37. I. Willner and Z. Goren, *J. Chem. Soc. Chem. Commun.*, **1986**, *2*, 172-173.

38. A. Henglein, *Topics in Current Chemistry*, Springer-Verlag, Berlin, **1988**.

39. A. Henglein, A. Fojtic and H. Weller, *Ber. Bunsen-Ges. Phys. Chem.*, **1987**, *91*, 441-446.

40. A. I. Nedoluzhko, I. A. Shumilin and V. V. Nikandrov, *J. Phys. Chem.*, **1996**, *100*, 17544-17550.

41. M. Kelm, J. Lilie and A. Henglein, *J. Chem. Soc., Faraday Trans. 1*, **1975**, *71*, 1132-1142.

42. A. Henglein, M. Gutierrez, M. Janata and B. G. Ershov, *J. Phys. Chem.*, **1992**, *96*, 4598-4602.

43. K. Hauffe and R. Bender, *Corrosion Handbook*, Wiley-VCH Verlag GmbH & Co. KGaA, **2008**.

44. I. W. F. Davidson, D. D. Sumner and J. C. Parker, *Drug Chem. Toxicol.*, **1982**, *5*, 1-87.

45. C.-Y. Hsiao, C.-L. Lee and D. F. Ollis, *J. Catal.*, **1983**, *82*, 418-423.

46. W. Choi and M. R. Hoffmann, *Environ. Sci. Technol.*, **1997**, *31*, 89-95.

47. C. Kormann, D. W. Bahnemann and M. R. Hoffmann, *Environ. Sci. Technol.*, **1991**, *25*, 494-500.

48. A. L. Pruden and D. F. Ollis, *Environ. Sci. Technol.*, **1983**, *17*, 628-631.

49. P. Calza, C. Minero and E. Pelizzetti, *Environ. Sci. Technol.*, **1997**, *31*, 2198-2203.

50. W. Choi and M. R. Hoffmann, *J. Phys. Chem.*, **1996**, *100*, 2161-2169.

51. C. K. Tan and T. C. Wang, *Environ. Sci. Technol.*, **1987**, *21*, 508-511.

52. T. C. Wang and C. K. Tan, *Environ. Sci. Technol.*, **1988**, *22*, 916-919.

53. J. Bockris, *Comprehensive Treatise of Electrochemistry: Electrochemical Processing*, Springer Science & Business Media, **2013**.

54. F. A. Cotton and G. Wilkinson, *Adv. Inorg. Chem.*, John Wiley & Sons, **1988**.

55. D. Griller and K. U. Ingold, *Acc. Chem. Res.*, **1976**, *9*, 13-19.

3. Task Specific Ionic Liquids as New Organic Photosensitizers

3.1. Synthesis and Characterization

3.1.1. Introduction

Investigation of chromophores used for visible-light sensitization utilized in photocatalysis and in generation of electric power by photovoltaics, is an essential part in research due to the increased interest in sustainable chemical conversions.[1] Metal complexes, usually consists of ruthenium with polypyridine ligands, have been intensively explored as photosensitizer (PS) due to their promising photoelectrochemical properties of their broad absorption bands, high stability of the photoexcited state and long lifetime. PSs based on metal-free organic compounds attracted much interest due to the increase demand of low-cost alternatives.

Metal-free organic PSs are structurally divided into an electron-donating and acceptor-donating moieties separated by a π-conjugated bridge, which are referred to as Donor-π-Acceptor (D-π-A) dyes. The design of the D-π-A structure possess a high diversity in its substructures which enables fine-tuning regarding the chemical and physical properties.

Table 3.1 shows selected examples of moieties to form D-π-A architectures. The donor consist of an electron-rich part, whereas arylamines like triphenylamine, indole or cumarin derivates are particularly suited. They should be sterically hindered and hydrophobic for suppressing agglomeration which results in loose of efficiency. (Poly)thiophenes and vinyl aromatics are proved as π-bridge serving as intramolecular charge transfer between the donor and acceptor moiety. For obtaining a push-pull character the selection of the acceptor part should be a withdrawing group. In applications with TiO_2, which is the most investigated and used semiconductor in light-driven applications, cyano acrylic acid and carboxyl groups are established as anchor group for efficient electron transfer. D-π-A dyes have been established as common PSs in photovoltaic and have not yet been explored in photocatalytic processes for synthesizing organic compounds.

Table 3.1 *Examples of donor, π-bridge and acceptor in D-π-A-type organic dyes.*

Donor	π-bridge	Acceptor

Ionic dyes are less common in photovoltaic and so far limited in structures based on cyanin (**3**) and squaraine (**4**), of which two examples are shown in Figure 3.1. They showed absorption in range of near infrared and visible light with high extinction coefficients of 10^5 L mol^{-1} cm^{-1} but moderate efficiency in conversion of solar power into electrical energy, compared to non-ionic D-π-A dyes.
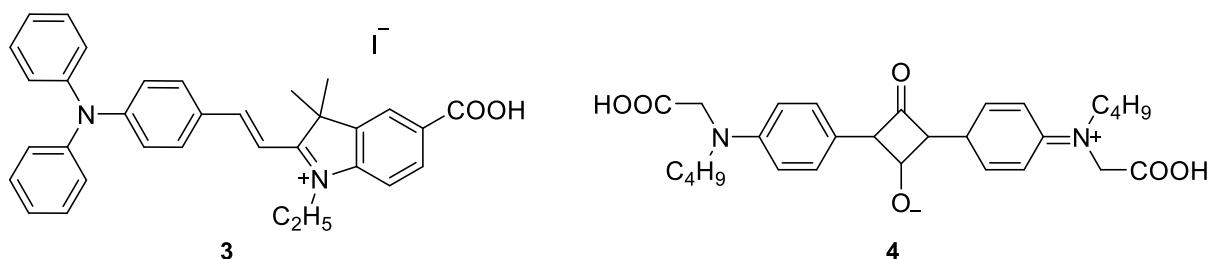
Figure 3.1 *Examples of ionic PSs based on cyanine (3) and squaraine (4).*

In this chapter new ionic PSs (**PS2** and **PS4**, Figure 3.2) were synthesized and characterized in order for their application as potential PS in photochemical reactions. Quaternized imidazolium and pyridinium were chosen as acceptor moiety, which build the most common structure of

ionic liquids (ILs) and extended by linked π-bridge of vinylbenzene or thiophene and triphenyl-amine as donor to give the desired D-π-A structure. They can be seen as task specific ILs. A theoretical background about ILs is given in chapter 4.1.
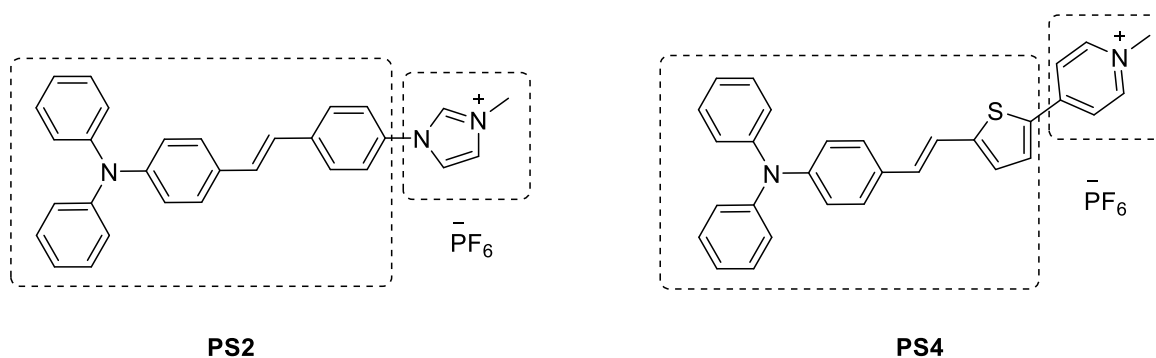
Figure 3.2   *Structure of synthesized D-π-A PSs with an ionic liquid as acceptor moiety.*

An imidazolium moiety in organic chromophores exhibited potential as fluorescent materials due to its aromaticity.[2-4] Shortly after our performed work, Tian *et al.*[5] published a synthesis route for **PS2** that was tested in applications in biomaging since the chromophore shows high quantum yield and long fluorescence lifetime. A structurally similar chromophore based on D-π-A structure (**5**) was studied in fluorescence turn-on senor and proofed as sensor for H_2PO_4 in MeCN and ClO_4^- in H_2O with high selectivity.[6] The chromophore **6** with similar structure to the pyridine-based **PS4** showed in preliminary tests a solar-to-energy conversion efficiency over 5% in DSSCs. A readily adsorption on TiO_2 was achieved by the cyano acrylic acid group.[7]
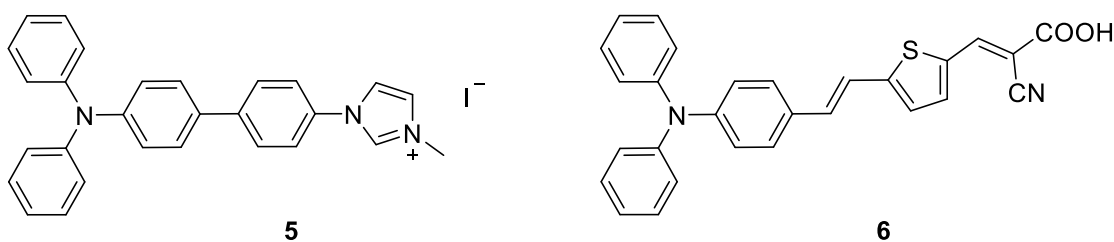
Figure 3.3   *Structure of similar organic chromophores in literature .[6-7]*

3.1.2. Results and Discussion

Synthesis

The basic structure is a D-π-A system consisting of triphenylamine as donor, vinylbenzene (**PS2**) and/or thiophene (**PS4**) as π-bridge and imidazole (**PS2**) and/or pyridine (**PS4**) as acceptor (Figure 3.4). The joint synthesis step is a Heck coupling constituting the π-bridge between the donor and acceptor moiety. The final step of quaterinzation of the N-atom in pyridinium or imidazolium by methylation and anion exchange with [PF₆] as counter anion resulted in the ionic **PS2** as dark yellow and **PS4** as purple solid.
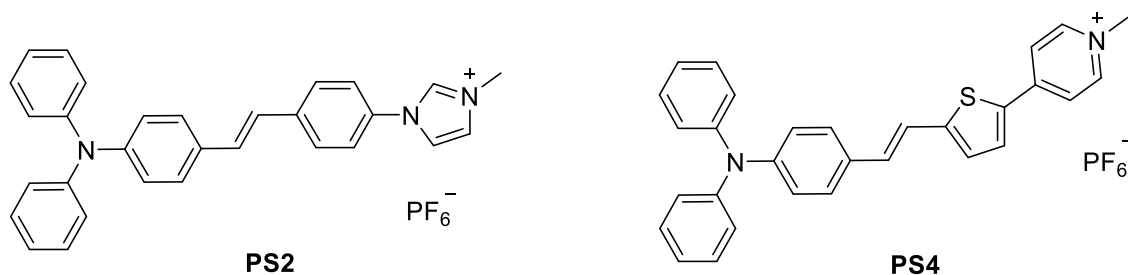
Figure 3.4 *Structure of PS2 and PS4.*

Synthesis of PS2

The synthesis of the imidazolium-based **PS2** started with a copper-catalyzed Ullmann arlyation of 1,4-dibromobenzene (**7**) with imidazole (**8**) to provide compound **10**. After Heck coupling of **10** and *N,N*-diphenyl-4-vinylaniline (**12**), which was synthesized from the commercially available 4-diphenylamino-benzaldehyde (**11**), **PS1** was obtained with a yield of 67%. The methylation by methyl iodide and the following anion exchange of iodide against hexafluorophosphate gave **PS2** in a yield of 98% (Scheme 3.1).
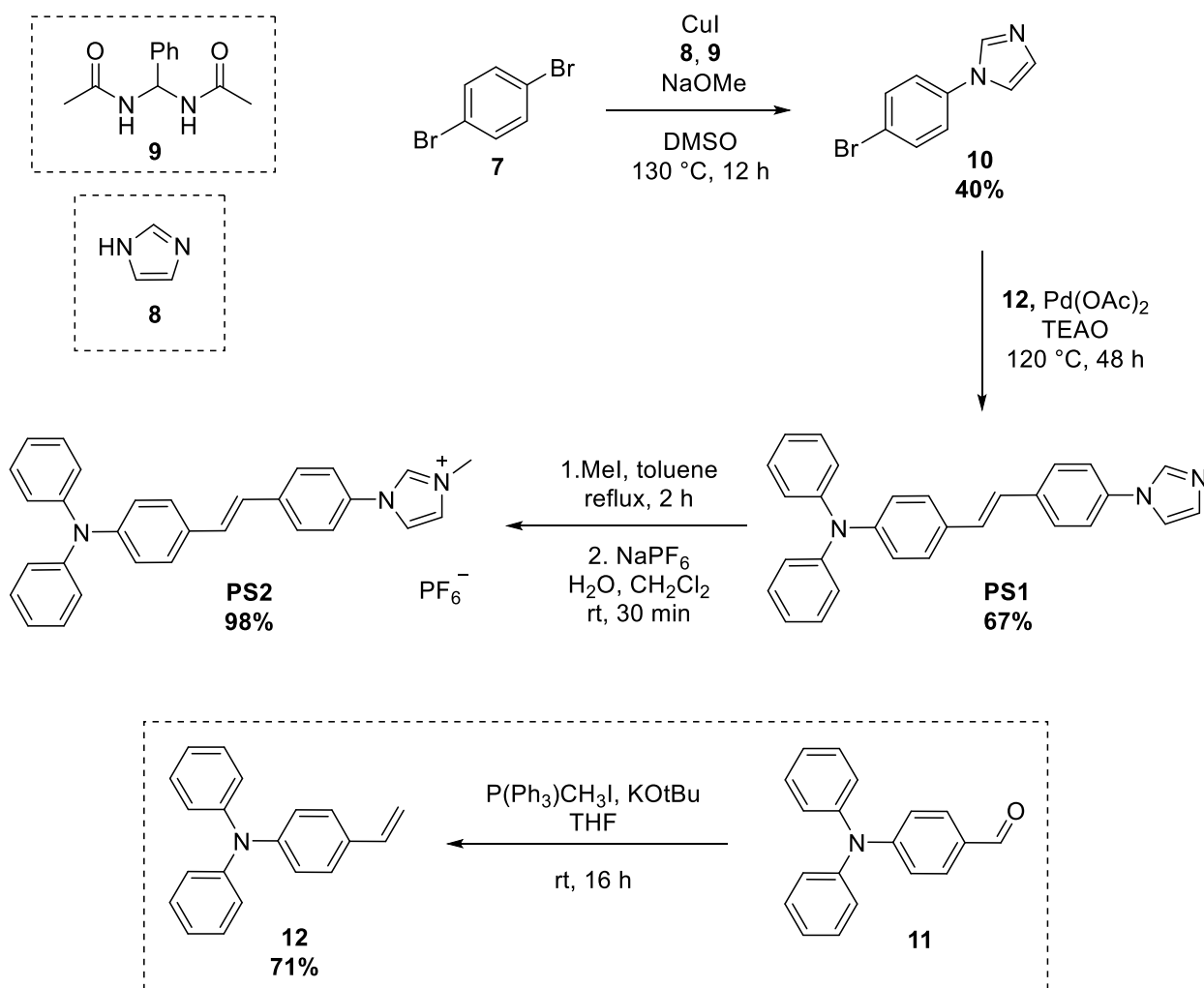
Scheme 3.1   *Synthesis route of organic PSs based on imidazole.*

The chromophore **13** with benzimidazole as acceptor and thiophene as part of the π-bridge was first planned to be synthesized as PS. The synthesis route to the target chromophore was proposed via Heck coupling between triphenylamine (**12**) and fragment **16**, which is framed by the dashed line in Scheme 3.2. Following cyclization by treating it with triethyl orthoformate and sodium hexafluorophosphate should give a benzimidazole moiety, which is a common synthesis strategy for imidazole-based ILs.[8] The fragment **16** was prepared by a Buchwald-Hartwig amination between 2,5-dibromothiophene (**15**) and *N*-methyl-1,2-phenyldiamine (**14**). Different equivalents of Pd₂(dba)₃ as catalyst, (±)-BINAP as ligands and NaOᵗBu as base were explored

according to literature procedures of Buchwald Hartwig amination with similar starting materials.[9-10] The purification of **16** proved difficult and also the yield was less than 10%. The same synthetic difficulties occurred by the use of imidazole (**8**) instead of *N*-methyl-1,2-phenyldiamine (**14**). Control reactions under the same conditions by using model reactions from the literature with the corresponding starting materials resulted in products with similar yields, which excluded synthetic errors on our part. A CuI catalyzed C-N bond formation via an Ullmann-type coupling reaction[11] between imidazole (**8**) and **15** led only to a coupled but debrominated species. A following bromination by N-bromosuccinimide (NBS) was not performed since the addition of bromine would probably take place at the C2 position of the imidazole.
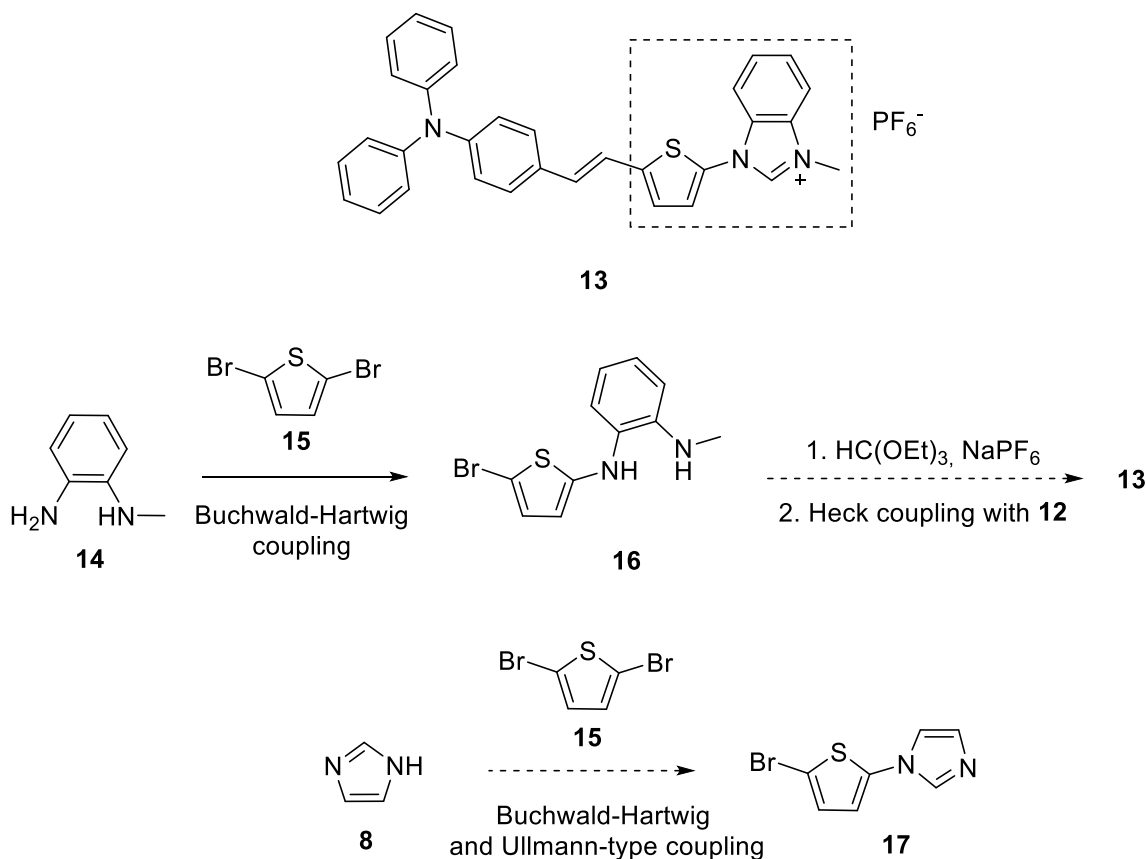
Scheme 3.2   *Structure of the planned chromophore (**13**) and synthesis of the fragments **16** and **17**.*

It has been decided to replace the thiophene against a benzene moiety, which resulted successfully in the synthesis of **PS1** and **PS2** (see synthesis route in Scheme 3.1). An analogue compound to **PS2** but with benzimidazole moiety was not synthesized, since DFT calculations

41

showed that imidazole exhibits no significant difference in UV-Vis absorption behavior compared to benzimidazole as acceptor unit.

Synthesis of PS4

For the synthesis of the pyridine-based **PS4**, compound **18** was coupled with 2-thienylboronic acid (**19**) by Suzuki reaction to give **20**. The latter was brominated by Wohl-Ziegler reaction with NBS at the thiophen unit for providing a following Heck coupling of **21** with **12**. By following quanternization and anion metathesis **PS4** was obtained with a yield of 97% (Scheme 3.3).
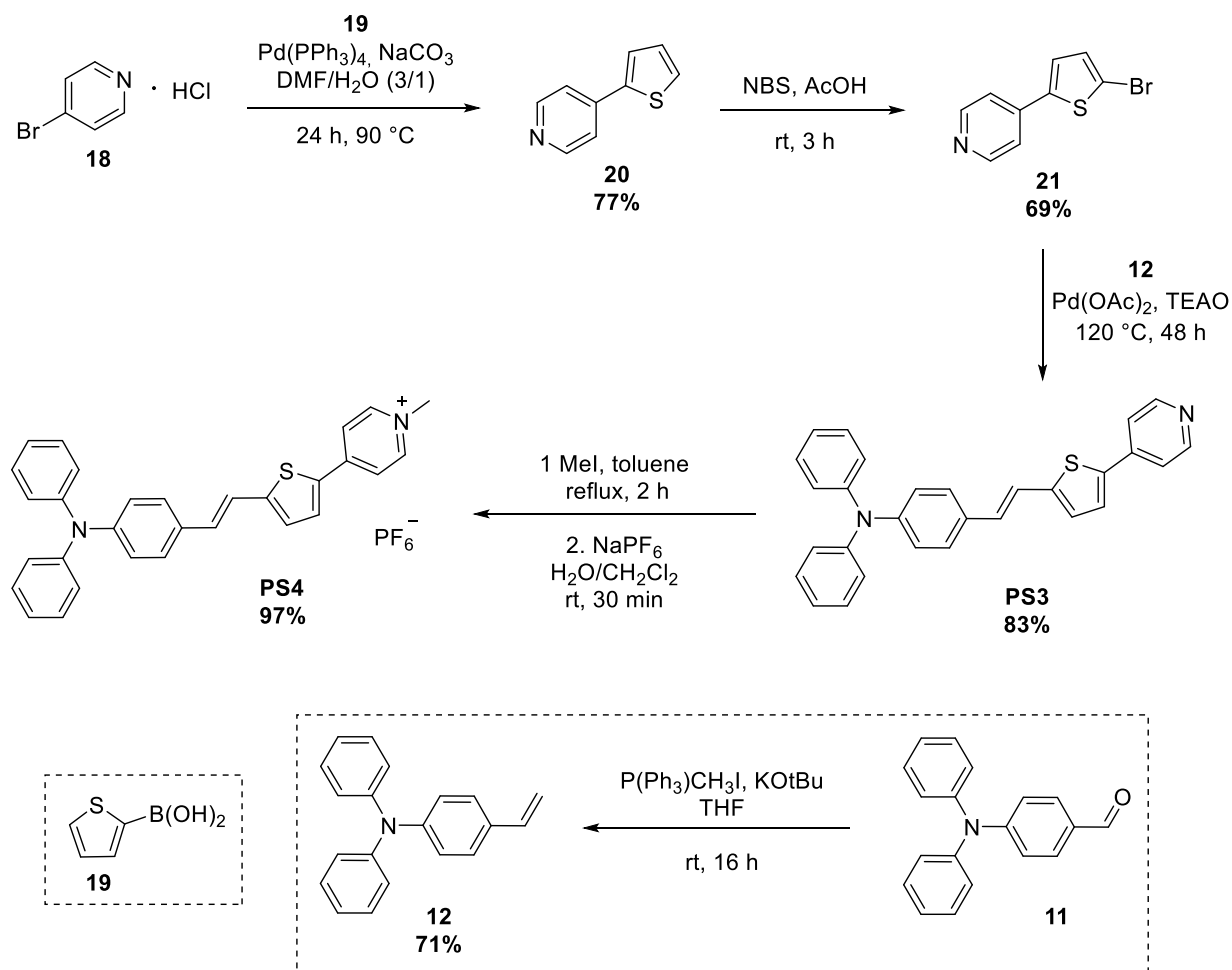
Scheme 3.3 *Synthesis route of organic PSs based on pyridine.*

The planned chromophore based on a pyridine acceptor initially contained a longer π-system by a double thiophene moiety (**28**, Scheme 3.4). The longer the π-bridge the more the photogenerated charges are separated from each other and the recombination is reduced. Further an extension of the π-system affects the light absorption to redshift.[12]
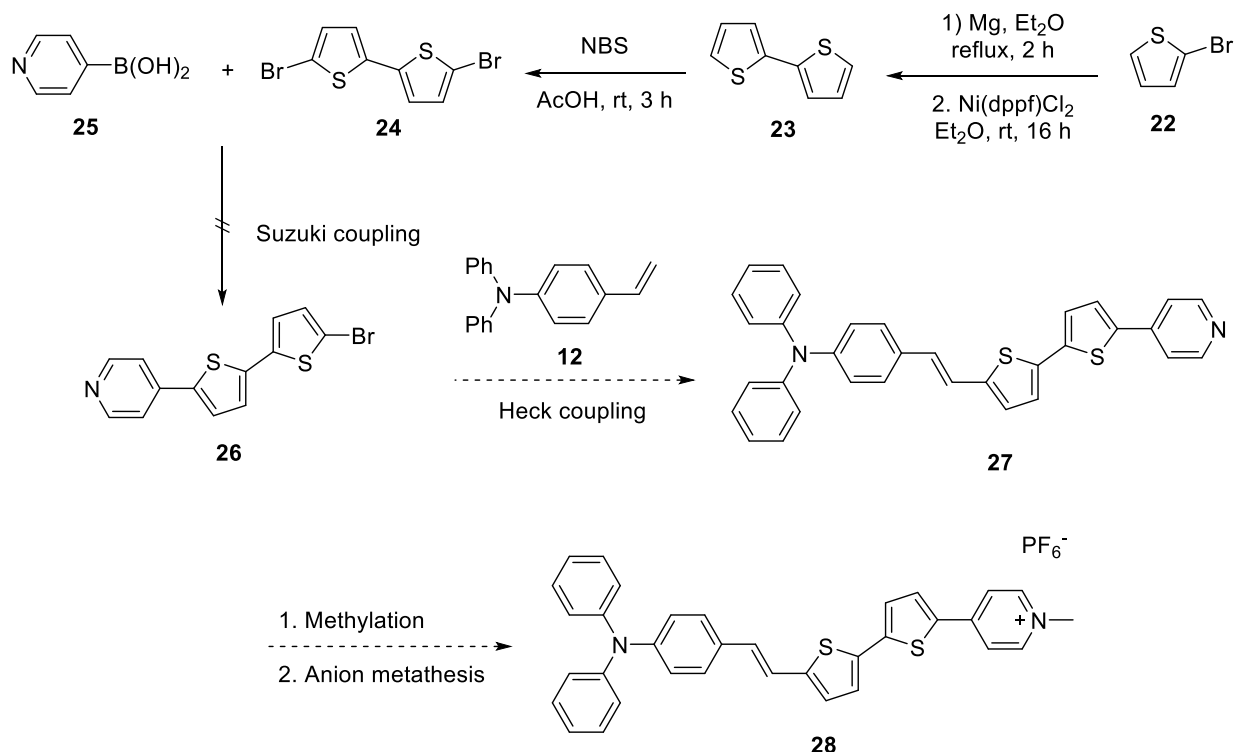
Scheme 3.4 *Planned synthesis route of fragment 28.*

The synthesis route contained a Suzuki coupling between both commercial available compounds **24** and **25** to obtain **26.** A following Heck coupling with **12** should give the neutral chromophore **27** that is transferred in the ionic structure of **28** by methylation and anion metathesis.

The fragment **24** was synthesized by a Grignard reagent of **22** that was linked with a further equivalent by Kumada coupling with Ni(dppf)Cl$_2$ as catalyst.[13] A bromination with NBS yielded the desired fragment **24**, which then should undergo in next step a Suzuki coupling with **25** to form **26**. In the first approach Pd(PPh$_3$)$_4$ as catalyst and Na$_2$CO$_3$ as base[14] did not result in the required fragment **26**. The ^{1}H-NMR showed side reactions and no pyridine group could be overserved. Since reactions with brominated thiophene-based compounds continuously did not result the desired products, the functional groups of bromine and boronic acid, which are required

43

in Suzuki coupling, were exchanged within the starting materials. Thiophen-2-ylboronic acid (**19**) is commercially available and was successfully coupled with 4-bromopyridine hydrochloride (**18**) according to a literature procedure,[15] which gave compound **20**, which was then brominated with NBS for enabling a following Heck coupling[16] with **12**. This resulted in a successfully synthesis of **PS3** and **PS4** (see synthesis route in Scheme 3.3). A brominated species of **19** was not applied in a Suzuki coupling to preclude a polymerization among each thiophene molecules.
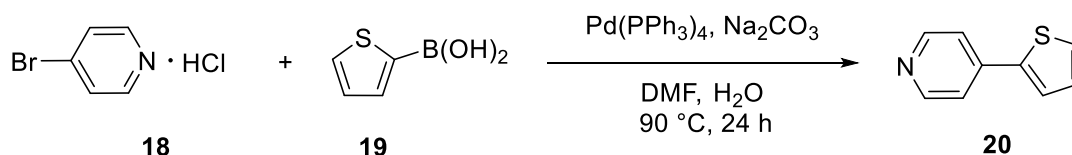
Scheme 3.5   *Synthesis of fragment 20.*[15]

Based on these synthetic observations an extended π-bridge of a doubled thiophene could be realized in further work according the proposed synthesis plan in Scheme 3.6 by Heck coupling between **21** and **7** as key step. The corresponding brominated compound **26** could then applied in the synthesis route proposed in Scheme 3.4 for yielding the previously planned chromophore **28**.
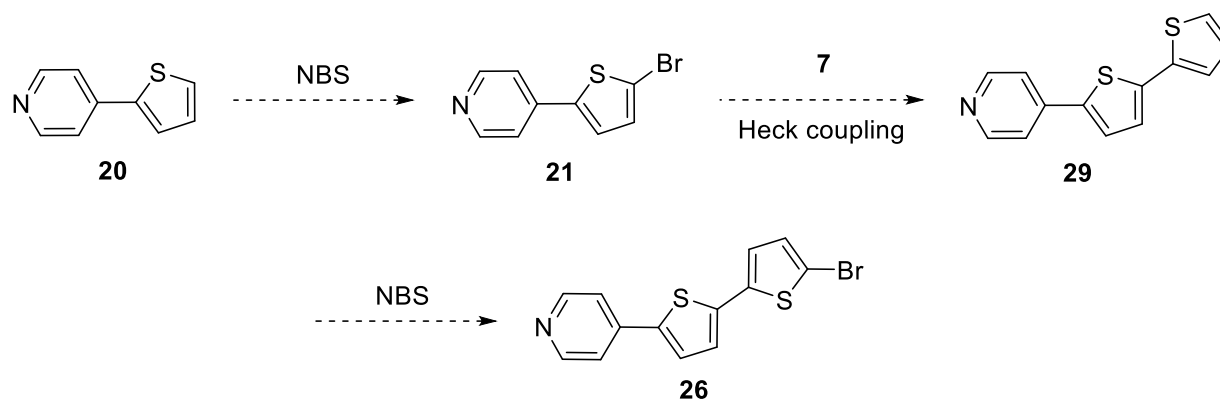
Scheme 3.6   *Proposed synthesis route for fragment 26.*

Characterization of PS1 and PS2

UV-Vis spectra of **PS2** and the non-ionic precursor **PS1** are given in Figure 3.5. **PS2** showed absorption maxima at 390 nm ($\varepsilon = 43701$ L mol^{-1} cm^{-1}) in CH$_2$Cl$_2$ and 368 nm ($\varepsilon = 20342$ L mol^{-1} cm^{-1}) in MeCN. By comparison of **PS1** with absorptions maxima at 377 nm ($\varepsilon = 42378$ L mol^{-1} cm^{-1}) in CH$_2$Cl$_2$ and 370 nm ($\varepsilon = 36093$ L mol^{-1} cm^{-1}) in MeCN, the quaternization of the imidazolium part shows no significant difference in absorption behavior in the visible range, except of the decreased extinction coefficient in MeCN. Unfortunately, only a minor part of the visible light range is covered by the imidazolium-based structures, thus they are not suited as PSs in application with visible light.
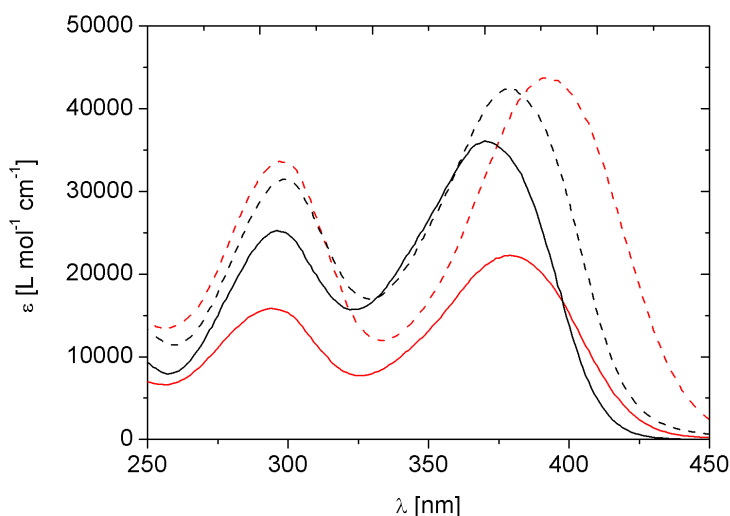
Figure 3.5   *UV-Vis spectra of **PS2** (red line) (c = 2.0·10^{-5} mol L^{-}) and **PS1** (black line) (c = 5.0·10^{-5} mol L^{-1}) in different solvents (MeCN = solid line, CH$_2$Cl$_2$ = dash line).*

CV of **PS2** was employed in a solution of dry CH$_2$Cl$_2$ with 0.2 M Bu$_4$NPF$_6$. The resulting CV is shown in Figure 3.6 in which the potentials are given relative to the redox couple ferrocen/ferrocenium (Fc/Fc$^+$). The measurement resulted in one oxidation peak with E$_{1/2}$ = 0.416 V vs. Fc/Fc$^+$ (ΔE = 90 mV) and implied a reversible oxidation. The corresponding square-wave CV exhibited several irreversible redox waves in the oxidation, since the signal is broad and asymmetrical. For that reason HOMO and LUMO of **PS2** might not be cleary experimentally determined.
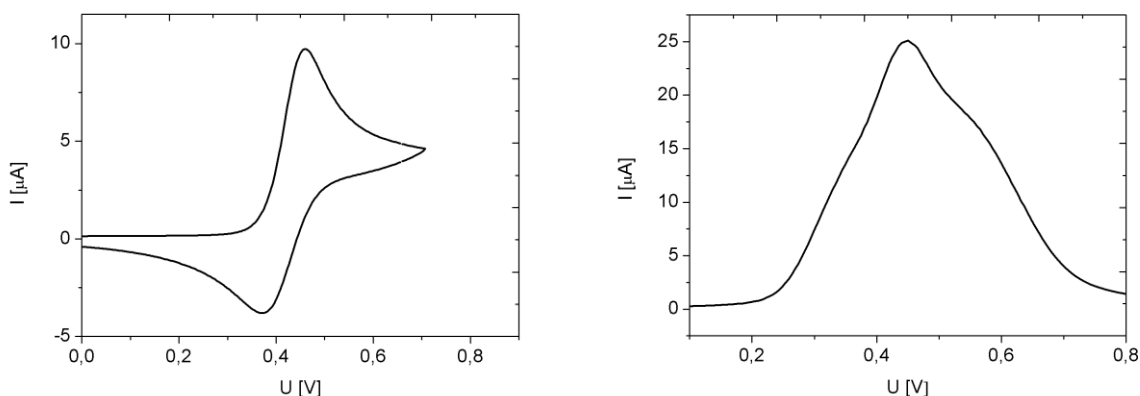
Figure 3.6 *Cyclic voltammetry (CV) of **PS2** [1.0 mmol L^{-1}] in CH_2Cl_2 vs. Fc/Fc$^+$ (0.1 mol L^{-1}) and corresponding cyclic square wave voltammetry (CSWV).*

The theoretically determined energy level by DFT (B3LYP - Correlation Consistent Double Zeta Basis Set) of **PS2** are −2.5 eV for the LUMO and −5.3 eV for the HOMO. Interestingly, the CV measurement provided that the oxidized state of non-ionic **PS1** is irreversible.

Characterization of PS3 and PS4

UV-Vis spectra of the pyridinium-based **PS4** is shown in Figure 3.7 with an absorption maxima at 487 nm (ε = 62823 L mol^{-1} cm^{-1}) in MeCN and 540 nm (ε = 23147 L mol^{-1} cm^{-1}) in CH_2Cl_2. The high extinction in MeCN is advantageous in view of photocatalytic application in aqueous reactions such as in water splitting, in which MeCN is usually used as organic solvent due to the miscibility. In case of heterogeneous applications with semiconductors, the higher the extinction coefficient is, the lower PS concentration is required which results in a lower agglomeration of the PS molecules. The impact by quaternization of the pyridinium is expressed in a significant redshift. The absorption maxima of the non-ionic intermediate **PS3** are 403 nm (ε = 49336 L mol^{-1} cm^{-1}) in MeCN and 411 nm (ε = 32340 L mol^{-1} cm^{-1}) in CH_2Cl_2.

CV of **PS4** was employed in a solution of dry CH_2Cl_2 and is shown in Figure 3.8, in which the potentials are given relative to (Fc/Fc$^+$). The half-wave potential of the oxidation is $E_{1/2}$ = 0.455 V vs. Fc/Fc$^+$ (ΔE = 70 mV) and can be assumed as reversible. A requirement in application as PS in solar cells or photocatalytic procesesss is a stable oxidized state of the PS that is reversibly

46

reducable. The reversibility of the oxidized state of **PS4** might be caused by the quaternization of the pyridine, since the non-ionic **PS3** showed no reversible oxidation behavior.
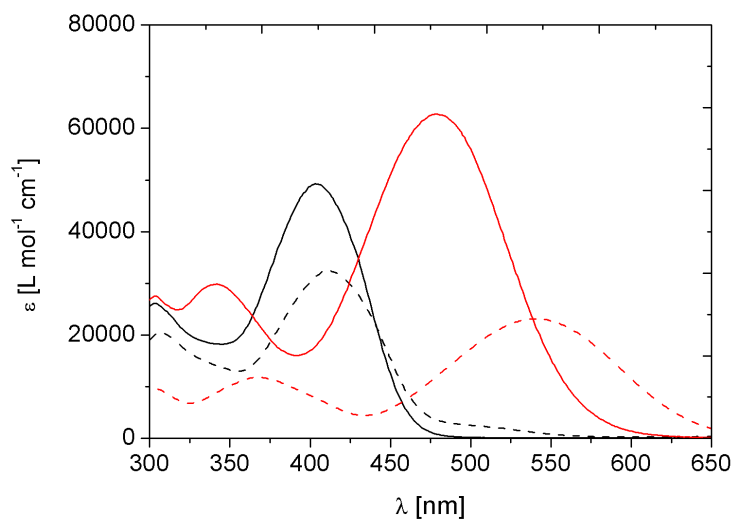

Figure 3.7. *UV-Vis spectra of **PS4** (red line) (c = 2.0·10^{-5} mol L^{-1}) and **PS3** (black line) (c = 5.0·10^{-5} mol L^{-1}) in different solvents (MeCN = solid line, CH$_2$Cl$_2$ = dash line).*
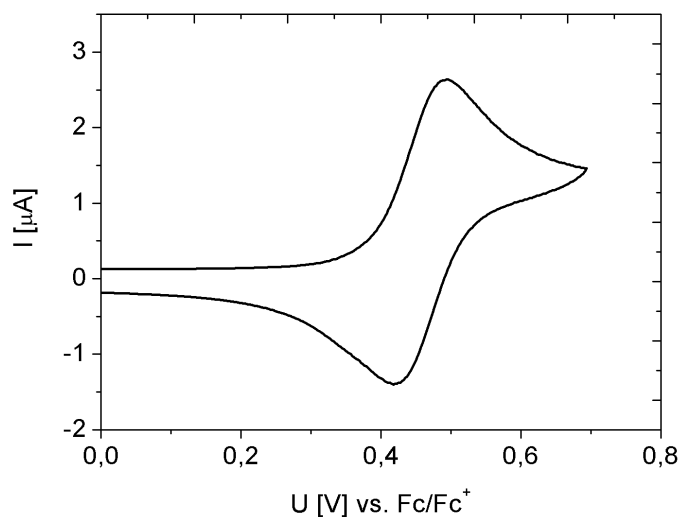
Figure 3.8 *CV of **PS4** (c = 1.0 mmol L^{-1}) in CH$_2$Cl$_2$ vs. Fc/Fc$^+$.*

Density functional theory (DFT) and time dependent density functional theory (TD-DFT) calculations were performed as implemented in Gaussian 09.[17] A localized cc-pVDZ basis set was

used and the electron exchange-correlation energy was modeled using the B3LYP functional. The HOMO-LUMO gap for the gas phase molecule is denoted to 2.23 eV. The HOMO was calculated at -5.48 eV and the LUMO at -3.25 eV with respect to the vacuum level. The frontier molecular orbitals (MOs) of the HOMO and LUMO of **PS4** are shown in Figure 3.9. The HOMO is mainly localized at the donor group, triphenylamine, whereas the LUMO is dominantly situated at the acceptor pyridine. The redistribution of the electron density is the essential characteristic of a push-pull type PS for enabling an efficient intramolecular charge separation. Both MOs also show some charge density at the π-bridge, vinylthiophene. The experimental HOMO/LUMO energy's in CH_2Cl_2 calculated from the half-wave potentials almost agree with the theoretically determined results by DFT (HOMO $= -3.2$ eV, LUMO $= -5.2$ eV). The PS fulfills the requirement of an efficient electron transfer in applications with TiO_2 since the LUMO of the PS is energetically positioned higher than the CB of titanium dioxide. The CB and VB edges of titanium dioxide are in the different modifications (rutile and anatase) at -4.0 eV and $-7.0 - -7.2$ eV in vacuum. Further, in view of the application in DSSCs the energy level of the HOMO is lower than the I_3^-/I_3 redox potential (-4.8 eV vs. vacuum)[18], which is usually used for regeneration of the oxidized PS.
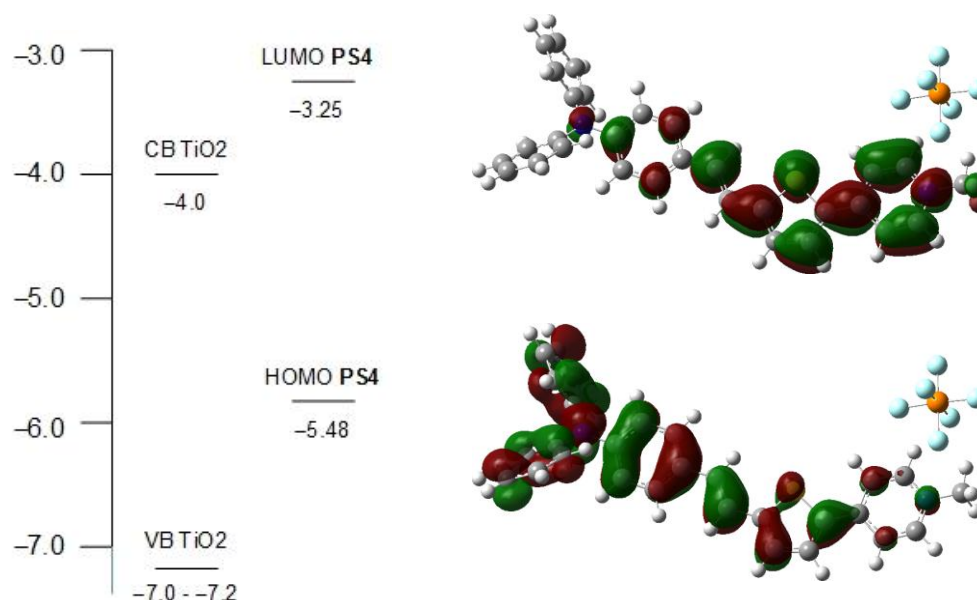
Figure 3.9 *Schematic energy level diagram of **PS4** in relation to TiO_2. Frontier molecular orbitals of the HOMO (bottom) and LUMO (top) of **PS4** are calculated by DFT.*

In order for application with TiO_2, a carboxyl group was attached to the acceptor moiety of pyridine, which resulted in **PS5**. The synthesis was proceeded by esterification of **PS3** with ethyl bromoacetate with following reduction with LiOH to give the carboxyl group. It shows already by UV-Vis measurement a broad absorption band with a remarkably high extinction coefficient of 118854 L mol^{-1} cm^{-1} at $\lambda = 478$ nm in MeOH (Figure 3.10). **PS5** is currently under investigation in our group in photocatalytic H_2 evolution and solar cells.

PS5
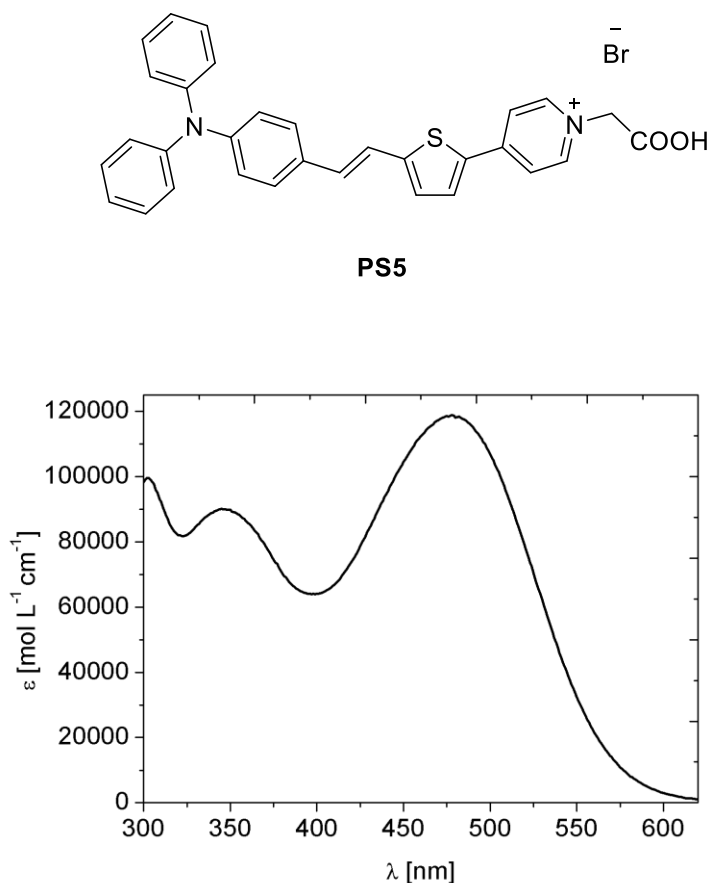
Figure 3.10 *Structure and UV-Vis spectra of **PS5** (c = 1.0·10^{-5} mol L^{-1}) in MeOH.*

3.1.3. Conclusion

Two ionic PSs (**PS2** and **PS4**) with D-π-A structure were synthesised and characterized by UV-Vis spectroscopy and CV. The idea of the structural design was an IL moiety as acceptor extended with chromophoric structure moieties to complete the D-π-A structure. **PS2** with imidazolium as acceptor exhibits poor absorption in the visible range that could be improved by expansion of the π-bridge as outlook. However **PS2** was not further investigated in this work. In contrast, **PS4** with a pyridinium acceptor appears as promising candidate as PS in photochemical reactions and was tested in H_2 evolution, presented in chapter 3.2. Further the structure of **PS4** was extended by an anchor in form of carboxyl group to give **PS5** in order to investigate its performance in photocatalytic applications adsorbed on TiO_2.

The quaternization of the acceptor moiety consisting of imidazole and/or pyridine to give an ionic structure had a positive impact on the electrochemical requirements that have to be fulfilled by a PS. In UV-Vis spectroscopy the impact was expressed in a significant redshift in absorption behavior. CV measurements showed only reversibility in oxidation in case of the ionic PS, while their non-ionic precursors **PS1** and **PS3** exhibited irreversible oxidation. Due to this observed fact, it is recommended to investigate if the efficiency of D-π-A dyes already explored in solar cells and photocatalyis could be improved by the transfer into an ionic structure. Further, the presence of a counter anion offers the possibility for easy tuning of chemical and physical properties by anion metathesis.

3.2. Photocatalytic Hydrogen Evolution

3.2.1. Introduction

Cobaloxime are established as Co(dmg)$_2$–based macrocyclic complexes formed by H-capped (**31**) or BF$_2$-capped (**32**) dimethyl glyoxime (dmg) ligands (Figure 3.11). Chloride and pyridine are in axial positions on the cobalt center and perpendicular to dmg. They were initially studied as model compounds for the active side of the coenzyme vitamin B12.[19] Later by observation of H$_2$ evolution in the presence of a sacrificial electron donor, cobaloximes attracted interest as proton reduction catalysts.[20] A three-component system has been established in photocatalytic proton reduction, consisting of a PS for absorbing light and transferring an electron to a molecular catalyst reducing protons and a SED for regeneration of the oxidized PS. The first cobaloxime reported in photocatalytic water reduction was in 1983 by the use of **30** with [Ru(bpy)$_3$]$^{2+}$ (**1**) as PS for absorbing light and triethanolamine (TEAO) as SED in aqueous medium.[21] Several derivates of cobaloxime have been reported and still explored in H$_2$ evolution.[22]
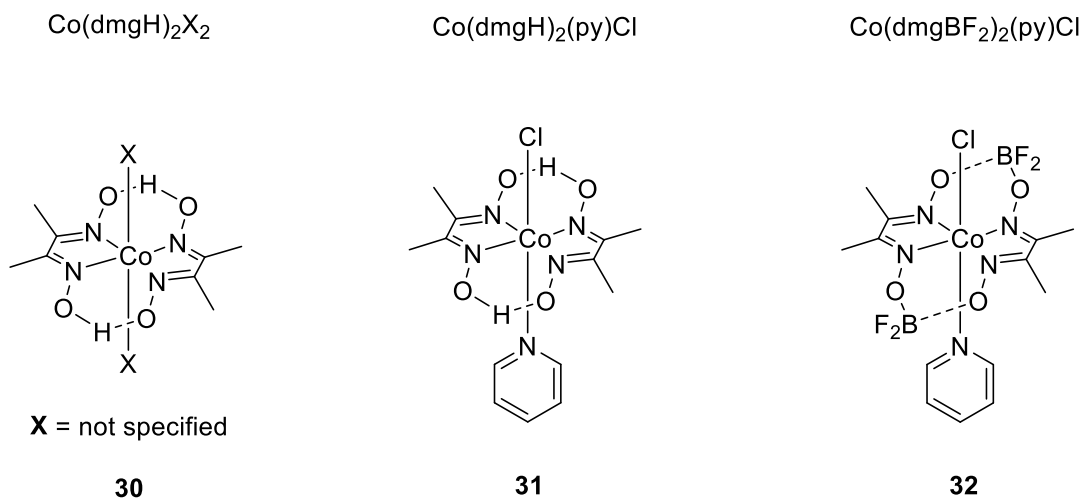
Figure 3.11 *Examples of cobaloximes used in photocatalytic H$_2$ evolution.*

The mechanism of H$_2$ evolution by cobaloxime is shown in a simplified scheme in Figure 3.12. Cobaloxime is reduced to a Co^I complex by electron transfer, which is then reacting with a proton source (H$^+$) to a Co^{III} hydride (Co^{III}H) complex to give the key component in H$_2$ evolution. The elimination of H$_2$ can undergo in a homolytic pathway by reacting of two Co(III) hydrides or in a heterolytic pathway by further protonation of Co^{III}H. However, Co^{III}H can be

further reduced to $Co^{II}H$, from which H_2 is released via analogous homolytic or heterolytic pathway.[22] From a kinetic point of view, the homolytic pathway is favorable and the heterolytic pathway is competitive in case of low catalyst or high acid concentration.[20]
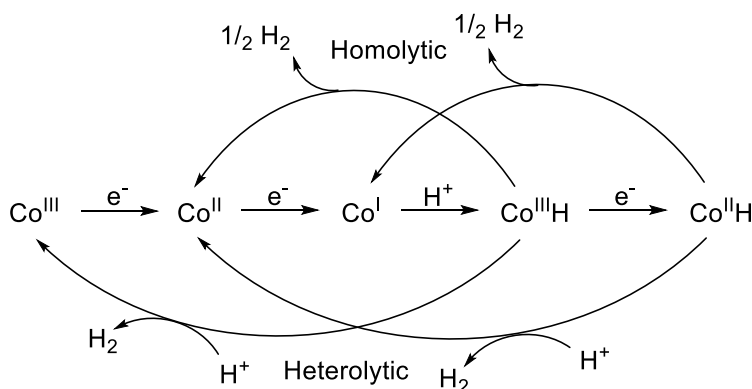

Figure 3.12 *Simplified scheme of the proton reduction mechanism by cobaloxime catalyst.*

Cobaloximes rank to the most studied proton reduction catalysts based on earth-abundant metal due to their simple synthesis and high tolerance against oxygen. The mechanism of H_2 evolution is well understood, so that they are representing an ideal platform for exploring new PSs.[23] Several PSs were investigated in H_2 photocatalysis with cobaloxime which are based on noble metals such as Pt^{24-26}, Ru^{27}, Re^{28-31}, Ir^{32} and recently organic PSs without noble metal. The first homogenous system for photocatalytic reduction of water containing no noble metal PSs was reported by Eisenberg *et al*. in 2009.[33] Hydrogen generation was explored with a photocatalytic system consisting of $(CoIII(dmgH)_2(py)Cl)$ (**2**) as catalyst, Eosin Y (**33**) or Rose Bengal (**34**) as PSs and TEAO as SED. The use of Eosin Y resulted in H_2 production for 5 h with a $TON_{Cat} = 72$ and TON_{PS} of 360. Cobaloximes tend to decompose by losing its diemthylgyloxime ligands. The durability was improved by addition of free $dmgH_2$ finally resulting in a $TON_{Cat} = 180$ and $TON_{PS} = 900$ during 10 h light irradiation. Bengal Rose (**34**) showed similar activities but was decomposed in about 2 h without the addition of $dmgH_2$. In a further report the rhodamine-based PS **35** showed activity with **2** in presence of TEAO, which resulted in a $TON_{Cat} = 51$ and $TON_{PS} = 3737$ after 5 h irradiation. The addition of $dmgH_2$ improved the turn over number up to $TON_{Cat} = 127$ and $TON_{PS} = 9384$ in 24 h.[34]

33 R$_1$ = R$_2$ = Br, R$_3$ = H
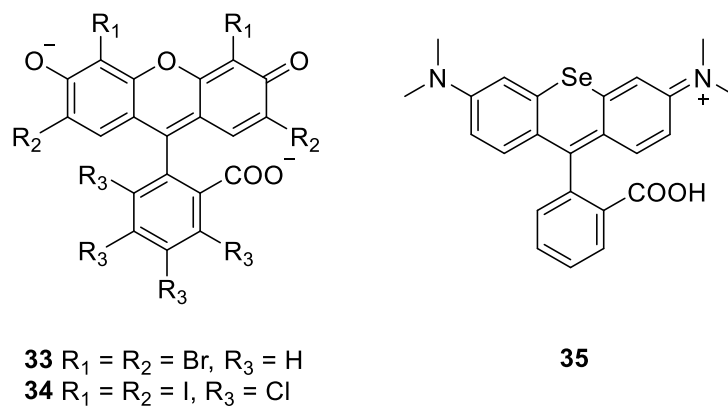**34** R$_1$ = R$_2$ = I, R$_3$ = Cl

35

Figure 3.13 *Noble metal-free PSs showing activity in H$_2$ evolution photocatalysis in systems with cobaloxime.*

36: X = H; R^1 = Me
37: X = BF$_2$; R^1 = Me
38: X = BF$_2$; R^1 = Ph

39

40: R^1 = H ; R^2 = Br
41: R^1 = H ; R^2 = I
42: R^1 = Me; R^2 = Br
43: R^1 = Me ; R^2 = I
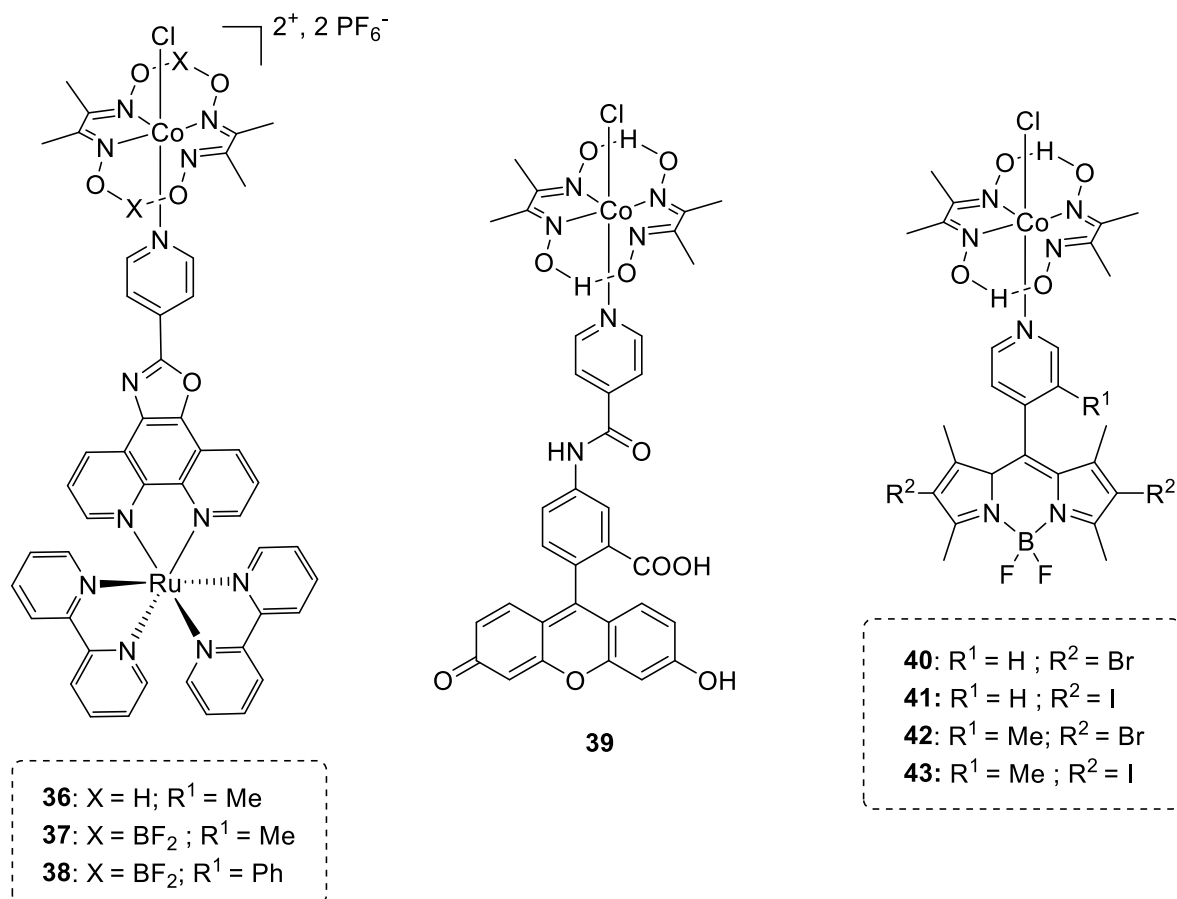
Figure 3.14 *Selected examples of combined-component systems based on cobaloxime and PS evolving photocatalytic H$_2$.*

Combined systems containing both photosensitizing and catalyzing properties in one complex by covalently or coordinatively attachment of PS to the Co center of cobaloxime are studied for enabling fast intramolecular electron transfer. The first complexes based on cobaloxime included ruthenium tris(diimine) moieties (**36** – **38**, Figure 3.14), whereby the highest TON = 103 was yielded with **37** after 15 h irradiation with visible light from a Hg lamp.[35] The systems showed compared to systems containing analogue PSs and catalysts but as separated components marginal increased activity by higher TONs. For example, the analogous iridium complex of **37** produced H_2 with a TON = 210 after 15 h irradiation which is up to date the highest TON that was obtained with a complex based on cobaloxime. The separated component system containing $[Ir(ppy)_2(phen)]^+$ and $[Co(dmgBF_2)_2(OH_2)_2]$ resulted in a TON = 165 after 15 h irradiation.[31]

Reports of combined systems based on earth-abundant metals are so far limited. A linked system of $Co(dmgH)_2(py)Cl$ (**2**) and fluorescein (**39**) with a pyridine moiety connected through an amide linker gave H_2 with a TON = 20 in 24 h, which was increased by the addition of free pyridine to a TON = 31. However, no covalent linkage produced H_2 with a TON = 63 in the same time. A labile pyridine group was assumed as reason for the lower activity by attaching catalyst and PS.[34] The second published complex is based on a linkage between H-capped cobaloxime and different *meso*-pyridyl boron dipyrromethene (BODIPY) (**40** – **43**), of which **43** showed highest activity by producing H_2 with a TON of nearly 31 after 17 h irradiation.[36]

To the best of our knowledge, no report is given about a photocatalytic system evolving H_2 in which a PS of a D-π-A structure commonly found in DSSCs was exploited as well as separated photosensitizing component or incorporated in a complex. In this chapter **PS4** was tested with cobloxime (**2**) as reduction catalyst and TEOA as SED in H_2 evolution. Further, a new system (**SC**) was designed consisting of **2** and the pyridine-based **PS3** and also explored (Figure 3.15).
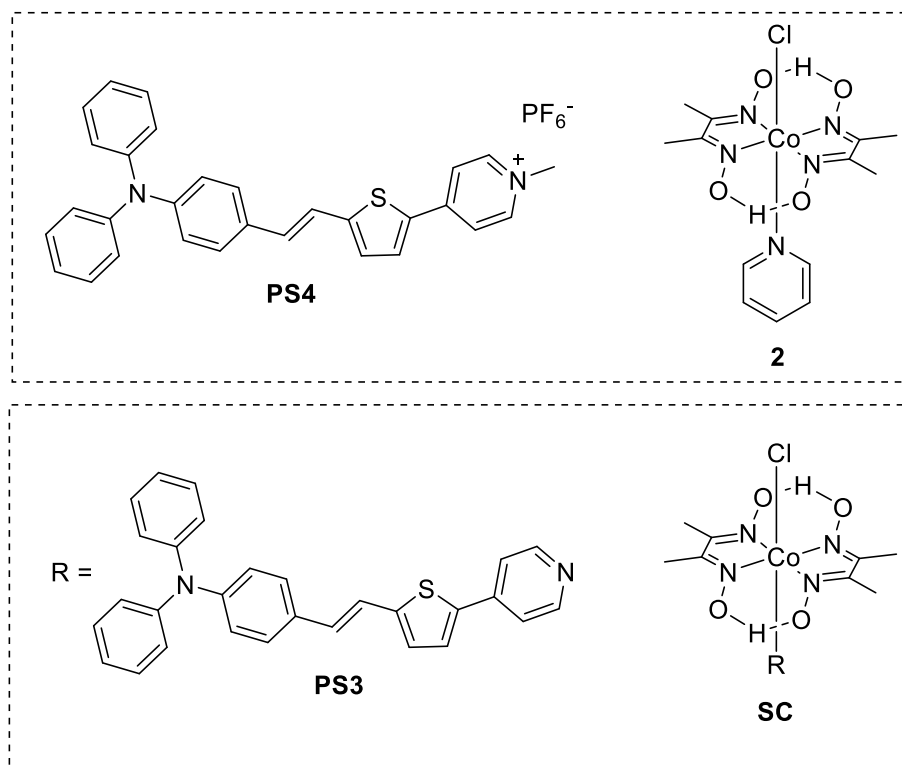
Figure 3.15 *Two photocatalytic systems tested in H$_2$ evolution. Separated system of **PS4** as PS and Co(dmgH)$_2$(py)Cl (**2**) as proton reduction catalyst and combined system in which **PS3** is covalently bounded axial via pyridine to cobaloxime.*

3.2.2.   Results and Discussion

First, the synthesis and characterization of the combined system **SC** is shown in Scheme 3.7 and was performed by complexation between cobaloxime **45** and **PS3** through axially coordinated pyridine with a yield of 68%. Compound **45** was prepared by the reaction of cobalt chloride hexahydrate and dimethylgyloxime (**44**) according literature procedure.[37]
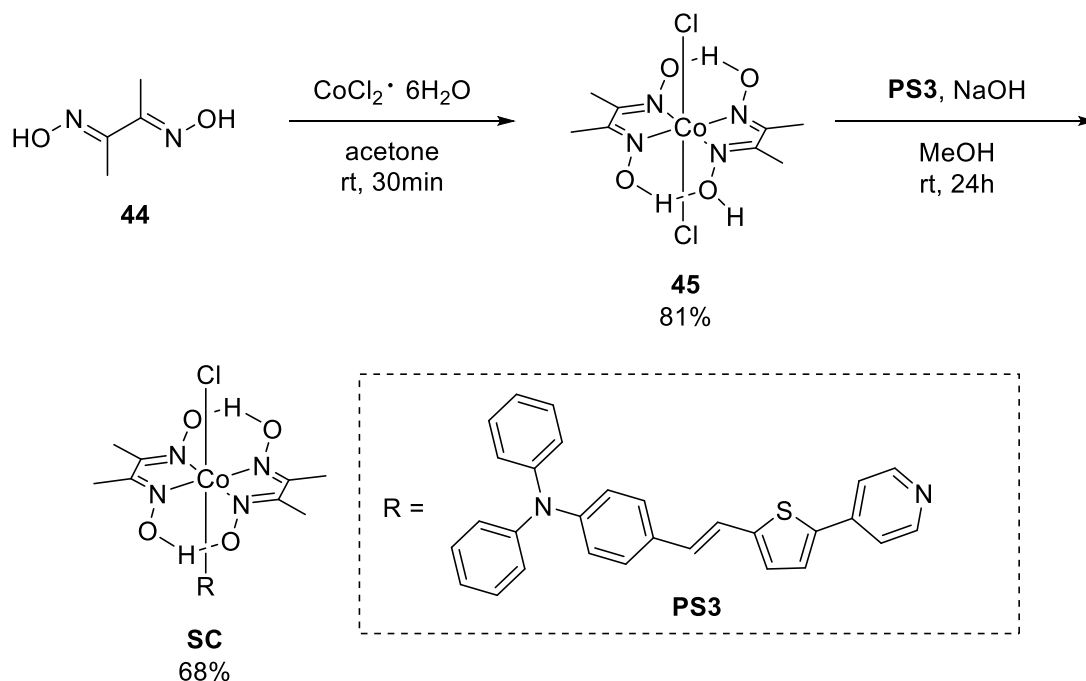
Scheme 3.7   *Synthesis route of SC.*

UV-Vis spectra of **SC** showed a broad absorption in visible range with a maxima at 499 nm (ε = 35473 L mol^{-1} cm^{-1}) in CH$_2$CL$_2$. The CV of **SC** was employed in a solution of dry CH$_2$Cl$_2$ with 0.2 M Bu$_4$NPF$_6$ and showed a reversible oxidation with a half-wave potential at E$_0$ = 0.435 V vs. Fc/Fc$^+$ (ΔE = 80 mV) and can be assumed as reversible (Figure 3.16).

In order to investigate the light-absorption behaviour of **PS4** and the complex **SC** incorporating the light-sensitive part, UV-Vis spectra were recorded of both in a solution of 15% TEOA in H$_2$O/MeCN, representing the conditions of photocatalytic performance. The absorption maximum of **PS4** is blueshifted at 474 nm (ε = 36634 L mol^{-1} cm^{-1}) and showed lower extinction in comparison when pure MeCN is used as solvent (Figure 3.16). The complex **SC** is poorly soluble in MeCN, but showed increased solubility in presence of TEOA, which results in the low exctintion with a maximum of 8229 L mol^{-1} cm^{-1} at 439 nm (Figure 3.17).
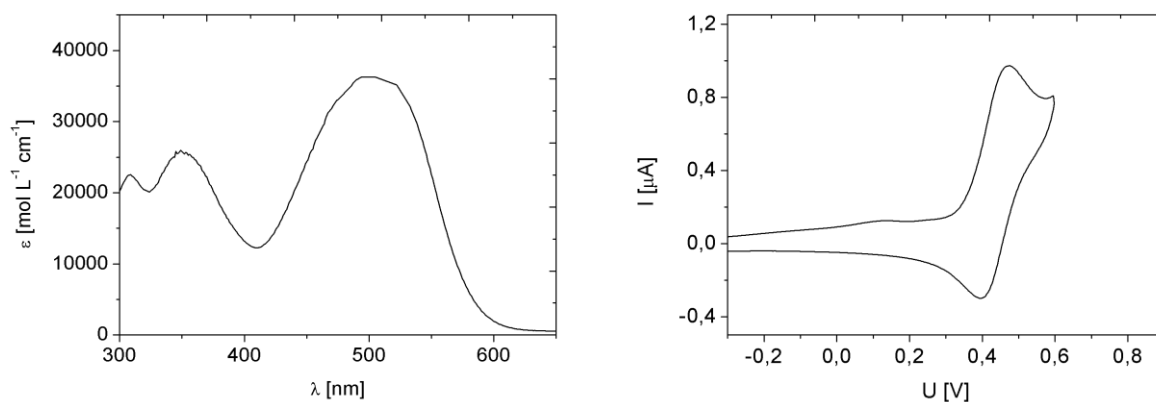
Figure 3.16 *UV-Vis spectra of SC (c =1.0·10^{-5} mol L^{-1}) in CH$_2$Cl$_2$ (left) and CV of SC (c = 1.0 mmol L^{-1}) in CH$_2$Cl$_2$ vs. Fc/Fc$^+$ (right).*
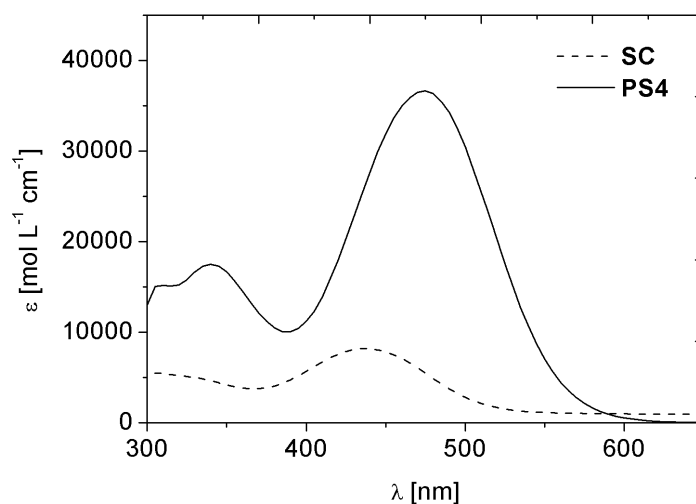
Figure 3.17 *UV-Vis spectra of SC and PS4 (both: c =1.0·10^{-4} mol L^{-1}) in solution of 15% TEOA in H$_2$O/MeCN (1/1).*
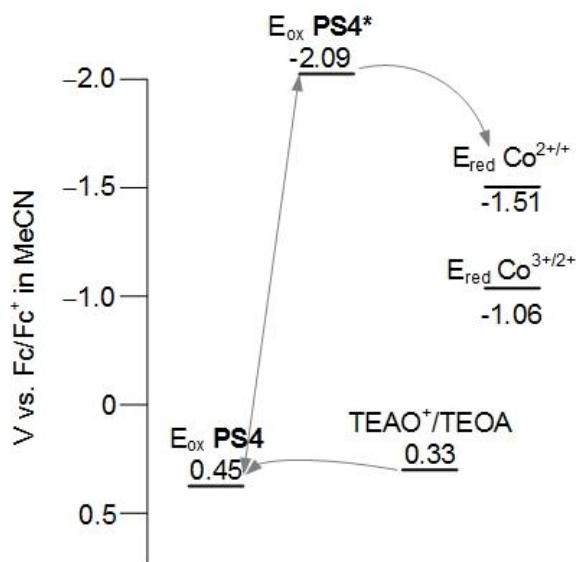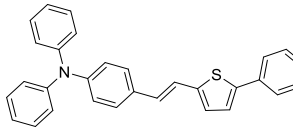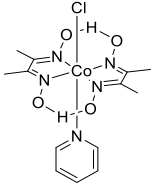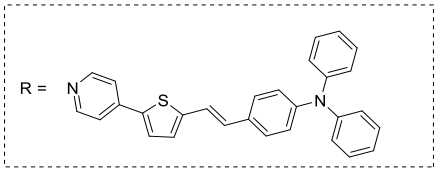
Figure 3.18 *Energy diagram of the ground state and excited state of **PS4**, reduction potential of hydrogen evolving catalyst **2** and oxidation potential of TEAO.*

Figure 3.18 showed the oxidation potentials in ground and excited state of **PS4** among with the reduction potentials of cobaloxime (**2**) utilized as catalyst and oxidation potential of TEOA as sacrifical donor. The redox potentials concluced that an oxidative quenching of the excited **PS4** and regeneration by TEOA is feasible. It should be noted, that only the singlet excited state is considered. The electron transfer can also occur via the triplet state, which can be significantly lower in energy.

Both systems show activity in H_2 evolution, whereby the system of combined PS and catalyst (**SC**) was more active than containing separated components. After 2 d light irradiation 2.8 mmol H_2 g_{CdS}^{-1} were obtained by using **PS4** and **2** as catalyst which corresponds to $TON_{Cat} = 1$ (Table 3.2, entry 1) and $TON_{PS} = 5.6$ In comparison, 9.2 mmol H_2 g_{CdS}^{-1} were achieved with the complex **SC** ($TON_{Cat} = 8$) (entry2).

Table 3.2 *Comparison of H$_2$ generation using separated and combined photocatalytic system after 2d light irradiation.[a]*

Entry	Photocatalytic system	H$_2$ [mmol g$_{cat}^{-1}$]	TON$_{Cat}$
1	**PS4** + **2**	2.8	1
2	R = ... **SC**	9.2	8

[a] Reaction conditions: λ = 455 nm, solution of 15% TEOA in H$_2$O/MeCN (1/1) containing **2** ($5.0 \cdot 10^{-4}$ mol L^{-1}) and **PS4** ($5.5 \cdot 10^{-5}$ mol L^{-1}) (entry 1) or $5.0 \; 10^{-4}$ mol L^{-1} **SC** (entry 2) at pH = 8.3.

Improved activity was achieved by increasing solubility of **SC** by changing the reaction medium. By increasing the part of MeCN with a ratio of 3/1 against H$_2$O, 40 mmol H$_2$ g$_{cat}^{-1}$ were generated, which corresponded a TON$_{Cat}$ = 14.5 (Table 3.3, entry 1). More effectivity was achieved by exchange of H$_2$O against MeOH, which resulted in 79 mmol H$_2$ g$_{cat}^{-1}$ after 2d, finally reaching 342 mmol H$_2$ g$_{CdS}^{-1}$ (TON$_{cat}$ = 122) after almost 9 d light irradation (entry 2). Compared to analogues reported systems,[33,36] in which an organic dye is linked to cobaloxime, the complex **SC** showed higher stability due to the long reaction time of 8.6 d and the fact that the H$_2$ evolution occurred almost linear (Figure 3.19). Interestingly, the use of 10% TEOA in MeCN/MeOH solution provided only 4 mmol H$_2$ g$_{cat}^{-1}$ with a TON$_{Cat}$ = 1.5 (entry 3). The use of triehtylamine (TEA) instead of TEOA resulted in 6.9 mmol, which corresponds to a TON$_{cat}$ = 2.5 after 72 h irradiation (entry 4).
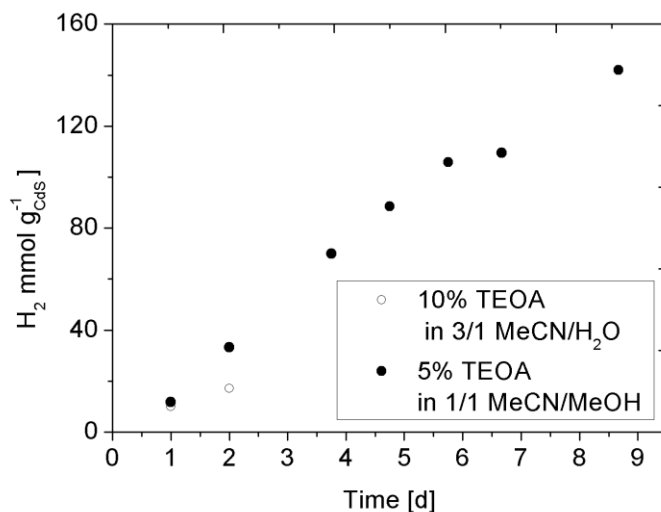
Figure 3.19 *Time course of photocatalytic H_2 generation by using **SC** ($5.0 \cdot 10^{-4}$ mol L^{-1}) in different solvents. [λ = 455 nm, pH = 8.3].*

Table 3.3 *Comparison of photocatalytic H_2 generation using **SC** under different conditions after light irradiation at respective time.[a]*

Entry	t [d]	Reaction conditions	H_2 [mmol g_{cat}^{-1}]	TON_{Cat}
1	2	10% TEOA, MeCN/H_2O (3/1)	40	14.5
2	8.6	5% TEOA, MeCN/MeOH (1/1)	342	122
3	4	10% TEOA, MeCN/H_2O (1/1)	4	1.5
4	3	5% TEA, MeCN/H_2O (1/1)	6.9	2.5

[a] Reaction conditions: λ = 455 nm, **SC** ($5.0 \cdot 10^{-4}$ mol L^{-1}), pH = 8

3.2.3. Conclusion

We are able to demonstrate photocatalytic H_2 evolution with compound **PS4** as PS acting with the proton reduction catalyst cobaloxime (**2**). Further a complex (**SC**) was synthesized, which contains both photosensitizing and catalyzing property in one compound by linkage of cobaloxime with a organic D-π-A dye (**PS3)** as ligand. The combined system has proven high stability and potential in photocatalytic evolving H_2 from a mixture of H_2O/MeOH (1/1) containing 5% TEOA as SED. The activity is expressed in 342 mmol H_2 g_{cat}^{-1}, which corresponds to a TON = 122. This value is much higher than the reached TONs of reported complexes with cobaloxime as proton reduction catalyst linked with organic dyes.[33,36] However the evolution occurs over a long reaction time of 8.6 d, which might be improved in further work.

3.3.   References

1.   A. Mishra, M. K. R. Fischer and P. Bäuerle, *Angew. Chem.*, **2009**, *121*, 2510-2536.

2.   A. J. Boydston, P. D. Vu, O. L. Dykhno, V. Chang, A. R. Wyatt, A. S. Stockett, E. T. Ritschdorff, J. B. Shear and C. W. Bielawski, *J. Am. Chem. Soc.*, **2008**, *130*, 3143-3156.

3.   S. Matsumoto, H. Abe and M. Akazome, *J. Org. Chem.*, **2013**, *78*, 2397-2404.

4.   G. Li, F. Song, D. Wu, J. Lan, X. Liu, J. Wu, S. Yang, D. Xiao and J. You, *Adv. Funct. Mater.*, **2014**, *24*, 747-753.

5.   Y. Zhu, L. Xiao, M. Zhao, J. Zhou, Q. Zhang, H. Wang, S. Li, H. Zhou, J. Wu and Y. Tian, *BioMed Res. Int.*, **2015**, *2015*.

6.   C. Gao, G. Gao, J. Lan and J. You, *Chem. Commun.*, **2014**, *50*, 5623-5625.

7.   T. Edvinsson and D. Hagberg, *Chem. Commun.*, **2006**, *21*, 2245-2247.

8.   C. M. Gordon, M. J. Muldoon, M. Wagner, C. Hilgers, J. H. Davis and P. Wasserscheid, *Ionic Liquids in Synthesis*, Wiley-VCH Verlag GmbH & Co. KGaA, **2008**, pp. 7-55.

9.   J. C. Peters, S. B. Harkins, S. D. Brown and M. W. Day, *Inorg. Chem.*, **2001**, *40*, 5083-5091.

10.   K. Vehlow, S. Maechling and S. Blechert, *Organometallics*, **2006**, *25*, 25-28.

11.   X. Lv, Z. Wang and W. Bao, *Tetrahedron*, **2006**, *62*, 4756-4761.

12.   A. Mishra, M. K. R. Fischer and P. Bäuerle, *Angew. Chem.*, **2009**, *121*, 2510-2536.

13.   C.-Y. Kuo, Y.-C. Huang, C.-Y. Hsiow, Y.-W. Yang, C.-I. Huang, S.-P. Rwei, H.-L. Wang and L. Wang, *Macromolecules*, **2013**, *46*, 5985-5997.

14.   Y.-F. Han, Y.-J. Lin, W.-G. Jia and G.-X. Jin, *Organometallics*, **2008**, *27*, 4088-4097.

15.   Y. Ooyama, S. Inoue, T. Nagano, K. Kushimoto, J. Ohshita, I. Imae, K. Komaguchi and Y. Harima, *Angew. Chem. Int. Ed.*, **2011**, *50*, 7429-7433.

16.   M. Jin, H. Xu, H. Hong, J.-P. Malval, Y. Zhang, A. Ren, D. Wan and H. Pu, *Chem. Commun.*, **2013**, *49*, 8480-8482.

17. M. Frisch, G. Trucks, H. Schlegel, G. Scuseria, M. Robb, J. Cheeseman, G. Scalmani, V. Barone, B. Mennucci and G. Petersson, *Gaussian 09 Revision B01*, Gaussian Inc., Wallingford, CT, **2009**.

18. M. G. Murali, X. Wang, Q. Wang and S. Valiyaveettil, *RSC Adv.*, **2016**, *6*, 57872-57879.

19. G. N. Schrauzer, *Angew. Chem. Int. Ed.*, **1976**, *15*, 417-426.

20. T.-H. Chao and J. H. Espenson, *J. Am. Chem. Soc.*, **1978**, *100*, 129-133.

21. J. Hawecker, J. M. LEHN and R. Ziessel, *Nouv. J. Chim.*, **1983**, *7*, 271-277.

22. J. L. Dempsey, B. S. Brunschwig, J. R. Winkler and H. B. Gray, *Acc. Chem. Res.*, **2009**, *42*, 1995-2004.

23. K. L. Mulfort, *C. R. Chim.*, **2016**, in press.

24. X. H. Wang, S. Goeb, Z. Q. Ji, N. A. Pogulaichenko and F. N. Castellano, *Inorg. Chem.*, **2011**, *50*, 705-707.

25. P. Du, J. Schneider, G. Luo, W. W. Brennessel and R. Eisenberg, *Inorg. Chem.*, **2009**, *48*, 4952-4962.

26. P. Du, K. Knowles and R. Eisenberg, *J. Am. Chem. Soc.*, **2008**, *130*, 12576-12577.

27. J. Hawecker, J. M. Lehn and R. Ziessel, *Nouv. J. Chim.*, **1983**, *7*, 271-277.

28. F. Kanoufi, Y. Zu and A. J. Bard, *J. Phys. Chem. B*, **2001**, *105*, 210-216.

29. B. Probst, A. Rodenberg, M. Guttentag, P. Hamm and R. Alberto, *Inorg. Chem.*, **2010**, *49*, 6453-6460.

30. P.-A. Jacques, V. Artero, J. Pécaut and M. Fontecave, *Proc. Natl. Acad. Sci. USA*, **2009**, *106*, 20627-20632.

31. A. Fihri, V. Artero, A. Pereira and M. Fontecave, *Dalton Trans.*, **2008**, *41*, 5567-5569.

32. P. J. DeLaive, T. K. Foreman, C. Giannotti and D. G. Whitten, *J. Am. Chem. Soc.*, **1980**, *102*, 5627-5631.

33. T. Lazarides, T. McCormick, P. Du, G. Luo, B. Lindley and R. Eisenberg, *J. Am. Chem. Soc.*, **2009**, *131*, 9192-9194.

34.   T. M. McCormick, Z. Han, D. J. Weinberg, W. W. Brennessel, P. L. Holland and R. Eisenberg, *Inorg. Chem.*, **2011**, *50*, 10660-10666.

35.   A. Fihri, V. Artero, M. Razavet, C. Baffert, W. Leibl and M. Fontecave, *Angew. Chem. Int. Ed.*, **2008**, *47*, 564-567.

36.   J. Bartelmess, A. J. Francis, K. A. El Roz, F. N. Castellano, W. W. Weare and R. D. Sommer, *Inorg. Chem.*, **2014**, *53*, 4527-4534.

37.   G. N. Schrauzer, *Inorg. Synth.*, **1968**, *11*, 61-70.

4. Ionic Liquids in Photocatalysis

4.1. Introduction

Ionic liquids (IL(s)) are salts composed of cations and anions, which are per definition liquid below 100 °C.[1] Due to the low melting point they differ to conventional salts like sodium chloride, which have high melting points. Variation of the anion and the cation results in various combinations of ionic liquids with different physical and chemical properties, so they can be used individually, as required. Figure 4.1 show common cations like imidazolium, pyridinium, ammonium, phosphonium and sulfonium and anions including halide, acetate, tetrafluoroborate, hexafluorophosphate, trifluoromethanesulfonate and tris(trifluoromethylsulfonyl)amide. The most researched ionic liquids composed of asymmetric *N,N*-alkylmethylimidazolium cations varied with different anions. Their cationic part is generally abbreviated as [$C_n$mim], whereby [mim] stands for methyl imidazolium and the length of the N-alkyl chain is expressed by the index n.
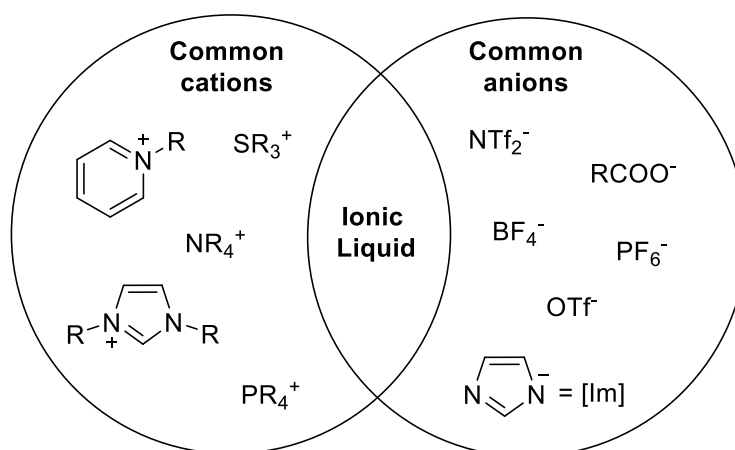
Figure 4.1   *Typically cations and anions in ILs.*

The reason for the low melting point is that the crystal structure forms only weak interactions due to the above average size and low symmetry of the ions. Ionic liquids, for which the lattice energy is overcome at room temperature, are referred as RTILs (Room Temperature Ionic Liquids). In general, the bigger and asymmetric the ions, the lower the melting point. However, if

the ions are too large or contain many aromatic groups, the melting point rises due to van der Waals and/or π-π-interactions.

R–N⁺–N–R X⁻   N⁺–R

R = Alkyl
X = AlCl₄, Al₂Cl₇, etc.

First generation of ionic liquids

R–N⁺–N–R X⁻

R = Alkyl
X = BF₄, PF₆, NTf₂, etc.

Second generation of ionic liquids

R–N⁺–N–FG X⁻

R = Alkyl
Functional group (FG)

OH, OR
COR
NR₂
SH
PR₂
Metal complex
Urea
etc.

Third generation of ionic liquids
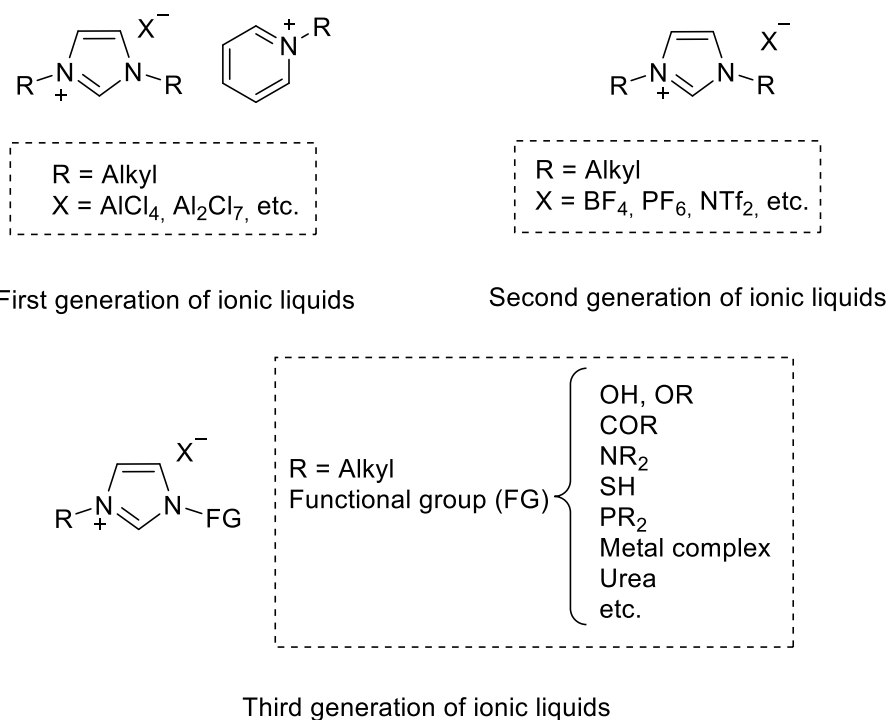
Figure 4.2   *First, second and third generation of ILs.[2]*

The start of the field of ILs was in the year 1914, when WALDEN *et al.* reported a new class of liquids, based on the salt ethylammonium nitrate [EtNH₃][NO₃], which has a melting point below room temperature.[3] Nevertheless no attention was given to the discovery. After World War II a significant breakthrough was achieved with the ascertainment that the melting point of a mixture of 1-ethylpyridinium bromide and AlCl₃ was below room temperature depending on the composition.[4-5] Since this observation, the research of chloroaluminate based ILs has increased, which are known as so-called first generation ILs, in which imidazolium or pyridinium serves as cation. They were mainly studied and used in electrochemical applications. The studies were dominated by U.S. Air Force research, which developed the ILs as electrolytes in batteries. Due to the AlCl₄-anions they are very sensitive to hydrolysis. In subsequent investigations the cations from the first generation were combined with hydrophobic anions such as tetrafluoroborate, hexafluorophosphate and perfluorinated ions like (trifluoromethylsufonyl) imide to form hydrolysis and air-stable ILs, known as the second generation ILs.[6]

In 2004 DAVIS *et al*. introduced the ILs, illustrated in Figure 4.2, in the group of the third generation.[1] In contrast to the first and second generation the cationic scaffolding of the ILs from the third Generation are not functionalized with alkyl groups but with functional groups such as carboxyl-, hydroxyl- and amino groups. Due to their possibility of variation, ionic liquids are common associated with the notion „designer solvents".

ILs received an increased attention since they have extraordinary solvent properties and are particularly suitable for electrochemical processes. They offer a high conductivity (up to 100 mS cm^{-1}) and a large electrochemical window (up to 5.8 V).[2] Further, they a considered as attractive alternatives to organic solvents due to their green properties of extremely low or no vapor pressure and high thermal stability, enabling product recovery and recycling ability.

In this chapter the impact of ILs was examined in photocatalytic H_2 evolution but also in reduction of CO_2 into hydrocarbons on TiO_2 in gas-solid phase.

4.2.   Reduction of Protons

4.2.1.   Introduction

ILs were described as promising mediates in water splitting in breaking hydrogen bridge bonds within the water molecules which result in an increase of the free energy of the water molecules. The reducing step might require less energy input.[3] The change of electronic structure due to the solvent effect of ILs could also have a positive effect in non-photolysis systems in which H_2 is not evolved from water molecules but from a proton source such as TEAO commonly applied as SED. However, no literature example is so far given of ILs promoting water splitting as solvent, which motivated us to this work.

ILs have been widely applied in stabilization and as structure-directing agent in preparation of nanoparticles.[4] TiO_2 in situ modified with imidazolium-based IL during the synthesis extended the absorption of visible light, which affect a higher photocatalytic activity in degradation of dye contaminants in aqueous solution compared to unmodified TiO_2.[5-7] Zhang *et al.* demonstrated an enhanced photocatalytic activity of IL-modified bismuth oxyiodide (BiOI) inhibiting the recombination of photogenerated electron-hole pairs. The IL could trap the photoexcited

67

electron at the CB of BiOI.[7] We investigated the impact of ILs as potential supporting medium under heterogeneous conditions.

4.2.2. Results and Discussion

Ionic Liquids as Solvent under Homogenous Conditions

The hydrophilic IL [C$_4$mim][OTf] (**46**) was tested in H$_2$ evolution as alternative to MeCN, which is usually used as water-miscible solvent in photocatalytic proton reduction. A simple photocatalytic system was selected which consisted the Ru(bpy)$_3$Cl$_2$ (**1**) as PS and cobaloxime (**2**) as catalyst in the presence of TEOA as SED in different ratios of H$_2$O and organic solvent of MeCN or IL (Figure 4.3).
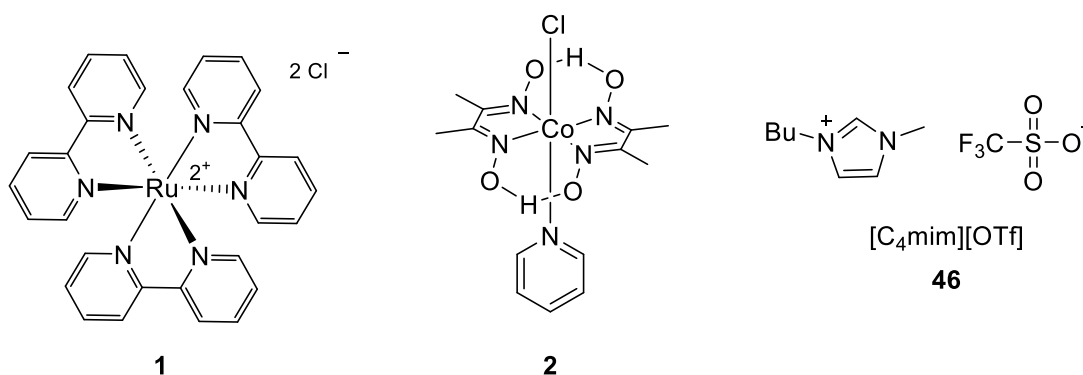
Figure 4.3   *Components used in photocatalytic H$_2$ evolution.*

The comparison of activity expressed in TON respective to the catalyst and PS is summarized in Table 4.1. In a ratio of higher share (entry 1) or equal share (entry 2) of H$_2$O, the IL [C$_4$mim][OTf] had a positive impact on the TON compared to MeCN as organic solvent. However, this is probably due to a higher solubility of the photocatalytic components in [C$_4$mim][OTf] than in MeCN, since by increasing the shares of organic solvents (entry $3 - 5$) the difference in TONs in both is minimal. From a ratio of a double share of organic solvent in relation to H$_2$O (entry 3), there is no significant difference in solubility of the photocatalytic components whether IL or MeCN is used. [C$_4$mim][OTf] provided to be a "green" alternative to MeCN but did not improve the activity in evolving H$_2$ under these performed conditions.

Table 4.1 *Photocatalytic hydrogen evolution with different ratios of H₂O and organic solvent of MeCN or [BMIM][OTf].[a]*

Entry	Ratio H₂O/Organic solvent	[C₄mim][OTf] TON_{Cat}	TON_{PS}	MeCN TON_{Cat}	TON_{PS}
1	2/1	38	153	17	66
2	1/1	96	386	58	231
3	1/2	136	545	140	560
4	1/3	174	696	159	637
5	1/4	197	787	213	837

[a] Reaction conditions: $\lambda = 455$ nm, 0.1 mL solution containing **1** (3.15^{-5} mol L^{-1}) and **2** (1.26^{-4} mol L^{-1}) in respective mixture of H₂O and organic solvent with TEOA (15% v/v) at pH 8.3, t = 24 h.

IL-supported SiO₂

Immobilization of homogenous catalysts on the surface of insoluble materials such as silica gel in order to turn them into heterogeneous ones, enables high local contraction and recycling and reuse ability.[8] The strong interaction ability of silica with molecules containing lipophilic functional groups have been already exploited by creating a photocatalytic system of immobilized silica with amphiphilic metal catalysts in H₂ evolution[9] and O₂ evolution.[10] A further approach is provided by the supported ionic liquid phase (SILP) technology, which means the dissolution of catalytic compounds in a layer of ionic liquid immobilized on a solid carrier material.[10] Inspired by this technology an IL-supported SiO₂ photocatalyst immobilized with amphiphilic **47** as PS and **48** as proton reduction catalyst was prepared and explored in photocatalytic proton reduction. Hydrophobic [C₈mim][PF₆] (**49**) containing an octyl chain as amphiphilic group was used as IL (Figure 4.4).
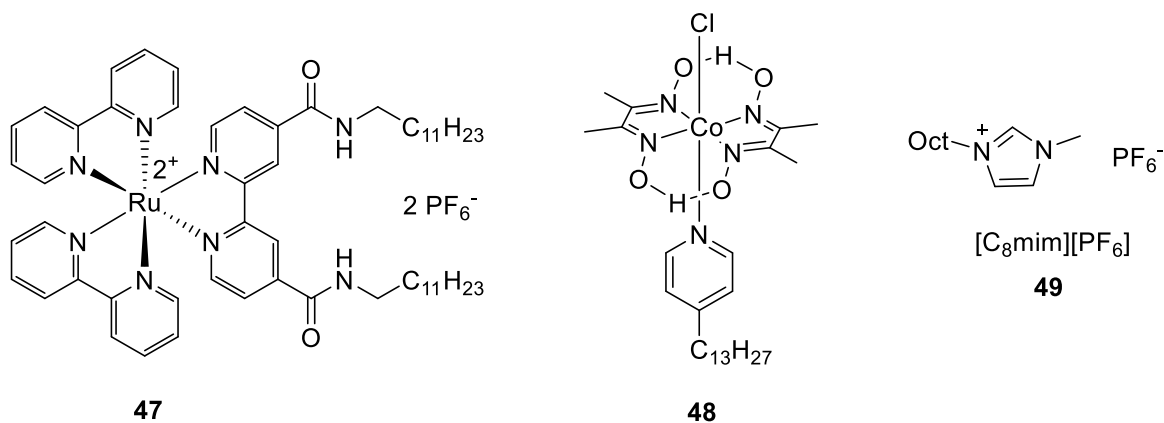
Figure 4.4   *Structures of the amphiphilic PS **47**, proton reduction catalyst **48** and hydro-*
*phobic IL **49** used as photocatalytic components in H_2 evolution.*

SiO_2 immobilized with **47** and **48** but unmodified with IL yielded a $TON_{cat} = 28$ and $TON_{PS} = 110$ in photocatalytic H_2 evolution (Table 4.2, entry 1). In comparison $[C_8mim][PF_6]$-supported SiO_2 led to decreased photocatalytic activity. With increased loading of IL on SiO_2 the TON is dropped steadily, demonstrated in entry 2 and 3.

Table 4.2   *ILs in H_2 evolution with SiO_2.* [a]

Entry	System	µq [C₈mim][PF₆]/mg SiO₂	TON$_{cat}$	TON$_{PS}$
1	SiO$_2$	none	28	110
2	IL-supported-SiO$_2$	12.4 µg/10 mg	18	74
3	IL-supported-SiO$_2$	24.8 µg/10 mg	13	54

[a] Reaction conditions: $\lambda = 455$ nm, 10.0 mg SiO_2 or IL-supported SiO_2 immobilized with **47** ($3.92 \cdot 10^{-5}$ mmol) and **48** ($1.53 \cdot 10^{-4}$ mmol), 1.0 mL solution of H_2O with TEOA (15% v/v) at pH 8.3, t = 24 h.

Ionic Liquid immobilized on Semiconductors

Further experiments were performed with IL-modified TiO_2. UV-irradiation with $\lambda = 365$ of pristine TiO_2 suspended in aqueous TEAO solution showed no H_2 evolution (Table 4.3, entry 1), so that the amphiphilic cobaloxime (**48**) was added as cocatalyst to the reaction solution,

which resulted in a TON = 41 per **48** (entry 3). A control experiment without TiO_2, in which no H_2 was evolved concludes an interaction by electron transfer between **48** and TiO_2 (entry 2). Modified TiO_2 with [C4mim][NTf2] (**50**) resulted in a drop of activity the higher loading of IL on TiO_2 is immobilized (entry 3 – 6).

Table 4.3   *ILs in H_2 evolution with TiO_2 [a]*

Entry	Photocatalyst	μq [C4mim][NTf2]/mg TiO2	TONcob[c]
1[b]	TiO_2	none	-
2	none	none	-
3	TiO_2	none	41
4	IL-supported TiO_2	(4 μg/1 mg)	37
5	IL-supported TiO_2	(6.2 μg/1 mg)	21
6	IL-supported TiO_2	(9 μg/1 mg)	8
7	IL-supported TiO_2	(13.2 μg/1 mg)	7

[a] Reaction conditions: λ = 356 nm, 1.0 mg photocatalyst, 1.0 mL aqueous solution containing **48** ($1.26 \cdot 10^{-4}$ mol L^{-1}) with TEOA (15% v/v) at pH 8.3, t = 24 h. [b] No cobaloxime (**48**). [c] No gas detection is expressed in "-".

[C4mim][Ntf2]

50
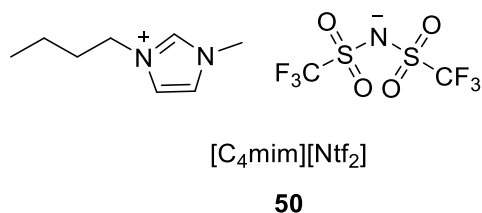
Figure 4.5   *Structure of [C4mim][NTf2].*

Same negative effect was observed with IL-supporting on CdS. While pristine CdS resulted in a TON_{CdS} = 58 (Table 4.4, entry 1), the use of IL-supported CdS led to a decreased TON the more IL is immobilized on the semiconductor (entry 2 and 3). Due to the absence of a proton

source which concludes that the protons originates from water molecules, the impact of hydrophilic [C$_4$mim][OTf] was also tested as solvent in breaking the bonds of H$_2$O for easier reduction. Nevertheless, a suspension of CdS in a mixture of [C$_4$mim][OTf] and H$_2$O in a ratio of 1/4 evolved H$_2$ with a low TON$_{CdS}$ = 2.

Table 4.4   *IL in H$_2$ evolution with CdS.[a]*

Entry	Photocatalyst	μq [C$_4$mim][NTf$_2$]/mg CdS	H$_2$ [mmol g$_{cat}^{-1}$]
1	CdS	none	58
2	IL-supported CdS	(4 μg/1 mg)	11
3	IL-supported CdS	(9 μg/1 mg)	7
4[b]	CdS	none	2

[a] Reaction conditions: λ = 455 nm, 1 mg photocatalyst, 1.0 mL aqueous solution of 0.35 mol L^{-1} Na$_2$S and 0.25 mol L^{-1} Na$_2$SO$_3$, t = 24 h. [b] 1.0 mL mixture of [C$_4$mim][OTf]/H$_2$O in ratio of 1/4.

In our experiments ILs exhibited consistently a negative influence in photocatalytic activity of H$_2$ evolving photocatalysts in both homogenous and heterogeneous conditions. A reason for lower activity could be that the IL is disturbing the charge transfer. Charge transfers from photoexcited TiO$_2$ nanorods to ILs are known[11] but there is no evidence about the transfer of charges in the reverse direction. A mass transfer could also be interrupted due to the increased viscosity of the IL. Examples of semiconductors exhibiting improved activity by modification with imidazolium-based ILs are mainly reported in photocatalytic degradation of the dyes. The increased activity is explained by enhanced separation of photogenerated electrons and holes caused by trapping of electrons by adsorbed C$_x$mim$^+$ ions on semiconductor surface, which is schematically drawn in Figure 4.6. In case of degradation of methylene orange, the adsorption of the negatively charged dye is enhanced by electrostatic attraction between the positively charged imidazolium cation and the methylene orange.[12]
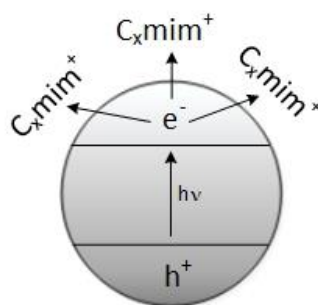
Figure 4.6   *Trapping of photogenerated electrons on the semiconductor surface by imidaz-
olium ([C$_x$mim])-based ILs.*

A recombination is suppressed and the electrons can be consumed in oxidative pathways. In turn the access to the holes is restricted, which suppresses the holes scavenging by the SED. This fact could be the determining factor in dropped activity with ILs, since the SED proved as an essential component in photocatalytic H$_2$ evolution systems with semiconductors. The splitting of water required ongoing supply of electrons per formation of an H$_2$ molecule. Dye degradation in aqueous solution is mainly initiated by OH radicals which are either formed by oxidation of water or reduction of oxygen.[13] This resulted in a radical chain reaction that can provide the degradation of several dye molecules per one triggered ·OH radical molecule. A further explanation for decreased activity could be a restriction of adsorbed protons on the semiconductor surface due to electrostatic repulsion between H$^+$ and the cation of the IL, whereby a reduction to H$_2$ is impeded.

4.2.3.   Conclusion

ILs were investigated in photocatalytic H$_2$ evolution in different approaches. The motivation of the series of experiments was that ILs exhibit a stabilizing effect on the photogenerated electron-hole pairs, which reduced the recombination rate of the charges. The experiments constantly resulted in dropped photoactivity in both under homogenous and heterogeneous conditions. The electrostatic attraction between a photoexcited photocatalyst and the cation of the IL could lead to a restricted access for the sacrificial donor and interrupted contact between photocatalyst and protons due to electrostatic repulsion. Both factors play an essential role in H$_2$ evolution, which

are probably blocked in the presence of ILs in direct contact to the photocatalyst and thus causes reduced activity compared to analogues IL-unmodified systems.

4.3.   Reduction of Carbon Dioxide

4.3.1.   Introduction

The rising interest of the change in the global energy supply to renewable energy provides decisive role in politics and science.[14] Renewable energy sources such as solar and wind are going to be increasingly used as energy supply in the future. Since their profit depends strongly on the weather conditions, it is essential to concentrate on the storage of solar or wind energy in chemical bonds, for later use. The energy, which is in the chemical bonds, mainly C-H, is an efficient way to storage energy. For example the storage density of chemical bonds in methane, which occurs in natural gas, is about one hundred times higher compared to batteries.[15] In order to decrease the rising CO_2 emission and the threatening risk of depletion of fossil fuels,[16] the current global research is increasingly focused to develop an alternative to the burning of fossil fuels. The chemical conversion of CO_2 to hydrocarbons combines for both global challenges a solution.

The reduction by photocatalysts provides the possibility to convert CO_2 in the presence of water vapour under mild conditions by using light (eq. (20)).

$$CO_2 + H_2O \xrightarrow{h\nu} CH_4 + 2O_2 \qquad (20)$$

Many studies in CO_2 photocatalytic reduction have been carried out since the first report in 1979 by Inoue *et al.*[17] However, the conversion to compounds with high value provides still a challenge. Systems generated yields below 10 μmol gcat^{-1} h^{-1}.[18] Among the various studied semiconductors, TiO_2 has proven as one of the most promising semiconductors in the heterogeneous reduction of CO_2.[19-20] TiO_2 is chemically stable, nontoxic, commercial available and also cheap. Due to the wide band gap (3.2 eV for anatase, which corresponds to the absorption of wavelengths < 400 nm) TiO_2 absorbs only 5% of the visible range. Moreover the doping and/or deposition

74

with metals facilitated visible light activity of TiO_2. Reactions were carried out with TiO_2 powder in liquid CO_2[21] or under conditions, in which solid TiO_2 was surrounded by gaseous CO_2 with water vapor.[22-23] But in the most cases TiO_2 was used as dispersion in an aqueous solutions saturated with CO_2.[24-25]

The mechanism pathway of CO_2 reduction to CH_4 over TiO_2 is still not proved and so far discussed in various studies which are commonly related on three proposed radical mechanisms attracting attention although no clear evidence is given.[26-28] The formation of a $\cdot CO_2^-$ anion radical is assumed as initial step in the photoreduction of CO_2.[29] A single-electron reduction of free CO_2 to an anion radical $\cdot CO_2^-$ has an electrochemical potential of 1.9 V vs. NHE (eq. (21)). Virtually no conduction band of any semiconductor, including TiO_2 (−0.5 V vs. NHE), is located at a more negative potential, whereby a required electron transfer onto CO_2 should not be possible.[30] This fact lead to the assumption of an initial activation of the CO_2 molecule which can be facilitated by absorption on semiconductor surfaces.

$$CO_2 + e^- \rightarrow \cdot CO_2^- \tag{21}$$

$$CO_2 + 2H^+ + 2e^- \rightarrow HCO_2H \tag{22}$$

$$CO_2 + 2H^+ + 2e^- \rightarrow CO + H_2O \tag{23}$$

$$CO_2 + 4H^+ + 4e^- \rightarrow HCHO + H_2O \tag{24}$$

$$CO_2 + 6H^+ + 6e^- \rightarrow CH_3OH + H_2O \tag{25}$$

$$CO_2 + 8H^+ + 8e^- \rightarrow CH_4 + 2H_2O \tag{26}$$
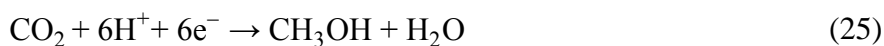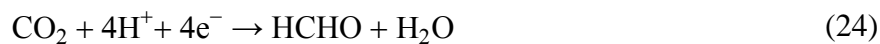
The proposed mechanisms involve C2 molecules such as formic acid, CO, formaldehyde and methanol as intermediates enabled by proton-assisted transfer of multiple electrons which is from a thermodynamics point of view more feasible in application with semiconductors. The electrochemical reduction potentials (vs. NHE) of CO_2 to the various products are summarized in eq. (22 – 26).

This fact lead to the assumption of an initial activation of the CO_2 molecule which can be facilitated by adsorption on semiconductor surfaces. One mechanism also involves the C2 molecule

glyoxal (OHC-CHO) as intermediated, resulted by dimerization of formyl radicals. C2 molecules are considered likely since they are more easily reduced than C1 molecules. However, the discussion about the mechanism is still a debate and recently CH_4 formation including the just mentioned intermediates of glyoxal were excluded by Strunk *et al.*[31] They proposed C2 molecules with methyl groups such as acetic acid and acetaldehyde as intermediates to give CH_4 according eq. (27 – 29).

$$CH_3COOH + h^+ \rightarrow \cdot CH_3 + CO_2 + H^+ \tag{27}$$

$$CH_3CHO + h^+ \rightarrow \cdot CH_3 + CO + H^+ \tag{28}$$

$$\cdot CH_3 + H^+ \rightarrow CH_4 \tag{29}$$
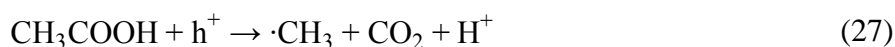
Ionic Liquids in Reduction of Carbon Dioxide

ILs are known to dissolve a high amount of carbon dioxide[32], which could increase the amount of generated methane and higher hydrocarbons. The sorption interaction could result to destabilization of free CO_2 molecule, which would make the formation of $\cdot CO_2^-$ anion radical more favourable.[33] Studies with imidazolium-based ionic liquids towards physical CO_2 sorption showed an enhanced but minimal influence with increased length of the alkyl chain of the imidazolium ring[34] and a major effect with increased fluoroalkyl groups in anions caused by Lewis acid-base interaction[35] between Fluor and CO_2.

Although, the use of ILs in the photocatalytic CO_2 conversion is limited.[36] Wang *et al.*[37] used the CO_2-sorption effect of imidazolium-based ionic liquids combined with a homogeneous photocatalytic system in the conversion of CO_2 to CO and H_2 under visible light irradiation ($\lambda >$ 420 nm). The system was consisted of $[Ru(bpy)_3]Cl_2$ and $CoCl_2$ as PS and catalyst and TEOA as sacrificial electron donor in organic/aqueous medium. By varying of the N-alkyl chain length and different anions they noticed the more viscosity of the ILs is increased, the more the activity in the CO_2 conversion is decreased. As described CO_2 sorption is enhanced with the length of N-alkyl chain, however a high viscosity caused by increased van der Waals interactions the longer the alkyl chain is, could limit rates of mass transfer.[38] Thus ILs of short N-alkyl chain lengths and fluorinated anions, most of which are less viscous[39], had the most positive influence. $[C_2mim][NTf_2]$ resulted as the best ionic liquid in promotion of the CO_2 conversion.

However, ILs are more represented in electrochemical reduction of CO_2.[36] The recently obser-vation was the enhanced yield in the electrocatalytic reduction of CO_2 to CO by TiO_2-passivated InP in [C_2mim][BF_4].[40]

In this chapter the impact of ILs was investigated in the photocataytic reduction of CO_2 in the presence of water vapor over solid TiO_2. A gas-solid phase photoreactor was built in which preliminary experiments were carried out by applying a layer of ILs on the TiO_2.

4.3.2.   Results and Discussion

The reduction of CO_2 into hydrocarbons was performed in a gas-tight photoreactor which was flooded with CO_2 and irradiated with light through a quartz glass. The CO_2 conversion was provided on a silicon wafer coated with TiO_2 and applied with various ILs shown in Figure 4.7.
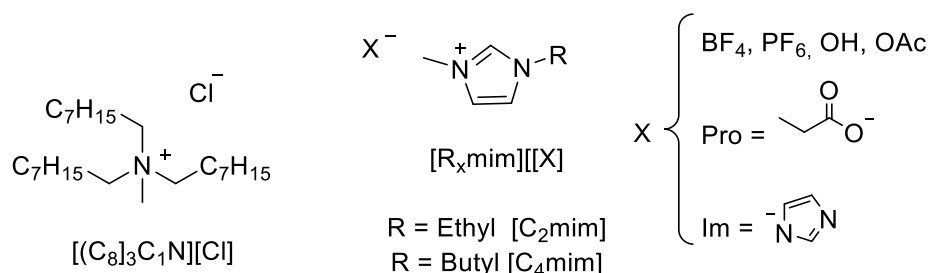
Figure 4.7   *ILs used in photocatalytic conversion of CO_2.*

TiO_2 exists in three modifications: rutile, anatase and brookite. However, the modification of brookite is rare and has no significance. Both, rutile and anatase absorb in the near UV region, the bandgap energy of anatase is 3.2 eV and for rutile 3.0 eV. Although rutile also absorbs some visible light, anatase has proven to be better which is based among others, that in rutile the charges recombine faster than in anatase.[17] Studies have shown that a mixture of mainly anatase and a smaller percentage of rutile shows higher photoacitivity in the photoreduction of CO_2 than the pure crystal modification.[41] The best photoactivity has TiO_2, which is marketed under the trade name Aeroxide ® TiO_2 P25 (Evonik) and led to use in this experiments. According to information from the producer the photocatalyst contained 80 wt% anatase and 20 wt% rutile and exhibit a specific surface area of 50 m^2 g^{-1}, a band gap energy of 3.38 eV and crystallite size of 25 and 54 nm.

The photocatalytic experiments were initially investigated under UV light irradiation due to the wide band gap which corresponds to the absorption of wavelengths < 400 nm. Pure TiO_2 irradiated with UV light for 1 h exclusively provided 2 ppm methane under this experimental conditions (Table 4.5, entry 1). The addition of various ionic liquids on TiO_2 resulted in an increased conversion of CO_2 into methane and also higher hydrocarbons. The use of $[C_2mim][BF_4]$ achieved 56 ppm of CH_4 which is the highest amount of formed methane among the studied ionic liquids under UV irradiation (entry 2). Further 47 ppm of ethane were evolved with $[C_2mim][BF_4]$. The increase of hydrophobicity by an longer alkyl chain at the imidazolium cation by using $[C_4mim][BF_4]$ shows no production of CH_4 but preferred formation of higher hydrocarbons (entry 3). We proposed that the hydrophobic property by a longer N-alkyl chain might lead to lower concentration of water at the surface and thus the combination of the radical intermediates to higher hydrocarbons could probably preferably compared to the deactivation by protons. The presumption that the formation of higher hydrocarbons is positively influenced by an hydrophobic cation, the long chain-based ionic liquid $[(C_8)_3 C_1N][Cl]$ was tested but provided no significant change (entry 4).

Table 4.5   *Evolved amount of hydrocarbons [ppm] in the photoreduction of CO_2 on TiO_2 under UV light by application of various ILs at respective irradiation time.[a]*

Entry	IL	CH$_4$	C$_2$H$_6$	C$_2$H$_4$	C$_3$H$_8$	C$_3$H$_6$
1[b]	none	2	-	-	-	-
2[b]	$[C_2mim][BF_4]$	56	47	-	-	-
3[c]	$[C_4mim][BF_4]$	-	4	16	3	6
4[c]	$[(C_8)_3C_1N][Cl]$	15	2	25	1	8
5[c]	$[C_2mim][PF_6]$	10	6	19	7	4
6[c]	$[C_4mim][Im]$	8	traces	-	-	-

[a] $\lambda = 365$ nm. Not detected gas is expressed by "-". [b] 1 h.
[c] 15 min.

An anion exchange from hydrophilic $[BF_4]$ to hydrophobic $[PF_6]$ showed similar behavior of selectivity in shift towards higher hydrocarbons (entry 5), which emphasizes our hypothesis that

a hydrophobic medium might promote the generation of higher hydrocarbons. Apart from the formation of higher hydrocarbon no increase in evolved amount of the gases is observed, which can be attributed to the fact, that the cation has a higher impact on the selectivity shift than the anion.

Increased pKa of anion lead to higher CO_2 capture[42] such as by formation of C(2) carbene of imidazolate[43] which led to the use of [C$_4$mim][Im]. However, imidazolate as high basic anion led to a drop of hydrocarbons formation (entry 6). This could be due to trapped protons by the high basicity.

It cannot be excluded that the IL is decomposed to hydrocarbons. TiO_2 offers highly oxidative holes in the VB, which may react with ionic liquids. However the photodegradation of ionic liquids on TiO_2 progresses much slower and more enhanced in the presence of the strong oxidizing agents H_2O_2.[44-45] NMR spectra of the irradiated ionic liquid contained no significant difference before and after reaction. Nevertheless in view of the small formed amounts of hydrocarbons in range of ppm, the corresponding low concentration of decomposed ionic liquid is not sensitive enough to be detectable by NMR spectroscopy.

In case of the use of acetate based ionic liquids a degradation was proofed. The intention to explore acetate based ionic liquids was due to their known reversible chemically dissolving of CO_2. The basic acetate abstracts a proton at the C(2) position of the imidazolium ring to form N-heterocyclic carbene, to which CO_2 can be easily binded.[46-48]

An hour UV irradiation of [C$_2$mim][OAc] offers an amount of 2191 ppm methane and 424 ppm ethylene (Table 4.6, entry 1). An irradiation of 15 min received about one quarter of the previously amount of methane and ethylene (entry 2). This was also reflected in the use of [C$_4$mim][OAc] with a longer N-alkyl chain, which offers 245 ppm methane and further higher hydrocarbons after a 15-min UV irradiation (entry 3). The control reaction without CO_2 led to methane concluding that CH_4 is originated from the decomposition of acetate (entry 4). Ethylene is probably formed by recombination of the CH_4 radical intermediates. According to expectations, propionate as anion show a marginal formation of CH_4 but increased formation of decomposed ethane and ethylene that originate from the C(2) alkyl chain of propionate (entry 5 and 6).

Table 4.6   *Generated amount of hydrocarbons [ppm] in the photoreduction of CO_2 on TiO_2 under UV light by application of various ILs at 1h irradiation time.[a]*
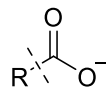
R = Me, Et

Entry	IL	CH$_4$	C$_2$H$_6$	C$_2$H$_4$	C$_2$H$_2$	C$_3$H$_8$	C$_3$H$_6$
1	[C$_2$mim][OAc]	2191	6	424	2	2	1
2[b]	[C$_2$mim][OAc]	593	-	74	1	2	-
3[b]	[C$_4$mim][OAc]	245	16	56	-	22	7
4[b,c]	[C$_2$mim][OAc]	437	-	32	-	-	-
5	[C$_2$mim][Pro]	2	477	82	-	-	-
6	[C$_4$mim][Pro]	10	629	188	-	-	2

[a] λ = 365 nm. Not detected gas is expressed by "-". [b] 15 min.
[c] Without CO_2.

In view of the interest in the use of sunlight as sustainable energy input, further experiments were performed with artificial sunlight by an AM1.5 lamp. For utilizing a broader range of visible light TiO_2 was sensitized with N3 dye (**51**) covalently bounded by the carboxyl groups (structure is shown in Figure 4.8) or a copper layer with a thickness of 4 nm by evaporation. The respective ionic liquid was applied by squeegee. In control experiment no gas evolution was observed by using pure TiO_2 (Table 4.7, entry 1). Copper-sensitized TiO_2 resulted exclusively in 2 ppm CH$_4$ and N3-senzitised showed no gas evolution under this conditions (entry 2 and 3).

51
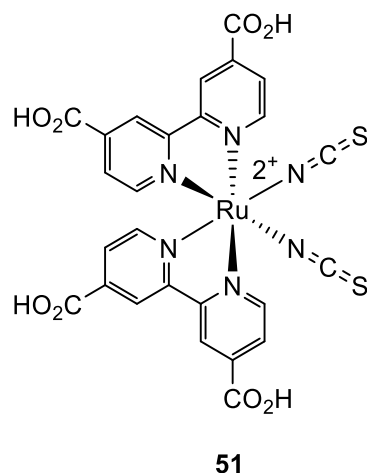
Figure 4.8   *Ruthenium-based N3 dye.*

First, the previously discussed acetate based ionic liquids were tested, since we expected less degradation by irradiation with low-energy light in form of artificial sunlight. Non-sensitized TiO_2 with applied [C_2mim][OAc] resulted in 25 ppm CH_4 and 6 ppm ethylene, which is attributed as degradation product caused by the containing UV light of the artificial sunlight (entry 3). Copper-sensitized TiO_2 gave 79 ppm CH_4, 267 ppm ethylene and traces of propylene and butane (entry 4) and 14 ppm CH_4 was achieved by N3-sensitization (entry 5). A control experiment without CO_2 resulted in no gas evolution (entry 6), which initially confirms that no degradation occurred under artificial sunlight. Nevertheless, it is also possible that a degradation rate of ionic liquids enriched with CO_2 is much faster due to structural change of the molecule. A further argument against degradation is the exclusively formation of CH_4 with [C_4mim][Pro] (entry 8 and 9). In case of degradation, a generation of higher hydrocarbons were expected according to the results obtained by UV-irradiation that resulted in the formation of ethane and ethylene from decomposition of propionate (Table 4.6, entry 5 and 6). The application of ILs of [C_2mim] cation and [BF_4], [PF_6] and [Im] as counter anion resulted in marginal evolution of hydrocarbons under irradiation with artificial sunlight (entry 10 – 16).

Table 4.7   *Generated amount of hydrocarbons [ppm] in the photoreduction of CO_2 on TiO₂ under AM1.5 light by application of various ILs on TiO₂ irradiated for 3 h.[a]*

Entry	IL	Sensitization	CH_4	C_2H_6	C_2H_4	C_2H_2	C_3H_6	C_4H_{10}
1	none	none	-	-	-	-	-	-
2	none	Cu	2	-	-	-	-	-
3	none	N3	-	-	-	-	-	-
4	[C₂mim][OAc]	none	25	-	6	-	-	-
5	[C₂mim][OAc]	Cu	79	-	267	-	traces	1
6	[C₂mim][OAc]	N3	14	-	-	-	-	-
7[b]	[C₂mim][OAc]	Cu	-	-	-	-	-	-
8	[C₂mim][Pro]	none	34	-	-	-	-	-
9	[C₂mim][Pro]	Cu	47	-	-	-	-	-
10	[C₂mim][BF₄]	none	-	-	-	-	-	-
11	[C₂mim][BF₄]	Cu	6	-	12	2	-	-
12	[C₂mim][BF₄]	N3	traces	-	-	-	-	-
13	[C₂mim][PF₆]	none	traces	-	-	-	-	-
14	[C₂mim][PF₆]	Cu	1	-	-	-	-	-
15	[C₂mim][Im]	none	-	2	-	-	-	-
16	[C₂mim][Im]	Cu	6	-	11	-	1	-

[a] Not detected gas is expressed by "-". [b] Without CO_2.

4.3.3. Conclusion

This chapter presents the first application of ILs in photocatalytic CO_2 reduction under heterogeneous conditions on TiO_2. A photoreactor was conceived and built, in which first preliminary experiments were performed. ILs showed the tendency to promote photocatalytic CO_2 reduction towards CH_4 and higher hydrocarbons in gas-solid phase. The catalytic efficiency of TiO_2 in conversion of gases is mainly relied on the gas solid contact, which could be increased by the CO_2 absorption property of ILs. The simple exchange of the ion enabled a high possibility of variation in chemical and physical properties which might lead to the desired hydrocarbon. A shift in selectivity towards higher hydrocarbons could be observed by increased hydrophobicity of the IL under UV irradiation. Nevertheless, the results in evolved amount of hydrocarbons are insignificant and the reproducibility was poor, whereby it is difficult to make a clear statement. As outlook it has to be find a photocatalytic system based on TiO_2 or other semiconductor, which produced already high amounts of hydrocarbons in order to subsequently investigate the impact of ILs

4.4. References

1. J. S. Wilkes, P. Wasserscheid and T. Welton, *Ionic Liquids in Synthesis*, Wiley-VCH Verlag GmbH & Co. KGaA, **2008**, pp. 1-6.

2. A. Winkel, TU Clausthal, *Synthese neuer chiraler ionischer Flüssigkeiten und deren Untersuchung in der chiralen Erkennung*, **2011**.

3. P. Walden, *Bull. Acad. Imper. Sci.*, **1914**, *8*, 405-422.

4. F. H. Hurley and T. P. Wier, *J. Electrochem. Soc.*, **1951**, *98*, 203-206.

5. F. H. Hurley and T. P. WIer, *J. Electrochem. Soc.*, **1951**, *98*, 207-212.

6. J. S. Wilkes and M. J. Zaworotko, *Chem. Commun.*, **1992**, *5*, 965-967.

7. J. H. Davis, James, *Chem. Lett.*, **2004**, *33*, 1072-1077.

8. T. Torimoto, T. Tsuda, K.-i. Okazaki and S. Kuwabata, *Adv. Mater.*, **2010**, *22*, 1196-1221.

9. D. R. MacFarlane, N. Tachikawa, M. Forsyth, J. M. Pringle, P. C. Howlett, G. D. Elliott, J. H. Davis, M. Watanabe, P. Simon and C. A. Angell, *Energy Environ. Sci.*, **2014**, *7*, 232-250.

10. Z. He and P. Alexandridis, *Phys. Chem. Chem. Phys.*, **2015**, *17*, 18238-18261.

11. S. Hu, A. Wang, X. Li, Y. Wang and H. Löwe, *Chem. Asian. J.*, **2010**, *5*, 1171-1177.

12. J. Yu, Q. Li, S. Liu and M. Jaroniec, *Chem. Eur. J.*, **2013**, *19*, 2433-2441.

13. Y. Wang, K. Deng and L. Zhang, *J. Phys. Chem., C*, **2011**, *115*, 14300-14308.

14. A. Kirschning, *Immobilized Cataysts*, Springer Heidelberg, **2004**.

15. C. Bachmann, B. Probst, M. Oberholzer, T. Fox and R. Alberto, *Chem. Sci.*, **2016**, *7*, 436-445.

16. C. Van Doorslaer, J. Wahlen, P. Mertens, K. Binnemans and D. De Vos, *Dalton Trans.*, **2010**, *39*, 8377-8390.

17. E. Binetti, A. Panniello, R. Tommasi, A. Agostiano, S. Fantini, M. L. Curri and M. Striccoli, *J. Phys. Chem. B*, **2012**, **116**, 3512-3518.

18. L. Qi, J. Yu and M. Jaroniec, *Adsorption*, **2013**, *19*, 557-561.

19. A. Ajmal, I. Majeed, R. N. Malik, H. Idriss and M. A. Nadeem, *RSC Adv.*, **2014**, *4*, 37003-37026.

20. R. E. H. Sims, *Sol. Energy*, **2004**, *76*, 9-17.

21. F. Schüth, *forschung*, **2010**, *35*, 50-55.

22. I. S. Nashawi, A. Malallah and M. Al-Bisharah, *Energy Fuels*, **2010**, *24*, 1788-1800.

23. T. Inoue, S. Fujishima, S. Konishi and K. Honda, *Nature*, **1979**, *277*, 637-638.

24. E. V. Kondratenko, G. Mul, J. Baltrusaitis, G. O. Larrazabal and J. Perez-Ramirez, *Energy Environ. Sci.*, **2013**, *6*, 3112-3135.

25. H. W. Slamet, E. Nasution, S. Purnama, J. Kosela and J. Gunlazuardi, *J. Catal. Commun.*, **2005**, *6*, 313-319.

26. Q. H. Zhang, W. D. Han and Y. J. H. G. Yu, *Catal. Today*, **2009**, *148*, 335-340.

27. S. Kaneco, H. Kurimoto, K. Ohta, K. Mizuno and T. Saji, *J. Photochem. Photobiol. A*, **1997**, *109*, 59-63.

28. M. Bellardita, A. Di Paola, E. García-López, V. Loddo, G. Marcì and L. Palmisano, *Curr. Org. Chem.*, **2013**, *17*, 2440-2448.

29. G. Marcì, E. I. García-López and L. Palmisano, *Catal. Commun.*, **2014**, *53*, 38-41.

30. G. R. Dey, A. D. Belapurkar and K. Kishore, *J. Photochem. Photobiol. A*, **2004**, *163*, 503-508.

31. S. Leytner and J. T. Hupp, *Chem. Phys. Lett.*, **2000**, *330*, 231-236.

32. I. A. Shkrob, T. W. Marin, H. He and P. Zapol, *J. Phys. Chem. C*, **2012**, *116*, 9450-9460.

33. K. Ikeue, H. Yamashita, M. Anpo and T. Takewaki, *J. Phys. Chem., B*, **2001**, *105*, 8350-8355.

34.   M. Subrahmanyam, S. Kaneco and N. Alonso-Vante, *Appl. Catal. B*, **1999**, *23*, 169-174.

35.   V. P. Indrakanti, J. D. Kubicki and H. H. Schobert, *Energy Environ. Sci.*, **2009**, *2*, 745-758.

36.   L. Schmidt-Mende, J. K. Stolarczyk and S. N. Habisreutinger, *Angew. Chem. Int. Ed.*, **2013**, *52*, 7372-7408.

37.   A. Pougin, M. Dilla and J. Strunk, *Phys. Chem. Chem. Phys.*, **2016**, *18*, 10809-10817.

38.   X. Zhang, X. Zhang, H. Dong, Z. Zhao, S. Zhang and Y. Huang, *Energy Environ. Sci.*, **2012**, *5*, 6668-6681.

39.   H. J. Freund and M. W. Roberts, *Surf. Sci. Rep.*, **1996**, *25*, 225-273.

40.   D. Almantariotis, T. Gefflaut, A. A. H. Pádua, J. Y. Coxam and M. F. Costa Gomes, *J. Phys. Chem., B*, **2010**, *114*, 3608-3617.

41.   S. G. Kazarian, B. J. Briscoe and T. Welton, *Chem. Commun.*, **2000**, *20*, 2047-2048.

42.   Y. Oh and X. Hu, *Chem. Soc. Rev.*, **2013**, *42*, 2253-2261.

43.   J. Lin, Z. Ding, Y. Hou and X. Wang, *Sci. Rep.*, **2013**, *3*, 1056 -1061.

44.   R. E. Baltus, B. H. Culbertson, S. Dai, H. Luo and D. W. DePaoli, *J. Phys. Chem., B*, **2004**, *108*, 721-727.

45.   H. Xue, R. Verma and J. n. M. Shreeve, *J. Fluor. Chem.*, **2006**, *127*, 159-176.

46.   G. Zeng, J. Qiu, B. Hou, H. Shi, Y. Lin, M. Hettick, A. Javey and S. B. Cronin, *Chem. Eur. J.*, **2015**, *21*, 13502-13507.

47.   K. Koci, L. Obalová and O. Solcová, *Chem. Process. Eng.*, **2010**, *31*, 395-407.

48.   C. Wang, X. Luo, H. Luo, D. Jiang, H. Li and S. Dai, *Angew. Chem. Int. Ed.*, **2011**, *21*, 4918-4922.

49.   Y. Zhang, Z. Wu, S. Chen, P. Yu and Y. Luo, *Chem. Eng. J.*, **2013**, *52*, 6069-6075.

50.   M. Czerwicka, S. Stolte, A. Müller, E. M. Siedlecka, M. Gołębiowski, J. Kumirska and P. Stepnowski, *J. Hazard. Mater.*, **2009**, *171*, 478-483.

51. P. Stepnowski and A. Zaleska, *J. Photochem. Photobiol., A*, **2005**, *170*, 45-50.

52. G. Gurau, H. Rodríguez, S. P. Kelley, P. Janiczek, R. S. Kalb and R. D. Rogers, *Angew. Chem. Int. Ed.*, **2011**, *50*, 12024-12026.

53. M. Besnard, M. I. Cabaço, F. Vaca Chávez, N. Pinaud, P. J. Sebastião, J. A. P. Coutinho, J. Mascetti and Y. Danten, *J. Phys. Chem., A*, **2012**, *116*, 4890-4901.

54. M. B. Shiflett, D. J. Kasprzak, C. P. Junk and A. Yokozeki, *J. Chem. Thermodyn.*, **2008**, *40*, 25-31.

5.   Experimental

5.1.   Experimental Chapter 2

5.1.1.   Instruments, Methods and Materials

Author contributions. Synthesis of CdS, photoreactions and analytics by Dagny Konieczna. Supervision by Prof. Dr. Burkhard König (University of Regensburg) and Prof. Dr. René Wilhelm (University of Paderborn).

Solvents and substrates. The reagents and solvents were purchased from commercial sources (Sigma Aldrich, Alfa Aesar and Acros Organics) and used without purification. CH_2Cl_2, THF and toluene were purified by distillation.

NMR spectroscopy. ^{1}H- and ^{13}C-NMR spectra were recorded at 500 MHz on a BRUKER Advance 500 and at 300 MHz at a BRUKER Advance 300. The measurement of the substances were performed in $CDCl_3$ (99.8%, DEUTERO). Chemical shifts δ are expressed in ppm.

Spectroscopy. ESI (electrospray ionization mass spectra were recorded using double-focussing sectorfield-MS DFS from Thermo Scientific. UV-Vis spectroscopy were performed with Varian Cary 50 UV-Vis spectrophotometer. The measurements were performed at room temperature in 10 mm Hellma quartz cuvettes. IR spectra were acquired on an FT-IR-spectrometer Vertex from BRUKER. The solids were measured as KBr pellets. The DRS spectra ($BaSO_4$ pellets) were measured with OMEGA 20 spectrophotometer with an integration of sphere module. The transmission measurements were conducted with a fiber optic spectrometer (USB200-Vis-NIR-ES from Ocean Optics). Krypton (ecoVis, Ocean Optics) was used as light source (400-2500 nm) equipped with a built-in cuvette holder.

Scanning Electron Microscopy. SEM images were recorded using a Zeiss Neon 40" scanning electron microscope equipped with an energy dispersive X-ray (EDX) detector.
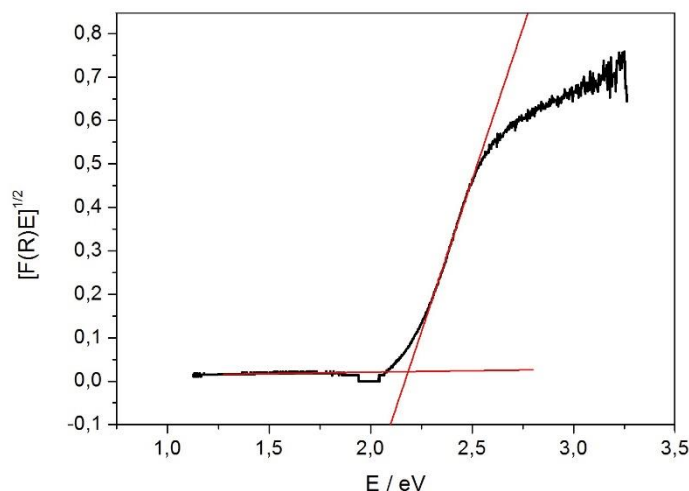
Figure 5.1   *DRS spectra of CdS transformed by Kubelka Munk function.*[1]

Cyclo voltammetry. CV and SWV were recorded at room temperature with a Metronohm-Autolab potentiostat PGSTAT 101 in a solution of CH_2Cl_2/0.2 M Bu_4NPF_6 and with a concentration of test substance of 1 M. All measurements was carried out under argon and in dry and degassed solvents with Pt as working electrode, Ag/0.01 M $AgNO_3$/MeCN as reference electrode and Pt as counter electrode. The potentials were given relative to redox couple ferrocene/ferrocenium (Fc/Fc$^+$) as an internal standard. The CV curves were calibrated using the Fc/Fc$^+$ redox couple as an external standard. The half-wave potential $E_{1/2}$ was estimated from eq. (30).

$$E_{1/2} = \left[\frac{E_{red} + E_{ox}}{2} \right] \ eV$$

(30)

with: E_{red} = Peak potential of reduction

       E_{ox} = Peak potential of oxidation

Nitrogen physiosorption. Measurements at 77 K were performed by a Quantachrome NOVA 4000. The samples were degassed at 120 °C for 24 h.

Powder X-ray diffraction. P-XRD was carried out on a Bruker AXS D8 Advance diffractometer with a secondary monochromator by using Cu-Kα radiation (40 kV, 40 mA). The average

crystallite size of CdS particles was estimated by application of Scherrer equation[2] on the XRD pattern according eq. (31)).

$$\text{size}_{\text{cryst}} = \frac{K \cdot \lambda}{\text{FWHM} \cdot \cos\theta}$$

(31)

with: K = Scherer constant (0 0.94)

   λ = Wavelength of x-ray radiation (0.154 nm)

   FWHM = Full width at half maximum of the peak

   θ = Angle of diffraction

Dynamic light scattering. DLS measurements were carried out on a Malvern Zetasizer Nano-ZS. The average particle size was calculated from the mean of triplicate (Figure 5.2).
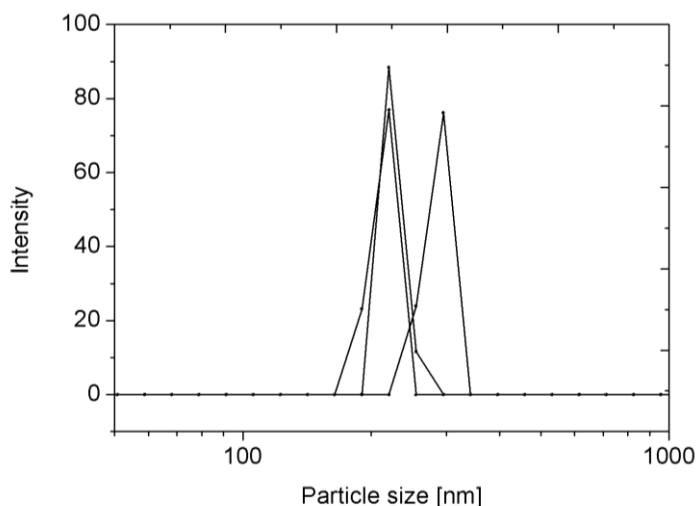
Figure 5.2   *DLS data of CdS powder.*

Apparent quantum yield determination. The AQY was determined by a method developed by Koenig *et al.*[3] A vial as blank sample with 2.0 mL solvent which was used in photocatalytic reaction and a stirring bar was placed in a light-covered apparatus above the 455 nm LED. The transmitted power [mW] was measured by a calibrated photodiode directly above the vial. Then the transmitted power [mW] of a vial with the reaction mixture was measured analogously to

the blank solution for a defined time. The quantum yield was calculated according eq. (32). The error was determined from 3 measurements per reaction.

$$\Phi=(\frac{N_{product}}{N_{photon}}=\frac{N_A \cdot n_{product}}{\dfrac{E_{light}}{E_{photon}}}=\frac{N_A \cdot n_{product}}{\dfrac{P_{absorbed} \cdot t}{\dfrac{h \cdot c}{\lambda}}}=\frac{h \cdot c \cdot N_A \cdot n_{product}}{\lambda \cdot (P_{ref}\text{-}P_{sample}) \cdot t}) \cdot 100 \tag{32}$$

with: Φ = Quantum yield

$N_{product}$ = Number of molecule created

N_{photon} = Number of photons absorbed

N_A = Avogadro's constant [mol^{-1}]

$N_{product}$ = Molar amount of molecules created [mol]

E_{light} = Energy of light absorbed [J]

$P_{absorbed}$ = Radiant power [W]

h = Planck's constant

c = Speed of light [m s^{-1}]

λ = Wavelength of the irradiation source [455 nm]

P_{ref} = Radiant power transmitted by a blank vial [W]

P_{sample} = Radiant power transmitted by the vial with reaction mixture [W]

Synthesis. CdS powder was prepared by precipitation from a $CdSO_4 \cdot \tfrac{8}{3} H_2O$ (25.7 g, 0.1 mol) solution with Na_2S (22.3 g, 0.1 mol) in aqueous NH_3 solution (10%, 200 mL) according litera-ture procedure.[4] Cobaloxime (**2**) was used from a batch synthesized by Dr. Stefan Troppmann (University of Regensburg).

5.1.2.   Photocatalytic Performance

Irradiation setup. The photocatalytic reactions were performed in sealed crimp-top vials and were irradiated with six high power LEDs (Osram Oslon SSL 80 royal-blue LEDs (λ = 455 nm $\pm$ 15 nm, 3.5 V, 700 mA)) from below. Temperature was kept constant on 20 °C by an enclosing aluminum cooling block connected to a thermostat.
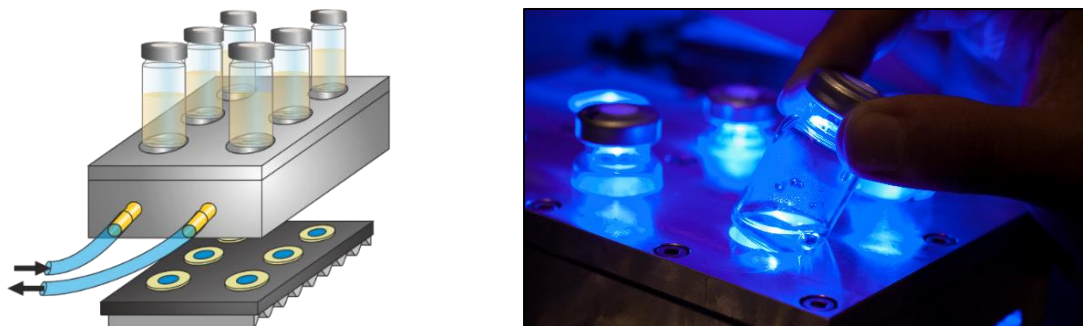
Figure 5.3   *Irradiation setup for photocatalytic H$_2$ evolution. Scheme drawn by Dr. Malte Hansen and photograph taken by Dr. Michal Poznik.*

Sample preparation (chapter 2.1 Reduction of Water). 63 μL of stock solution of cobaloxime (2.0 mmol L^{-1}) was added to a crimp-top vial and evaporated under vigorous shaking by a thermo shaker at defined temperature. After the addition of 0.5 mg of CdS, 0.1 mL of MeCN, 0.9 mL of aqueous solution containing Na$_2$S (0.35M) and Na$_2$SO$_3$ (0.25M) and a magnetic stirring bar, the crimp top vial was closed with a septum cap. Water was deionized using a Milli-Q-Plus water purification system (~ 18.2 MΩcm). The samples were degassed by bubbling nitrogen through the solution for 5 minutes and then irradiated according the irradiation setup shown in Figure 5.3.

Gas chromatography. The determination of the amount of H$_2$ was performed by gas chromatography (Inficon Micro GC 3000) with 5Å molecular sieves column and a thermal conductivity detector. Argon was used as a carrier gas. The amount [μmol g^{-1}] of evolved H$_2$ was determined in triplicate and the mean was plotted against time. The slope of the linear regression over 10 hours gave the maximal H$_2$ evolution rate [μmol g^{-1} h^{-1}].
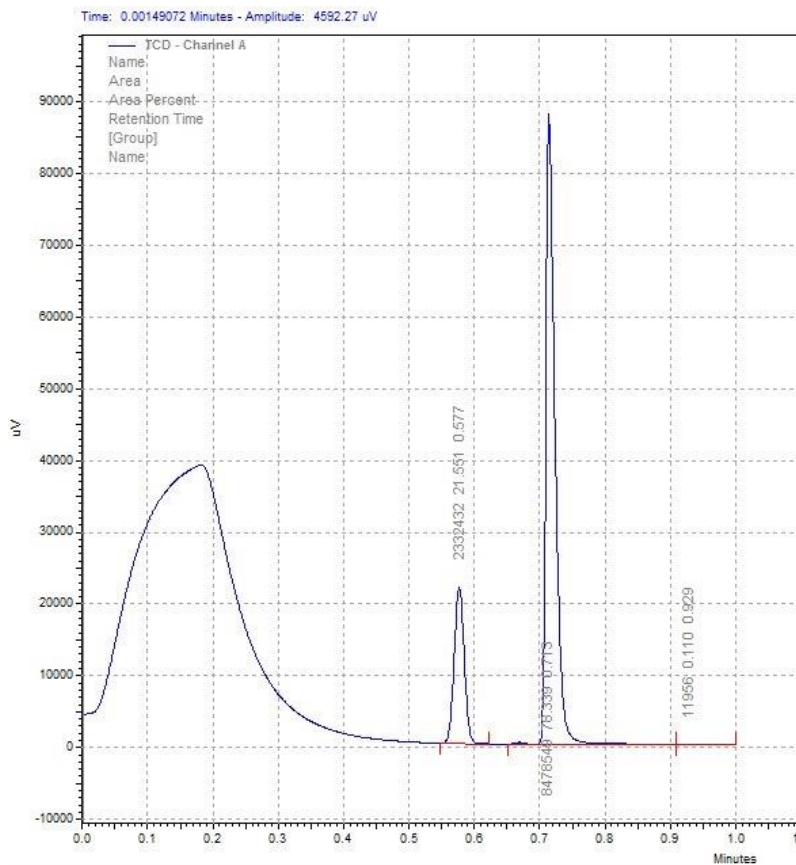
Figure 5.4   *Chromatography of H_2 (RT = 0.58 min) evolved by the photocatalytic system containing 0.5 mg CdS and $1.26 \cdot 10^{-4}$ mol L^{-1} CoIII(dmgH)$_2$(py)Cl in 1.0 mL mixture of MeCN (0.1 mL and H$_2$O (0.9 mL) solution of 0.35 mol L^{-1} Na$_2$S and 0.25 mol L^{-1} Na$_2$SO$_3$. Atmospheric O$_2$ and N$_2$ was eluted at RT = 0.71 min.*

Sample preparation (chapter 2.2 Reduction of Sodium Formate). 0.1 mg CdS powder and 2 mL water containing 4 mol L^{-1} NaHCO$_2$ were added with a magnetic stirring bar to a crimptop vial. Water was deionized using a SG water purification system ($\sim$ 0.055 μS cm^{-1}). After the suspension was sonicated for 5 minutes in an ultrasonic bath, the crimp top vial was closed with a septum cap. The samples were degassed by bubbling nitrogen through the solution for 5 minutes and then irradiated according the irradiation setup shown in Figure 5.3.

Gas chromatography. The determination of the amount of the gases (CO and H$_2$) was performed by gas chromatography carried out on Agilent 6890 equipped with a ShinCarbon ST column (100/120 mesh) and thermal conductivity detector.
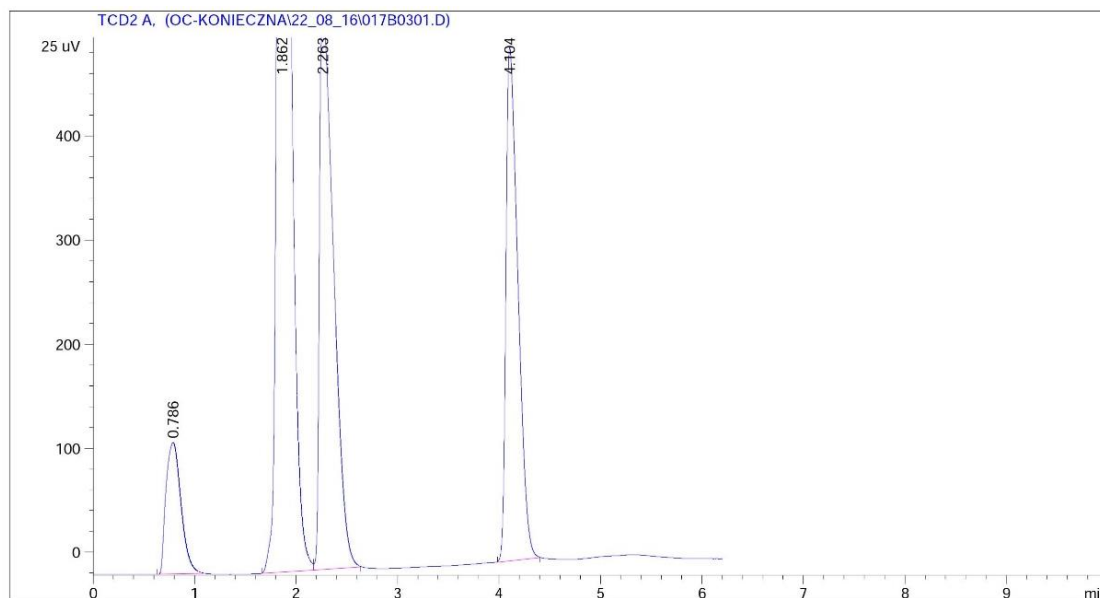
Figure 5.5   *Chromatography of H₂ (RT = 0.78 min) and CO (RT = 2.26 min) and CH₄ (RT = 4.10 min) evolved by the photocatalytic system containing 1.0 mg CdS in 2.0 mL aqueous solution of 4.0 mol L⁻¹ NaHCO₂ and 50 μL of CHCl₃. Atmospheric O₂ and N₂ was eluted at RT = 2.26 min.*

Sample preparation (chapter 2.3 Reductive Dehalogenation). A defined amount of halogenated compound was added to a reaction sample which was identically prepared such as in chapter 2.2. The photocatalytic performance and analytic was also done according experimental procedure from chapter 2.2

Yield determination. The conversion of dehalogenated products was calculated from ^{1}H NMR following eq. 33.

$$\text{Conversion [\%]} \frac{\dfrac{I_{Product}}{N_{Product}}}{\left(\dfrac{I_{Product}}{N_{Product}} + \dfrac{I_{Educt}}{N_{Educt}}\right)} \cdot 100 \tag{33}$$

with I = Integral area of the signal peak

         N = Number of protons of the signal

The related area of the signal peaks was acquired by setting the transmitter offset (O1P) in the middle of the selected signals with a scan rate of 128. Selected singlet peaks were carefully integrated after baseline correction.
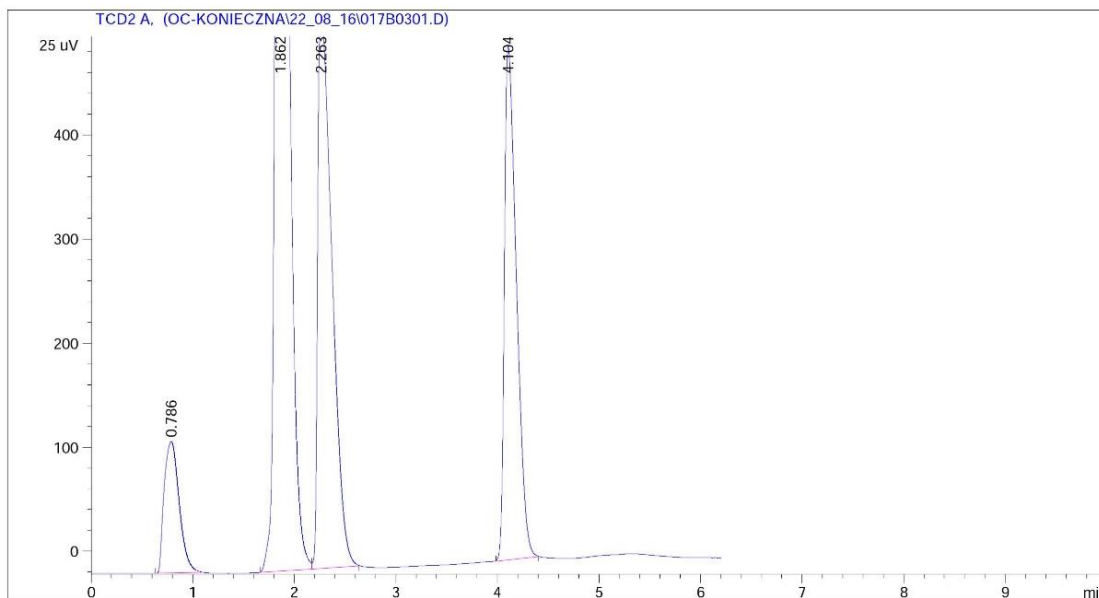
Figure 5.6 *Chromatography of H$_2$ (RT = 0.78 min) and CO (RT = 2.26 min) and CH$_4$ (RT = 4.10 min) evolved by the photocatalytic system containing 1.0 mg CdS in 2 mL aqueous solution of 4 mol L^{-1} NaHCO$_2$ and 50 μl of CHCl$_3$. Atmospheric O$_2$ and N$_2$ was eluted at RT = 2.26 min.*

5.1.3. References

1. H. Kisch, *Angew. Chem. Int. Ed.*, **2013**, *52*, 812-847.

2. P. Scherrer, *Nachrichten von der Gesellschaft der Wissenschaften zu Göttingen, Mathematisch-Physikalische Klasse*, **1918**, *2*, 98-100.

3. U. Megerle, R. Lechner, B. Konig and E. Riedle, *Photochem. Photobiol. Sci.*, **2010**, *9*, 1400-1406.

4. A. Reinheimer, R. van Eldik and H. Kisch, *J. Phys. Chem. B*, **2000**, *104*, 1014-1024.

5.2. Experimental Chapter 3

5.2.1. Instruments, Methods and Materials

Author contributions. Synthesis, characterization and photocatalytic performance by Dagny Konieczna. DFT calculations and description (p. 48) by Matthias Witte (University of Paderborn). The Supervision by Prof. Dr. René Wilhelm (University of Paderborn).

Solvents and substrates. The reagents were purchased from commercial sources (Sigma Aldrich, Alfa Aesar, Acros Organics) and used without further purification. The reactions were prepared under argon atmosphere using Schlenk techniques[1] unless otherwise stated. CH_2Cl_2 and THF were purified by distillation. The reactions were supervised by thin layer chromatography on glass plates with silica gel (MERCK TLC Silica gel F254). The detection of compounds was carried out by irradiation with UV light at 254 and 366 nm. Column chromatography was performed using silica gel 60. Water used in photocatalytic samples was deionized using a Milli-Q-Plus water purification system (~ 18.2 MΩcm).

NMR spectroscopy. ^1H- and ^{13}C-NMR spectra were recorded at 500 MHz on a Bruker Advance 500 and at 300 MHz at a Bruker Advance. The measurement of the substances were performed in $CDCl_3$, DMSO-d6, acetone-D6 and CD_3OD from DEUTERO (all 99.8%). Chemical shifts δ are expressed in ppm and the spin-spin coupling constant is given in Hertz (Hz). Regarding multiplicity the evaluation was carried out with the following abbreviations: s = singlet, d = doublet, dd = double doublet = triplet, q = quartet, m = multiplet).

Spectroscopy. ESI (electrospray ionization) mass spectra were recorded using double-focusing sectorfield-MS DFS from Thermo Scientific. UV-Vis spectroscopy were performed with Varian Cary 50 UV-Vis spectrophotometer. The measurements were performed at room temperature in 10 mm Hellma quartz cuvettes. IR spectra were acquired on an FT-IR-spectrometer Vertex from BRUKER. The solids were measured as KBr pellets.

Melting point. The determination of melting points was performed in open-end-capillary tubes on a BÜCHI B-545 melting point apparatus

Elemental analysis. EA were performed with a vario MICRO cube analysator from Elementar.

Cyclo voltammetry. CV and SWV were recorded at room temperature with a Metrohom-Autolab potentiostat PGSTAT 101 in a solution of $CH_2Cl_2/0.2$ 1.0 mol L^{-1} Bu_4NPF_6 and with a concentration of test substance of 1.0 mol L^{-1}. All measurements was carried out under argon and in dry and degassed solvents with Pt as working electrode, Ag/0.01 M $AgNO_3$/MeCN as reference electrode and Pt as counter electrode. The potentials were given relative to the redox couple ferrocene/ferrocenium (Fc/Fc^+) as an internal standard. The CV curves were calibrated using the Fc/Fc^+ redox couple as an external standard. The half-wave potential $E_{1/2}$ was estimated from eq. (20) (chapter 2.1.10).

The HOMO is approximately equal to the ionization potential I_p and the LUMO to the electron affinity E_a, that are calculated according the empirical relationship by Bredas *et al.*[2] from the onset potentials being compared to ferrocene (4.4 eV vs. vacuum)[3] (eq. 34 and 35). The onset potential were estimated from the intersection of two tangents dawn at the rising signal current and baseline current of the CV.

$$HOMO = I_p = -\left[E_{onset,\,ox} + 4.4 \right] eV \tag{34}$$

$$LUMO = E_a = -\left[E_{onset,\,red} + 4.4 \right] eV \tag{35}$$

with: $E_{onset,ox}$ = Onset potential of oxidation

  $E_{onset,red}$ = Onset potential of reduction

The reduction potentials of cobaloxime (**2**) from Co^{3+} to Co^{2+} (−1.06 V) and further reduction to Co^+ (−1.51 V) and the redox potential of TEOA ($E_{1/2}$ = 0.51 V) are literature-known.[4-5] The potentials were adjusted to Fc/Fc^+.[6] The excited oxidation potential E_{ox} (PS^*/PS^{-1}) of **PS4** was calculated by the Rehm Weller equation[7] (eq. 36):

$$E_{ox}(PS^*/PS^{-1}) = E_{ox}(PS/PS^{-1}) - E_{0,0} \tag{36}$$

with: $E_{0,0}$ = Zero, zero transition energy of excited state, estimated by the absorption maximum from emission spectra of **PS4** in MeCN

Calculation of turnover number: The TON for a homogenous catalyst was estimated according to eq. (37):

$$\text{TON} = \frac{\text{total number of moles product}}{\text{mole catalyst}} \tag{37}$$

Irradiation setup. See chapter 1.7 Experimental – Photocatalytic Performance.

Sample preparation. A solution of **PS4** ($5.0 \cdot 10^{-4}$) and **2** ($5.5 \, 10^{-5}$ mol L^{-1}) in 2.0 mL mixture of MeCN/H_2O (1/1) with 15% TEOA or **SC** ($5.0 \, 10^{-4}$ mol L^{-1}) in 2.0 mL appropriate solvent containing TEOA or TEA and a magnetic stirring bar was added to a crimp-top vial. The aqueous solution was adjusted to pH = 8.3 by HCl. The samples were degassed by bubbling nitrogen through the solution for 5 minutes and then irradiated for a defined time with $\lambda = 455$ nm.

Gas chromatography. GC was carried out on Agilent 6890N equipped with a ShinCarbon ST column (100/120 mesh) and thermal conductivity detector. The quantitative determination of H_2 was performed by preparing a calibration curve.

5.2.2. Synthesis
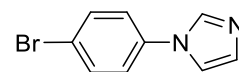
Synthesis of 1-(4-bromopheny)-1*H*-imidazole[8] (10). Copper(I) iodide (1.26 mmol, 240 mg, 0.1 eq) and *N,N'*-(phenylmethylene)diacetamide (1.27 mmol, 261 mg, 0.1 eq) were dissolved in DMSO (18 mL) and stirred for 5 minutes. After addition of dibromobenzene (12.8 mmol, 3 g, 1.0 eq), imidazole (12.8 mmol, 870 mg, 1.0 eq) and sodium methoxide (25.0 mmol, 1.38 g, 2 eq) the reaction solution was stirred overnight at 130 °C. The solution was cooled down and diluted with a mixture of ethyl acetate and H_2O and filtrated by Celite®. Extraction with ethyl acetate (3 x 10 mL) and purification by column chromatography on silica gel using ethyl acetate/*n*-hexane (7/3 v/v %) gave **10** as light yellow solid (5.16 mmol, 1.15 g, 40%). Spectral data were consistent with literature values.[8]

^{1}H-NMR: (500 MHz, CDCl$_3$): δ = 7.78 (s, 1H), 7.54-7.52 (m, 2H) 7.23-7.19 (m, 3H), 7.14 (s, 1H) ppm.

^{13}C-NMR: (300 MHz, CDCl$_3$): δ = 136.3, 135.4, 132.9, 130.6, 123.1, 120.8, 118.1 ppm.
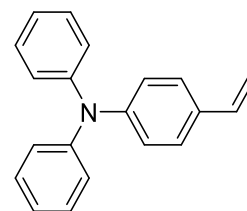
Synthesis of 4-(*N*,*N*-diphenyl-4-vinylaniline[9] (12). 4-(*N*,*N*-diphenylamino)-benzaldehyde (**11**) (3.31 g, 12.11 mmol, 1.0 eq) was dissolved in THF (10 mL) and added to KOtBu (2.10 g, 18.71 mmol, 1.5 eq) and methyltriphenyl phosphonium iodide (7.23 g, 17.89 mmol, 1.5 eq). The solution was stirred for 4 h, changing the color from yellow to brown. After addition of distilled water, the crude product was extracted with methylene chloride, dried over MgSO$_4$ and evaporated to dryness. The product was then purified by column chromatography on silica gel using *n*-hexane. A further purification by precipitation of the obtained residue into methylene chloride /methanol (1/20 v/v %) give **12** as light yellow solid (2.03 g, 7.49 mmol, 62%). Spectral data were consistent with literature values.[9]

^{1}H-NMR: (500 MHz, DMSO-d$_6$): δ = 7.37 (d, J = 8.5 Hz, 2H), 7.30 (m, 4H) 7.06-7.00 (m, 6H), 6.93 (d, J = 8.6 Hz, 2H), 6,66 (dd, ^3J = 17.6, 10.9 Hz, 1H), 5.68 (dd, ^3J = 17.6, 1.0 Hz, 1H), 5.17 (dd, J = 10.9, 0.9 Hz, 1H) ppm.

^{13}C-NMR: (300 MHz, DMSO-d$_6$): δ = 147.5, 147.4, 136.5, 131.9, 130.0, 127.7, 124.5, 123.6, 123.5, 113.1 ppm.
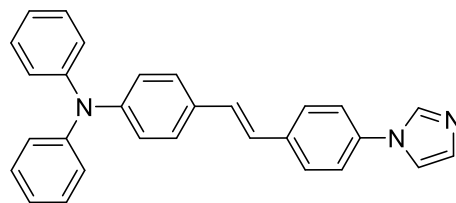
Synthesis of (*E*)-4-(4-(1*H*-imidazol-1-yl)styryl)-*N*,*N*-diphenylaniline (PS1): 1-(4-Bromophenyl)-1*H*-imidazole (**10**) (0.181 g, 0.811 mmol, 1.1.0 eq), *N*,*N*-diphenyl-4-vinylaniline (**12**) (0.20 g, 0.738 mmol, 1.0 eq) and palladium(II) acetate (0.0017 g, 7.38 µmol, 0.01 eq) were stirred in TEAO (14 mL) for 24 h at 120 °C. After cooling the reaction mixture was diluted with water and extracted with ethyl acetate (3 x 10 mL). The organic phases were combined and evaporated to dryness. Purification by column chromatography on silica gel using ethyl acetate/*n*-hexane (7/3 v/v %) gave **PS1** as yellow solid (0.23 g, 0.558 mmol, 76%).

^{1}H-NMR: (500 MHz, CDCl$_3$): δ = 7.92 (s, 1H), 7.58 (d, J_{HH}=14.1 Hz, 2H), 7.38 (q, J_{HH} = 8.6 Hz, 4H) 7.30-7.24 (m, 6H), 7.12-6.98 (m, 10H) ppm.

^{13}C-NMR: (125 MHz, CDCl$_3$): δ = 147.8, 147.5, 137.2, 136.0, 130.8, 130.2, 129.4, 129.3, 127.5, 127.4, 125.3, 124.6, 123.3, 123.2, 121.6 ppm.

^{15}N-NMR: (51 MHz, CDCl$_3$): δ = 150.2 ppm, 109.5, 104.2 ppm.

HRMS (ESI): calcd. for [C$_{29}$H$_{24}$N$_3$]$^+$, 414.1965; found 414.1971.

IR $\tilde{v}$ (KBR pellets, cm^{-1}): 3436, 3081, 2925, 1586, 1521, 1490, 1419, 1384, 1330, 1274, 1172, 1110, 1048, 960, 900, 832, 740, 693, 651, 616, 541, 504, 404.

EA: Anal. calcd for C$_{29}$H$_{23}$N$_3$: C 84.23, H 5.61, N 10.16; found, C, 83.79; H, 5.42; N, 10.15.

M. p.: 243 °C
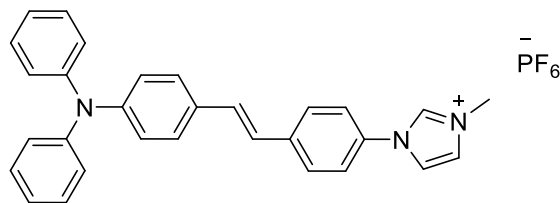
Synthesis of (*E*)-4-(5-(4-(diphenylamino)styryl)thiophen-2-yl)-1-methylpyridin-1-ium ex-afluorophosphate (PS2): Methyl iodide (0.16 mL, 2.52 mmol, 12.0 eq) was added to a solution of (*E*)-*N*,*N*-diphenyl-4-(2-(5-(pyridin-4-yl)thiophen-2-yl)vinyl)aniline (**PS1**) (95 mg, 0.21 mmol, 1.0 eq) in CH_2Cl_2 (7 mL). After stirring overnight the solvent was removed under reduced pressure to give (*E*)-4-(5-(4-(diphenylamino)styryl)thiophen-2-yl)-1-methylpyridin-1-ium iodide as deep violet solid, which was dissolved in CH_2Cl_2 (7 mL) and treated with an aqueous solution of $NaPF_6$ (5.0 mL, 0.05 mol L^{-1}, 1.5 eq). The reaction mixture was vigorously stirred for 4 h. The organic phase was separated and dried over $MgSO_4$ and the solvent was removed under reduced pressure. The crude product was dissolved in a small amount of hot $CHCl_3$ and finally precipitated in *n*-hexane to give **PS2** as yellow solid (99.6 g, 0.168 mmol, 97%).

^{1}H-NMR: (500 MHz, $CDCl_3$): δ = 9.76 (s, 1H), 7.95 (t, *J* = 1.7 Hz, 1H), 7.85 (d, *J* = 8.8 Hz, 1H), 7.76 (d, *J* = 8.8 Hz, 2H), 7.55 (d, *J* = 8.7 Hz, 2H), 7.38-7.32 (m, 5H), 7.21 (d, *J* = 16.4 Hz, 1H), 7.11-7.05 (m, 6H), 6.98 (d, *J* = 8.6 Hz, 2H), 4.96 (s, 3H) ppm.

^{13}C-NMR: (125 MHz, $CDCl_3$): δ = 147.7, 147.3, 139.3, 136.2, 133.7, 133.5 131.2, 130.6, 130.1, 128.4, 128.1, 125.4, 124.9, 124.8, 124.7, 123.9, 123.1, 122.4, 121.3, 36.6 ppm.

^{19}F-NMR: (280 MHz, DMSO-D6): δ = -70.2 (d, *J* = 710.0 Hz) ppm.

^{15}N-NMR: (51 MHz, DMSO-D6): δ = 101.0, 158.2 ppm. (Third N-Atom was not observed).

^{31}P-NMR: (200 MHz, DMSO-D6): δ = −144.1 (sept, *J* = 711.2 Hz) ppm.

IR $\tilde{v}$ (KBR pellets, cm^{-1}): 3432, 3077, 2925, 1545, 1508, 1500, 1419, 1354, 132, 1232, 1080, 1048, 1020, 960, 930, 832, 740, 651, 541, 504, 404.

HRMS (ESI): calcd. for $[C_{30}H_{26}N_3]^+$ 428.2121; found 428.2132

EA: Anal. calcd. for $C_{30}H_{26}N_3PF_6$: C, 62.83; H, 4.57; N, 7.33; S, 5.43; found C, 62.70; H, 4.30; N, 7.12.

M. p.: 235 °C
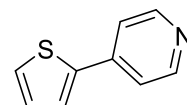
Synthesis of 4-(thiophen-2-yl)pyridine[10] (20): The reagents 4-bromopyridine hydrochloride (**18**) (810 mg, 4.14 mmol, 1.0 eq), thiophen-2-ylboronic acid (**19**) (530 mg, 4.14 mmol, 1.0 eq) and tetrakis(triphenylphosphine)palladium(0) were dissolved in a mixture of aqueous solution containing sodium carbonate (4.2 mL, 1 M) and CH_2Cl_2 (12 mL). The reaction solution was degassed by purging with argon and then stirred for 24 h at 90 °C. After cooling the solvent was evaporated and the residue was dissolved in CH_2Cl_2 (100 mL) and washed with water. The organic phase was dried over $MgSO_4$, filtrated and evaporated to dryness. Purification by column chromatography on silica gel using CH_2Cl_2/ethyl acetate (1/1 v/v %) to give **20** as white solid (151 mg, 0.71 mmol, 77%). Spectral data were consistent with literature values.[10]

^{1}H-NMR (500 MHz, CDCl$_3$): δ = 8.59 (d, J = 3.5 Hz, 2H), 7.50 (dd, J = PS1 Hz, 1.1 Hz, 1H), 7.48 (d, J = 6.1 Hz, 2H), 7.41 (dd, J = 5.0 Hz, 1.1 Hz, 1H), 7.13 (dd, J = 5.2 Hz, 3.6 Hz, 1H) ppm.

^{13}C-NMR (300 MHz, CDCl$_3$): δ = 150.3, 141.4, 141.2, 128.4, 127.2, 125.3, 119.9 ppm.
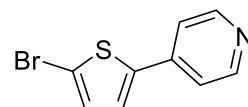
Synthesis of 4-(5-bromothiophen-2-yl)pyridine[11] (21): 4-(Thiophen-2-yl)pyridine (**20**) (172 mg, 1.07 mmol, 1.0 eq) was dissolved in acetic acid (12 mL) and treated with *N*-bromosuccinimide (200 mg, 1.2 mmol, 1.12 eq). The reaction mixture was stirred for 3 h in the absence of light. After the addition of distilled water the aqueous solution is extracted with CH_2Cl_2 (3 x 5 mL). The combined organic phase was washed with water, dried over $MgSO_4$, filtrated and

evaporated to dryness. Purification by column chromatography on silica gel using CH_2Cl_2/ethyl acetate (1/1 v/v %) yielded **21** as light yellow solid (177 mg, 0.74 mmol, 69%). Spectral data were consistent with literature values.[11]

^{1}H-NMR: (500 MHz, $CDCl_3$): δ = 8.60 (d, J = 6.3 Hz, 2H), 7.42 (d, J = 6.3 Hz, 2H) 7.28 (d, J = 3.9 Hz, 1H), 7.411 (d, J = 3.9 Hz, 1H) ppm.

^{13}C-NMR: (300 MHz, $CDCl_3$): δ = 149.4, 142.1, 141.5, 131.5, 126.1, 119.6, 115.2 ppm.
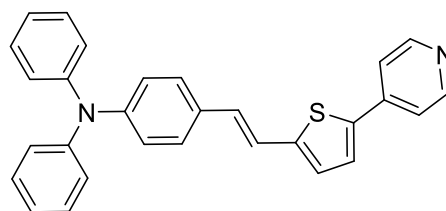
Synthesis of (*E*)-*N,N*-diphenl-4-(2-(5-(pyridine-4-yl)thiophen-2-yl)vinyl)aniline (PS3): *N,N*-diphenyl-4-vinylaniline (**12**) (562 mg, 2.08 mmol, 1.0 eq), 4-(5-bromothiophen-2-yl)pyridine (**21**) (500 mg, 2.08 mmol, 1.0 eq) and palladium(II) acetate (4.7 mg, 0.02 mmol, 0.01 eq) were dissolved in triethanolamine (10 mL) and degassed by purging with argon. The reaction mixture was stirred for 48 h at 120 °C. After cooling the reaction mixture was diluted with distilled water and extracted four times with CH_2Cl_2. The organic phase was washed with distilled water, dried over $MgSO_4$ and filtrated and evaporated to dryness. Purification by column chromatography on silica gel using *n*-hexane/ethyl acetate (1/1 v/v % %) give **PS3** as yellow solid (490 mg, 53%).

^{1}H-NMR: (500 MHz, $CDCl_3$): δ = 8.57 (d, J = 6.1 Hz, 2H), 7.46 (dd, ^3J = 4.5 Hz, 1.6 Hz, 2H), 7.42 (d, J = 3.8 Hz, 1H), 7.35 (d, J = 8.5 Hz, 2H), 7.28-7.25 (m, 4H), 7.12-7.09 (m, 4H), 7.06-7.03 (m, 6H), 6.94 (d, J = 16 Hz, 1H) ppm.

^{13}C-NMR: (300 MHz, $CDCl_3$): δ = 149.9, 147.8, 147.3, 145.6, 130.4, 129.6, 129.3, 127.4, 126.7, 126.2, 124.7 123.3, 123.1, 119.4 ppm.

^{15}N-NMR: (51 MHz, DMSO-D6): δ =102.3 ppm (2nd N-Atom was not observed).

IR $\tilde{\nu}$ (KBR pellets, cm^{-1}): 3435, 3031, 2923, 1783, 1733, 1677, 1583, 1486, 1407, 1328, 1270, 1174, 1077, 1027, 989, 954, 888, 856, 800, 752, 692, 615.

HRMS (ESI): calcd. for $[C_{29}H_{23}N_2S]^+$ 431.1576; found 431.1583.

EA: Anal. calcd. for $C_{29}H_{22}N_2S$: C, 80.90; H, 5.15; N, 6.51; S, 7.45; found C, 80.69, H, 5.15, N, 6.34, S, 7.45.

M.p.: 201 °C.
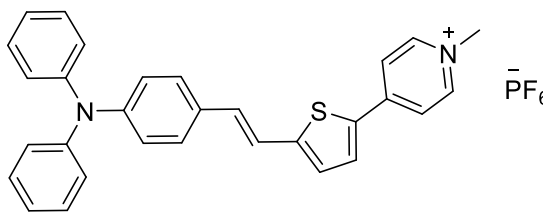
Synthesis of (*E*)-*N*,*N*-diphenyl-4-(2-(5-(pyrdin-4-yl)thiohphen-2-yl)-1-methylpyridin-1-ium hexafluorophosphate (PS4): (*E*)-*N*,*N*-Diphenyl-4-(2-(5-(pyrdin-4-yl)thiohphen-2-yl)vinly)aniline (**PS3**) (95 mg, 0.21 mmol, 1.0 eq) was dissolved in CH$_2$Cl$_2$ (7 mL) and treated with methyl iodide (0.16 mL, 2.52 mmol, 12 eq). The reaction mixture was stirred overnight and then evaporated to dryness. (*E*)-*N*,*N*-diphenyl-4-(2-(5-(pyrdin-4-yl)thiohphen-2-yl)-1-methylpyridin-1-ium iodide was obtained as violet solid and was directly dissolved in CH$_2$Cl$_2$ (7 mL) and treated with an aqueous NaPF$_6$ solution (5 mL, 0.05 L mol^{-1}, 1.5 eq). The reaction mixture was vigorously stirred. The organic phase was separated, dried over magnesium sulfate, filtrated and evaporated to dryness. The crude product was dissolved in hot CHCl$_3$ and precipitated by addition of an excess of *n*-hexane. After filtration and drying under high vacuum give **PS4** as red solid (96 mg, 0.17 mmol, 97%).

^{1}H-NMR: (500 MHz, acetone-D6): δ = 8.89 (d, J = 6.9 Hz, 2H), 8.30 (d, J = 7.1 Hz, 2H), 8.13 (d, J = 4.1 Hz, 1H), 7.52 (d, J = 8.6 Hz, 2H), 7.41-7.38 (m, 2H), 7.35-7.32 (m, 4H), 7.23 (d, J = 16.1 Hz, 1H), 7.12-7.09 (m, 6H), 6.99 (d, J = 8.7, 2H), 4.50 (s, 3H) ppm.

^{13}C-NMR: 300 MHz, acetone-D6): δ = 154.3, 152.8, 149.6, 148.1, 146.2, 135.3, 134.0, 133.3, 130.7, 130.5, 129.1, 129.0, 125.9, 128.9, 124.7, 123.2, 122.6, 119.62, 111.3, 48.0 ppm.

^{15}N-NMR: (51 MHz, acetone-D6): $\delta = 190.9, 101.8$ ppm.

^{19}F-NMR: (280 MHz, acetone-D6): $\delta = -72.51$ (d, $J = 707.8$ Hz).

^{31}P-NMR: (200 MHz, acetone-D6): $\delta = -144.12$ (sept, $J = 707.8$ Hz).

IR absorption (KBR pellets, cm^{-1}): 3440, 3032, 1642, 1588, 1536.8, 1507, 1441, 1329, 1232, 1198, 1072, 961, 831, 752, 694, 621.

HRMS (ESI, m/z): $[C_{30}H_{25}N_2S]^+$ calcd for $C_{30}H_{25}N_2S$ 445.1733; found 445.1742.

EA: Anal. calcd. for $C_{30}H_{25}N_2SPF_6$: C, 61.01; H, 4.27; N, 4.74; S, 5.43; found C, 60.11; H, 4.49; N, 4.84; S, 5.48.

M.p.: 235 °C.
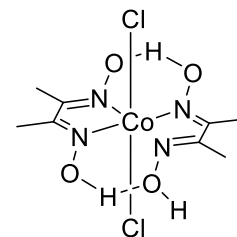
Synthesis of Bis-dimethylglyoximcobalt-dichloride.[12] (45): Cobalt(II) hexahydrate (0.954 g, 4 mmol, 1.0 eq) and **44** (0.978 g, 8.5 mmol, 2.1 eq) were dissolved in acetone and vigorously stirred for 30 min under airflow. A dark green solid precipitated and the reaction mixture was cooled in an ice bath and then filtrated cold. The residue was washed with cooled acetone and dried under high vacuum. The compound **45** was obtained as dark green solid (1.176 g, 3.25 mmol, 68%). Spectral data were consistent with literature values.[12]

^{1}H-NMR: (500 MHz, DMSO-D$_6$): $\delta = 9.32$ (s, 1H), 2.34 (s, 12H) ppm.

^{13}C-NMR: (125 MHz, DMSO-D$_6$): $\delta = 150.0, 12.4$ ppm.
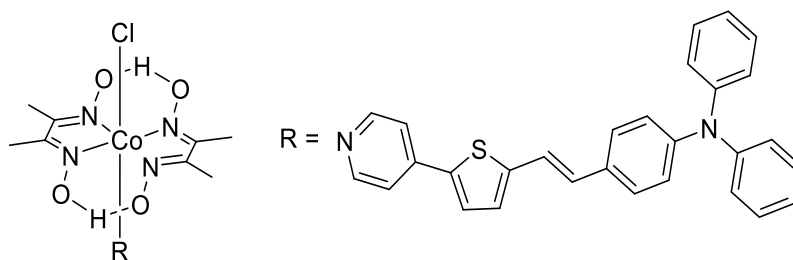
Synthesis of CoCl(dmgH)₂-(*E*)-*N*,*N*-diphenl-4-(2-(5-(pyridine-4-yl)thiophen-2-yl)vinyl)aniline (SC). Compound **45** (160 mg, 0.443 mmol, 1.0 eq) was dissolved in methanol (20 mL), to which NaOH (17.7 mg, 0.443 mmol, 1.0 eq) and compound **PS3** (198 mg, 0,443 mmol, 1.0 eq) was added. The reaction mixture was stirred at rt for 24 h. By slow addition of acetic acid the raw product was precipitated. The reaction solution was filtrated and the residue was washed with CH_2Cl_3 by column chromatograph to give **SC** as orange solid (230 mg, 0.305 mmol, 68%).

^{1}H-NMR: (500 MHz, CDCl₃): δ = 8.11 (d, *J* = 6.8 Hz, 2H), 7.41 (d, *J* = 4.2 Hz, 1H), 7.32 (d, *J* = 8.8 Hz, 2H), 7.30 (d, *J* = 6.8 Hz, 2H), 7.27 (t, *J* = 7.0 Hz 4H), 7.11 (dd, ^3J = 8.7 Hz, 1.1 Hz, 4H), 7.06 (t, *J* = 7.31 Hz, 2H), 7.04-7.00 (m, 4H), 6.95 (d, *J* = 16 Hz, 1H) ppm.

^{13}C-NMR: (125 MHz, CDCl₃): δ = 152.4, 150.8, 148.4, 148.3, 147.3, 143.9, 135.3, 131,8, 129.6, 129.4, 128.6, 127.6, 126.9, 124.9, 123.5, 122.7, 120.6, 118.6 ppm.

^{15}N-NMR: (50 MHz, CDCl₃): δ = 316.4, 199.7, 102.4 ppm.

IR $\tilde{\nu}$ (KBR pellets, cm^{-1}): 3855, 3823, 3753, 3448, 3034, 2362, 1614, 1587, 1508, 1446, 1371, 1328, 1272, 1240, 1176, 1093, 1028, 968, 898, 821, 754, 698, 617, 588, 561, 512, 391.

HRMS (ESI): calcd. for $[C_{37}H_{36}N_6O_4SClCo]^+$ 431.1576; found, 431.1583.

EA: Anal. calcd for $C_{37}H_{36}N_6O_4SClCo$: C, 58.85; H, 4.81; N, 11.13; S, 4.25; found C, 57.30; H, 4.98; N, 10.51; S, 4.17.

M.p.: 201 °C.
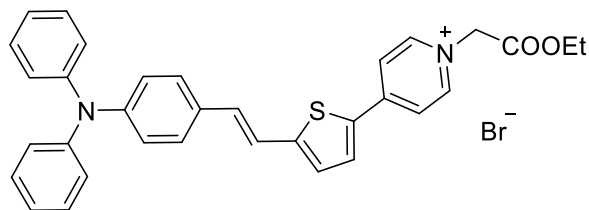
Synthesis of (*E*)-4-(5-(4-(diphenylamino)styryl)thiophen-2-yl)-1-(2-ethoxy-2-oxoethyl)pyridin-1-ium bromide. The synthesis procedure is derived from literature.[13] Ethyl bromoacetate (15 µL, 0.135 mmol) was added to a solution of compound **PS3** (40 mg, 0.09 mmol) in MeCN (15 mL) and stirred overnight under reflux. The reaction mixture was cooled and the solvent evaporated. Purification by column chromatography on silica gel using CH_2Cl_2//MeOH (20/1 v/v %) gave a red solid (40 mg, 0.077 mmol, 85%).

^{1}H-NMR: (500 MHz, MeOD): δ = 8.66 (dd, *J* = 7.2 Hz, 1.1 Hz, 2H), 8.19 (d, *J* = 7.2 Hz, 2H), 8.07 (d, *J* = 4.0 Hz, 2H), 7.46 (d, *J* = 8.6 Hz, 2H), 7.33 (d, *J* = 4.0 Hz, 1H), 7.32-7.26 (m, 5H, 7.20 (d, *J* = 16.0 Hz, 1H), 7.11-7.06 (m, 6H), 6.97 (d, *J* = 8.7 Hz, 2H), 4.33 (q, *J* = 7.1 Hz, 2H), 3.87 (s, 2H), 1.34 (t, *J* = 7.2 Hz, 3H) ppm.

^{13}C-NMR: (125 MHz, MeOD): δ = 166.3, 153.3, 149.8, 148.7, 147.2, 145.2, 134.0, 133.6, 132.8, 129.6, 129.2, 128.0, 127.8, 124.8, 123.5, 122.0, 121.0, 118.2, 62.7, 52.5, 12.9 ppm.
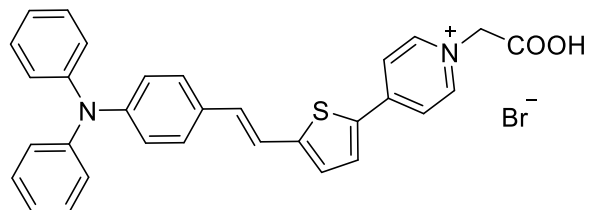
Synthesis of (*E*)-1-(carboxymethyl)-4-(5-(4-(diphenylamino)styryl)thiophen-2-yl)pyridin-1-ium bromide (PS5). The synthesis procedure is derived from literature.[14] A solution of compound **51** (40 mg, 0.077 mmol) in a mixture of EtOH/H_2O (10 mL, 9/1 v/v %) was treated with LiOH·H_2O (64 mg, 1.54 mmol) and stirred at rt for 24 h. The pH was adjusted at 2-3 by diluted HCl solution (1.0 mol L^{-1}). The ethanol was evaporated and the remaining aqueous solution was

extracted with CH_2Cl_2 (3 x 30 mL). After evaporation of the organic phase to dryness, the purification by column chromatography on silica gel using CH_2Cl_2/MeOH 5/1 v/v %) gave **PS5** as red solid (312 mg, 0.063 mmol, 81%).

^{1}H-NMR: (500 MHz, MeOD): δ = 8.59 (d, J = 7.2 Hz, 2H), 8.12 (d, J = 7.2 Hz, 2H), 8.01 (d, J = 4.0 Hz, 1H), 7.46 (d, J = 8.6 Hz, 2H), 7.31-7.26 (m, 6H), 7.17 (d, J = 16.0 Hz, 1H), 7.10-7.06 (m, 6H), 6.97 (d, J = 8.7 Hz, 2H), 5.03 (s, 2H) ppm.

^{13}C-NMR: (125 MHz, MeOD): δ = 168.9, 152.0, 148.6, 147.3, 144.9, 134.4, 132.5, 132.2, 129.8, 129.1 129.0 127.7, 124.8, 123.4, 122.2, 120.8, 118.4, 62.3, ppm.

^{15}N-NMR: (125 MHz, MeOD): δ = 197.3, 102.3 ppm.

IR $\tilde{v}$ (KBR pellets, cm^{-1}): 3435, 3034, 2361, 1637, 1587, 1508, 1440, 1384, 1274, 1226, 1192, 1068, 956, 819, 752, 696, 619, 586, 557, 503, 470.

HRMS (ESI): calcd. for $[C_{31}H_{25}N_2O_2S]^+$ 489.1631; found 489.1640

EA: Anal. calcd for $C_{37}H_{36}N_6O_4SClCo$: C, 58.85; H, 4.81; N, 11.13; S, 4.25; found C, 57.30; H, 4.98; N, 10.51; S, 4.17.

M. p.: 98 -100°C

¹H NMR spectra of new compounds

¹H NMR (500 MHz, CDCl₃)
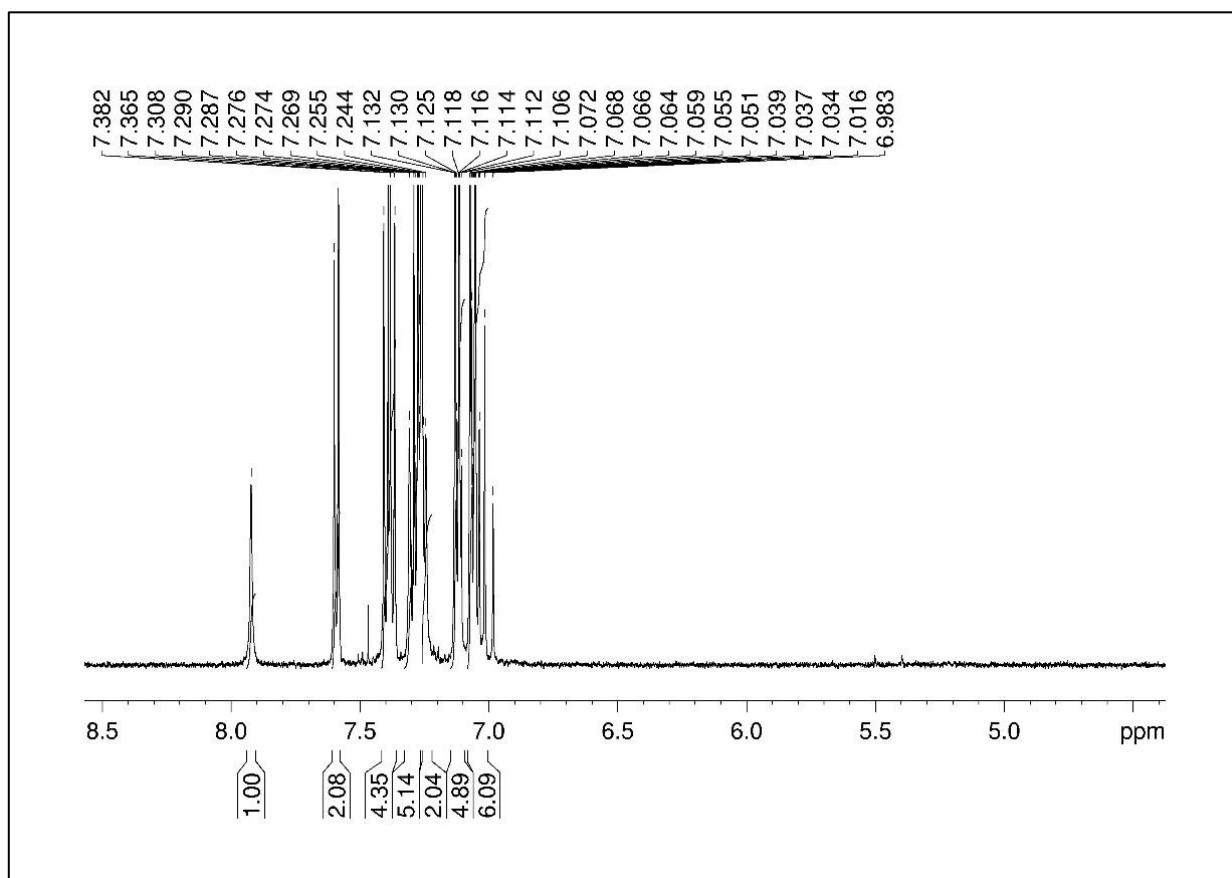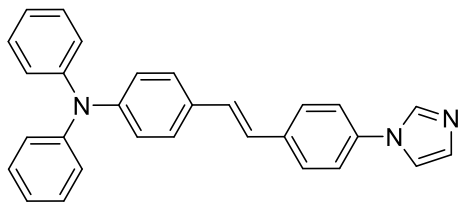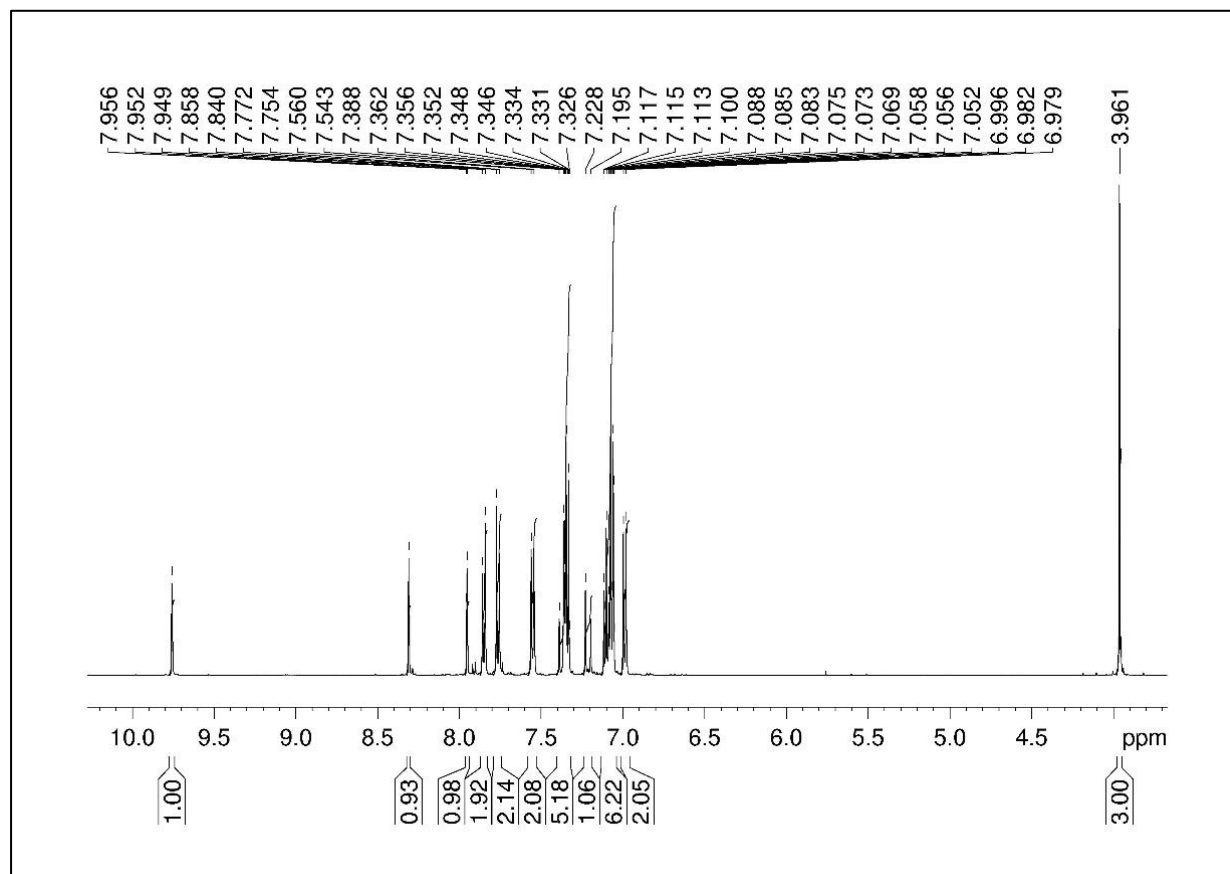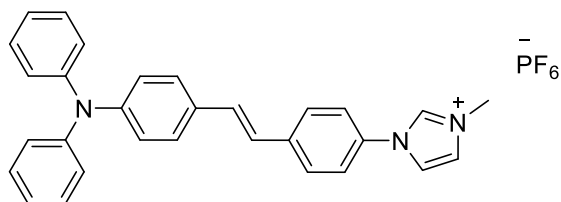
¹H NMR (500 MHz, CDCl₃)
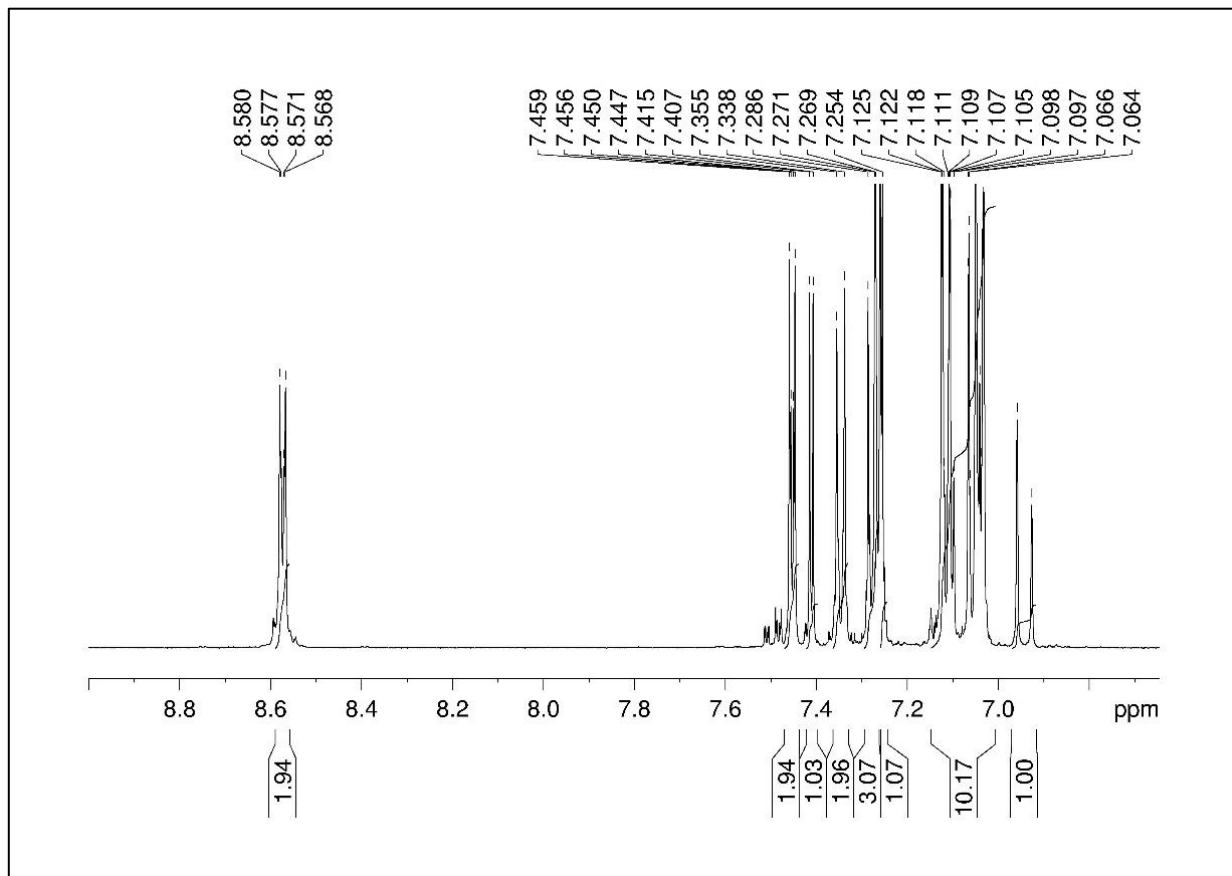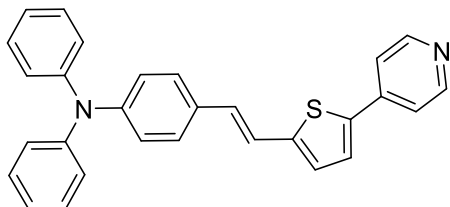
¹H NMR (500 MHz, CDCl₃)

¹H NMR (500 MHz, acetone-D6
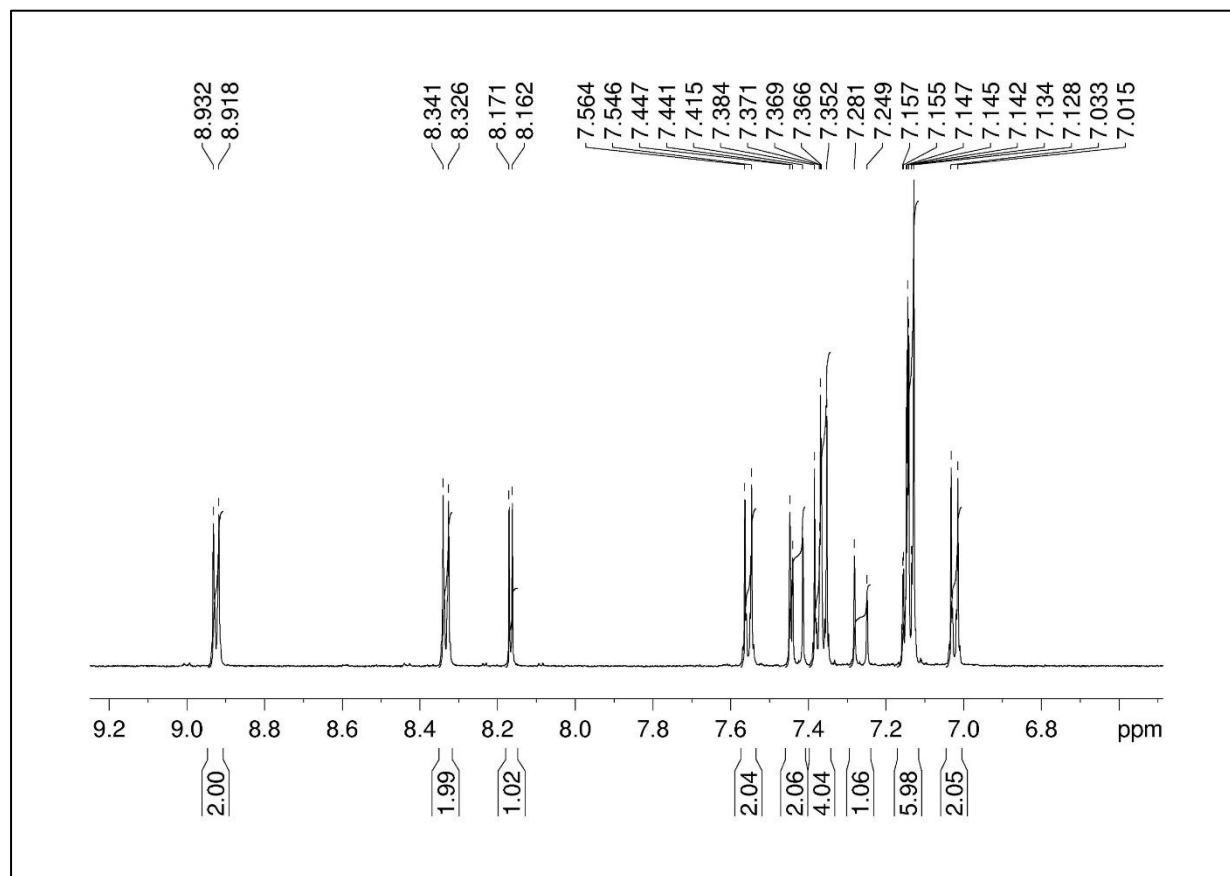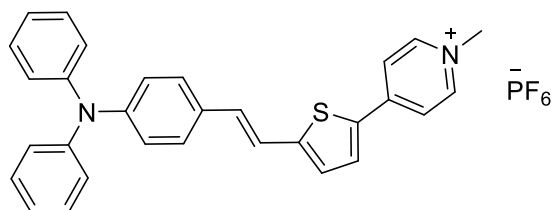
¹H NMR (500 MHz, MeOD)

^{1}H NMR (500 MHz, CDCl$_3$)

7.313
7.310
7.305
7.297
7.292
7.291
7.281
7.266
7.193
7.161
7.094
7.093
7.088
7.086
7.082
7.079
7.075
7.071
7.069
7.067
7.064
6.989
6.986
6.976
6.972
5.030
4.805
3.313
3.310
3.307

2.00
2.03
0.98
2.03
6.01
1.11
5.95
2.28
1.94
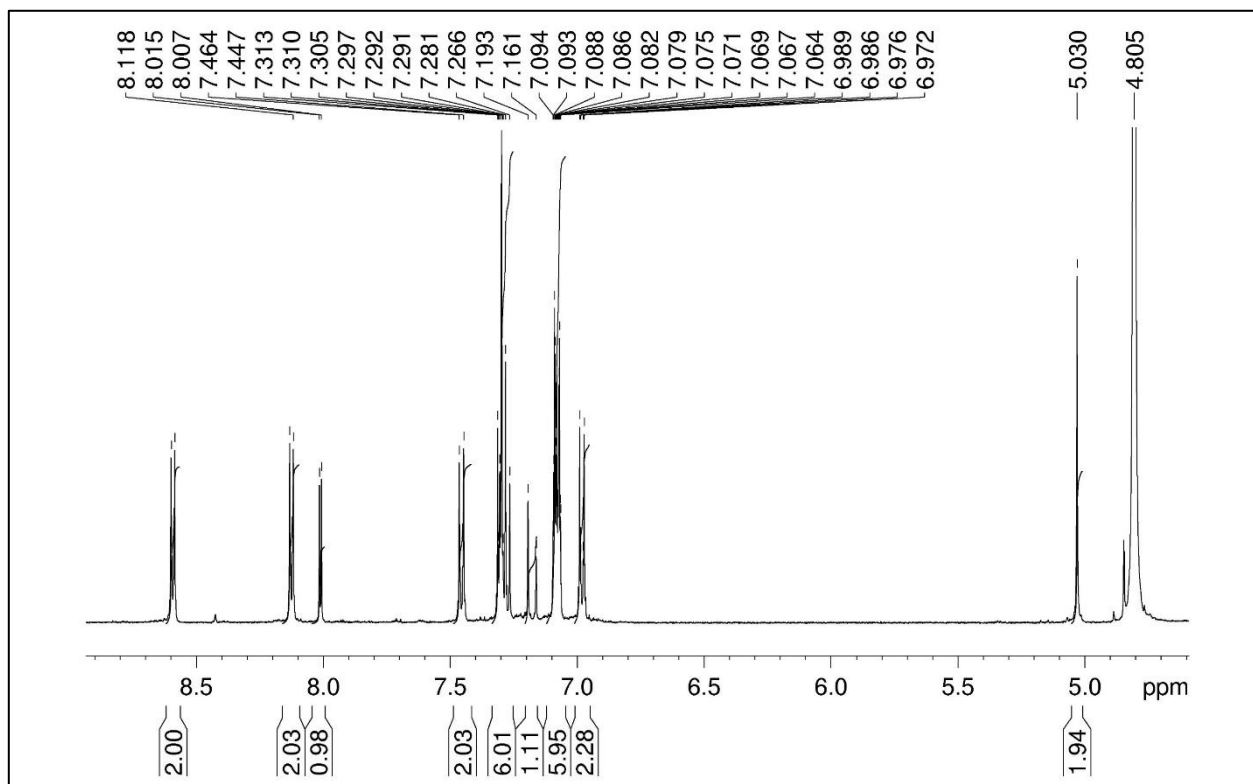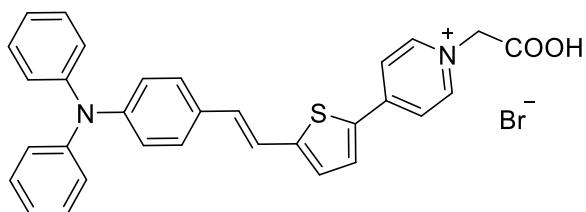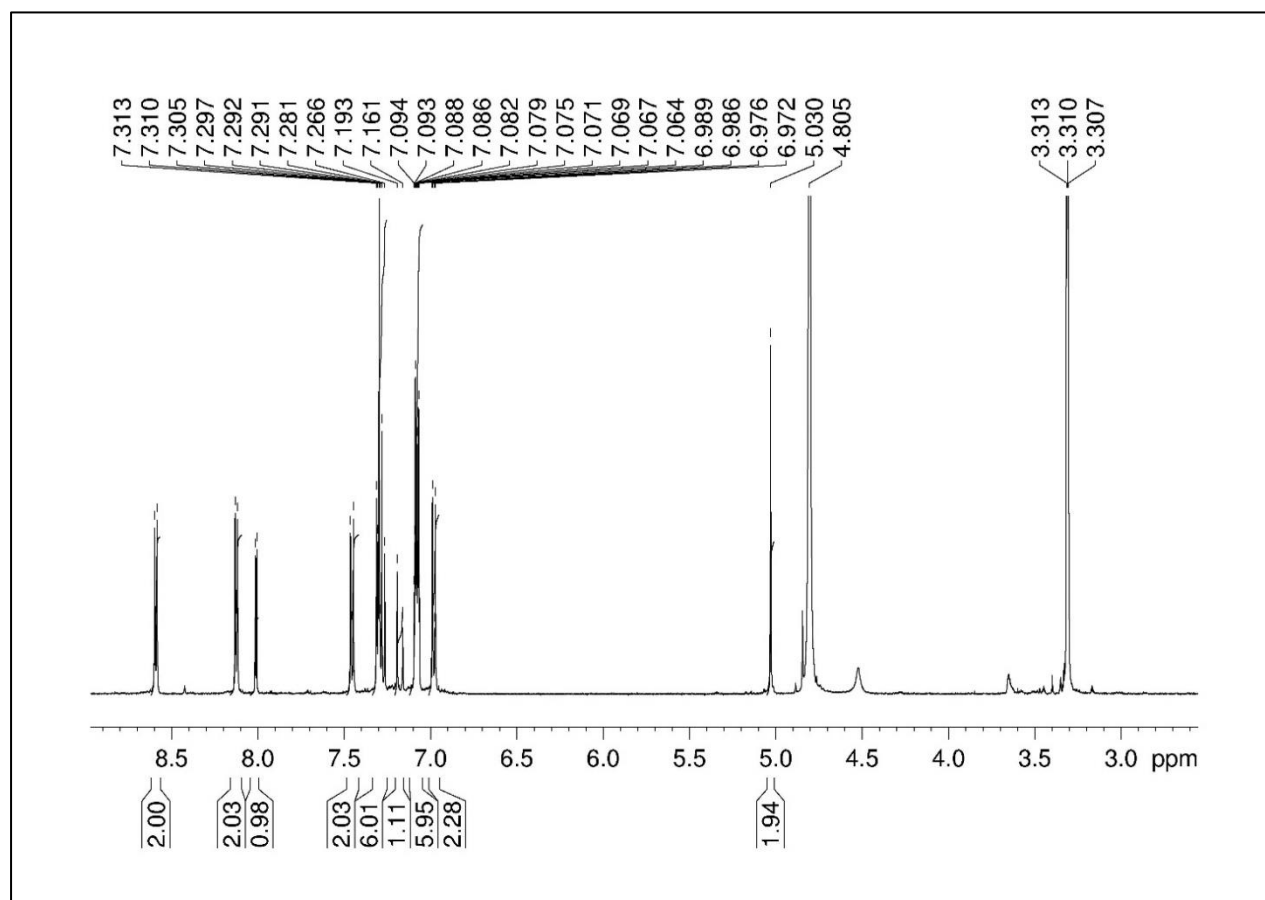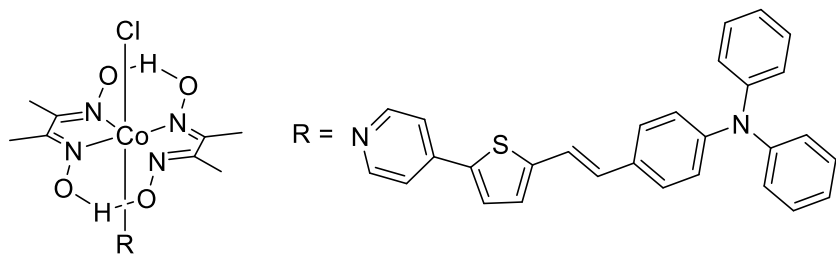
5.2.3. References

1. L. Beyer and J. Angulo Cornejo, *Koordinationschemie*, Vieweg+Teubner Verlag, Wiesbaden, **2012**.

2. J. L. Bredas, R. Silbey, D. S. Boudreaux and R. R. Chance, *J. Am. Chem. Soc.*, **1983**, *105*, 6555-6559.

3. A. K. Agrawal and S. A. Jenekhe, *Chem. Mater.*, **1996**, *8*, 579-589.

4. P. Du, University of Rochester, *Platinum (II) polypyridyl complexes for visible light-driven hydrogen production from water*, **2009**.

5. G. Ruiz, F. Rodriguez-Nieto, E. Wolcan and M. R. Féliz, *J. Photochem. Photobiol. A*, **1997**, *107*, 47-54.

6. V. V. Pavlishchuk and A. W. Addison, *Inorg. Chim. Acta*, **2000**, *298*, 97-102.

7. G. J. Kavarnos and N. J. Turro, *Chem. Rev.*, **1986**, *86*, 401-449.

8. J.-P. Wan, Y.-F. Chai, J.-M. Wu and Y.-J. Pan, *Synlett*, **2008**, *19*, 3068-3072.

9. S. Hwang, J. H. Lee, C. Park, H. Lee, C. Kim, C. Park, M.-H. Lee, W. Lee, J. Park, K. Kim, N.-G. Park and C. Kim, *Chem. Commun.*, **2007**, *46*, 4887-4889.

10. Y. Ooyama, S. Inoue, T. Nagano, K. Kushimoto, J. Ohshita, I. Imae, K. Komaguchi and Y. Harima, *Angew. Chem. Int. Ed.*, **2011**, *50*, 7429-7433.

11. L. Wang, X. Yang, S. Li, M. Cheng and L. Sun, *RSC Adv.*, **2013**, *3*, 13677-13680.

12. G. N. Schrauzer, *Angew. Chem. Int. Ed.*, **1976**, *15*, 417-426.

13. T.-Y. Li, C. Su, S. B. Akula, W.-G. Sun, H.-M. Chien and W.-R. Li, *Org. Lett.*, **2016**, *18*, 3386-3389.

14. M. Cheng, X. Yang, F. Zhang, J. Zhao and L. Sun, *J. Phys. Chem. C*, **2013**, *117*, 9076-9083.

5.3. Experimental Chapter 4

5.3.1. Instruments, Methods, and Materials

Author contributions. Chapter "*Reduction of Carbon Dioxide*" by Dagny Konieczna in collaboration with André Kleine (group of Prof. Dr. Ullrich Hilleringmann, University of Paderborn) under supervision of Prof Dr. René Wilhelm (University of Paderborn). Conception and construction of the photoreactor by Dagny Konieczna, André Kleine and Dr. Heinz Weber (University of Paderborn). Chapter "*Reduction of Protons*" by Dagny Konieczna under supervision of Prof. Dr. Burkhard König.

Solvents and substrates. The reagents were purchased from commercial sources (Sigma Aldrich, Alfa Aesar and Acros Organics. SiO_2 (pore size = 60 Å, particle size = 63 – 200 μm) was purchased from Macherey Nagel, TiO_2 (Aeroxid P25®) from Evonik and ILs from Iolitec and used without purification. The reactions were prepared under argon atmosphere using Schlenk techniques[1] unless otherwise stated. Water used in photocatalytic samples was deionized using a Milli-Q-Plus water purification system (~ 18.2 MΩcm).

Nuclear magnetic resonance spectroscopy. ^{1}H- and ^{13}C -NMR spectra were recorded at 500 MHz on a BRUKER Advance 500 and at 300 MHz at a BRUKER Advance 300. The measurement of the substances were performed in d6-DMSO (99.8%, DEUTERO). Chemical shifts δ are expressed in ppm and the spin-spin coupling constant is given in Hertz (Hz). Regarding multiplicity the evaluation was carried out with the following abbreviations: br = broad, s = singlet, d = doublet, dd = double doublet = triplet, q = quartet, m = multiplet).

5.3.2. Experimental Chapter 4.2

Synthesis of photocatalytic components **2** and **47**, **48** were synthesized by Dr. Stefan Troppmann (University of Regensburg).[2]

Calculation of turnover number: The TON for a homogenous catalyst was estimated according to eq. (37) (see chapter 5.2).

Irradiation setup. See chapter 1.7 Experimental – Photocatalytic Performance.

Sample preparation for homogenous H_2 evolution. 63 μL of stock solution of **2** (2.0 mmol L^{-1}) and 31.5 μL of **1** (1.0 mmol L^{-1}) was added to a crimp-top vial and evaporated under vigorous shaking by a thermo shaker at defined temperature. An appropriate ratio of H_2O and organic solvent MeCN or [C_4mim][OTf]) with TEOA (15% v/v) and a magnetic stirring bar was added to a crimp-top vial and gas-tight closed. The aqueous solution was adjusted to pH = 8.3 by HCl. The samples were degassed by bubbling nitrogen through the solution for 5 minutes and then irradiated for a defined time with λ = 455 nm.

Preparation of IL-supported SiO_2 catalyst. An appropriate amount of IL [C_8mim][PF_6] (Table 5.1) was added to a solution of **47** (1.26 mg, 0.98 μmol) and **48** (2.24 mg, 3.82 μmol) dissolved in $CHCl_3$ (10 mL) and stirred for 5 min. Afterward 250 mg of SiO_2 was added and stirred for 30 min. MeOH was removed in vacuum to give a red powder in quantitative yield. The immobilization of SiO_2 with **47** and **48** without supported IL was prepared in the same way but without the addition of IL.

Table 5.1   *Amount of IL in preparation of IL-supported SiO_2 photocatalyst.*

Amount of [C_8mim][PF_6]	Table, entry
0.25 mL, 0.31 mg	Table 4.2, 2
0.50 mL, 0.62 mg	Table 4.2, 3

Sample preparation with SiO_2 catalyst. 10.0 mg of the photocatalyst, 1.0 mL of H_2O with TEOA (15% v/v) and a magnetic stirring bar were added to to a crimp-top vial and the aqueous solution was adjusted to pH = 8.3 by HCl. The samples were degassed by bubbling nitrogen through the solution for 5 minutes and then irradiated for a defined time with λ = 455 nm.

General preparation of IL-supported semiconductor catalyst. An appropriate amount of IL [C_4mim][NTf_2] (Table 5.2) was added to a suspension of 50 mg of semiconductor TiO_2 in MeOH (5.0 mL) and stirred for 30 min. $CHCl_3$ was removed in vacuum to give a semiconductor powder in quantitative yield.

Table 5.2   *Amount of IL in preparation of IL-supported semiconductor photocatalyst.*

Semiconductor	Amount of [C4mim][NTf2]	Table, entry
TiO$_2$	0.14 mL, 0.20 mg	Table 4.3, 4
TiO$_2$	0.22 mL, 0.31 mg	Table 4.2, 5
TiO$_2$	0.31 mL, 0.45 mg	Table 4.2, 6
TiO$_2$	0.46 mL, 0.66 mg	Table 4.2, 7
CdS	0.14 mL, 0.20 mg	Table 4.7, 2
CdS	0.31 mL, 0.45 mg	Table 4.7, 3

Sample preparation with TiO$_2$ catalyst. 1.0 mg of the photocatalyst, 1.0 mL of H$_2$O containing TEOA (15% v/v) and a magnetic stirring bar were added to a crimp-top vial and gas-tight closed. The aqueous solution was adjusted to pH = 8.3 by HCl. The samples were degassed by bubbling nitrogen through the solution for 5 minutes and then irradiated for a defined time with λ = 455 nm.

Sample preparation with CdS catalyst. 1.0 mg of the photocatalyst, 1.0 mL of H$_2$O containing **48** (1.26·10^{-4} mol L^{-1}), Na$_2$S (0.35 mol L^{-1}) and Na$_2$SO$_3$ (0.25 mol L^{-1}) and a magnetic stirring bar were added to to a crimp-top vial and gas-tight closed. The aqueous solution was adjusted to pH = 8.3 by HCl. The samples were degassed by bubbling nitrogen through the solution for 5 minutes and then irradiated for a defined time with λ = 455 nm.

Gas chromatography. GC was carried out on Inficon Micro GC 3000) with a 5Å molecular sieve column and a thermal conductivity detector. Argon was used as a carrier gas. The amount of evolved H$_2$ was determined in triplicate for each reaction.

5.3.3. Experimental Chapter 4.3

Preparation of the photocatalyst. TiO_2 was applied as a dispersion via spin coating on a silicon wafer. The dispersion was composed of 3.0 g of TiO_2 in 10.0 mL of suspension. The compositions of the suspension consisted of 1.25 mL of acetylacetone, 2.5 mL of Triton X-100 in deionized water (extracted from 1.0 mL of Triton X-100 in 5 mL of deionized water, 5.0 mL of polyethylene glycol in deionized water (extracted from 1.0 g of polyethylene glycol in 10.0 mL of deionized water) and 50.0 mL of deionized water. It resulted in a 5 μm TiO_2 layer, which was then sintered at 450 °C for 1 h in a 3-zone furnace under standard atmosphere.

The application of the IL on TiO_2 was performed via squeegee resulting in a film of a thickness of 50 μm, which is shown in Figure 5.7.
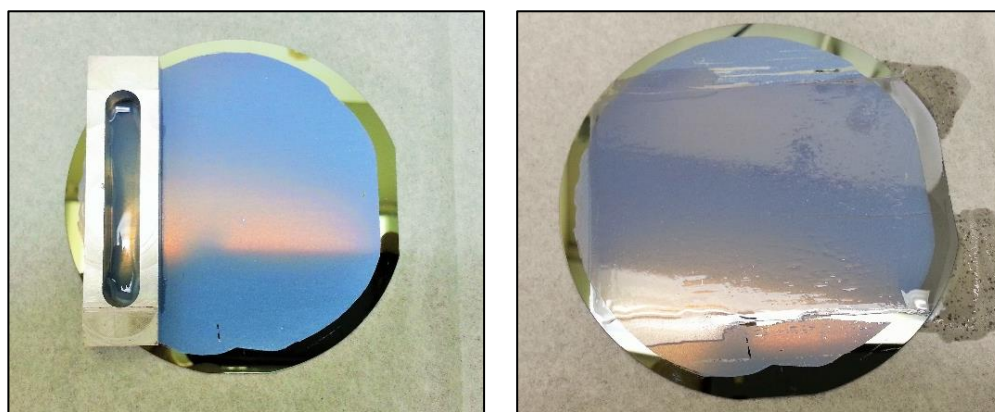
Figure 5.7   *Photographs of the coating of IL by squeegee on TiO_2 applied on silicon wafer.*

The copper layer was coated on TiO_2 via physical evaporative deposition (PVD) in a Varian Coater 3119 apparatus. The cooper source was heated to a vapor stream inside a high vacuum chamber, and is coated as film with thickness of 4 nm that corresponds to 0.75 mg cm^{-2} by hitting the TiO_2 substrate.

For sensitizing of TiO_2 with N3 dye (**51**), ruthenizer 535-bisTBA (37 mg/100 mL) and chenodeoxycholic acid (5 mmol L^{-1}) were dissolved in 100 mL ethanol and stirred overnight. After completely dissolution of the PS, the silicon wafer with TiO_2 was placed for 12 h at room temperature in this solution. Then the wafer was washed with ethanol and dried under high vacuum.

Photocatalytic performance. The reduction was carried out in a steel photoreactor with a volume of about 300 cm^3, shown in Figure 5.8. The reaction chamber is equipped with a delivery

and removal gas tap and temperature and pressure sensor. The sampling took place via a septum using a syringe. For each reaction, the photoreactor was purified with acetone, isopropyl alcohol and demineralized water and finally baked out at 120 °C for 1 h. The coated silicon wafer was placed into the photoreactor, which was then flooded with CO_2 for 30 minutes with a flow approximately of 231.9 mL/min. Around the placed silicon wafer a small amount of water was filled in an integrated notch for enriching the carbon dioxide with water. The photoreactor was then gas-tight closed by a quartz glass and the silicon wafer was irradiated with UV light (Edixeon EDEV-SLPS2-03 l = 395 - 410 nm, Imax 700 mA, 3.00 W) or AM1.5 light (300 W) for a defined time.
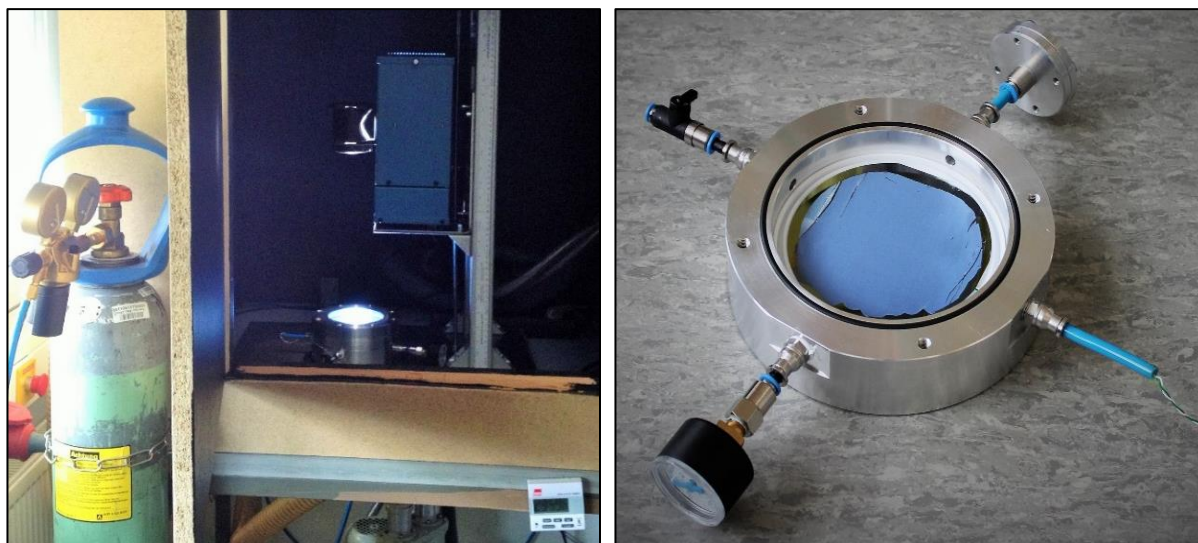
Figure 5.8   *Photograph of experimental setup of CO_2 reduction during irradiation with AM1.5 light (left) and photoreactor for CO_2 conversion with inside placed silicon wafer applied with TiO_2 (right).*

Figure 5.9 shows the recorded time course of temperature inside the photoreactor that increased from 20.5 – 35 ° C during 3 h irradiation with AM1.5 lamp.
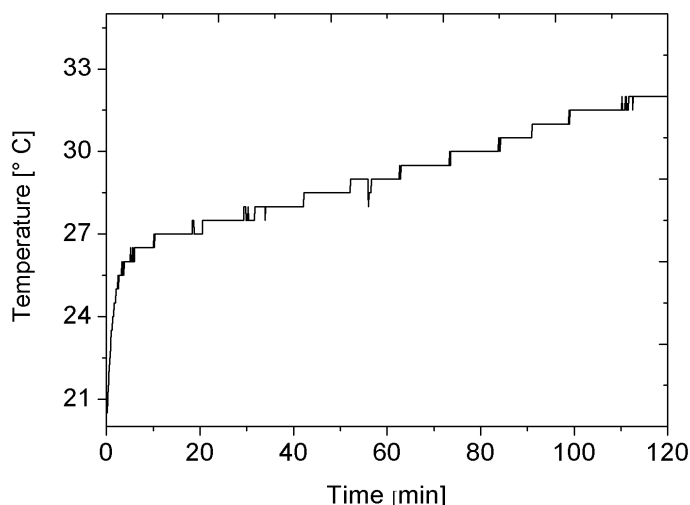
Figure 5.9 *Time course of internal temperature in the photoreactor during 3 h irradiation with AM1.5 lamp.*

Gas chromatography. GC was carried out on Agilent 6890N equipped with a flame ionization detector (FID) and a fused silica capillary column (50 m x 320 m x 5 μm) coated with Al_2O_3/KCl. The quantitative determination of methane, ethylene and *n*-butane was performed by preparing a calibration curve. The evolved amount of the other hydrocarbons were calculated on the basis of gas mixture containing 15 ppm of each gas.

Synthesis
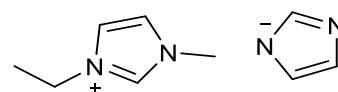
Synthesis of 3-ethyl-1-methyl-1*H*-imidazol-3-ium imidazole-1-ide[3] Imidazole (1.87 g, 27.4 mmol, 1.0 eq) was added to a solution of sodium hydroxide (1.0 g, 27.4 mmol, 1.0 eq) in dry methanol (5 mL) and stirred for 1 h at rt. After the addition of the 3-ethyl-1-methyl-1*H*-imidaz-oli-3-ium chloride (4 g, 27.4 mmol, 1.0 eq) and dry methanol (5 mL) the resulting light yellow solution was stirred overnight at rt. After adding of diethyl ether (5 mL), the solution was stirred again for 3 h. The product was obtained after filtration and evaporating under vacuum to give the desired product as dark yellow oil (3.42 g, 19.2 mmol, 71%).

121

^{1}H-NMR: (500 MHz, DMSO-d$_6$): δ = 7.78 (d, J = 1.9 Hz, 1H), 7.69 (d, J = 1.9 Hz, 1H), 7.13 (s, 1H), 6.70 (d, J = 0.85 Hz, 2 H), 4.16 (q, J = 7.31 Hz, 2H), 3.82 (s, 3H), 1.41 (t, J = 7.32 Hz, 3H) ppm.

^{13}C-NMR: (300 MHz, DMSO-d$_6$): δ = 142.8, 137.1, 125.0, 124.0, 122.4, 48.6, 44.5, 36.1, 15.6 ppm.

General procedure of *N,N* Dialkylimidazolium propionate.[4] 1-Ethyl-3-methylimidazolium chloride (1.0 eq) was stirred with sodium propionate (1.0 eq) in EtOH for 24 h. The resulting NaCl was removed by filtration and EtOH was evaporated under vacuum. The obtained crude product was dissolved in CH$_2$Cl$_2$ and filtered again for removing residue of sodium chloride. After evaporation the obtained viscous liquid was dried under vacuum overnight to give the desired product.
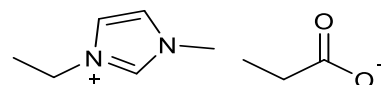
Synthesis of 3-ethyl-1-methyl-1*H*-imidazol-3-ium propionate. From 3-Ethyl-1-methyl-imidazolium chloride (4.1 g, 27.4 mmol, 1.0 eq) and sodium propionate (2.63 g, 27.4 mmol, 1.0 eq). Yellow oil. Yield: 2.52 g, 17.2 mmol, 62%. Spectroscopic data is consistent with literature values.[4]

^{1}H-NMR: (500 MHz, DMSO-d$_6$): δ = 9.59 (s, 1H), 7.81 (br s, 1H), 7.73 (br s, 1H), 4.21 (q, J = 7.31 Hz, 2H), 3.87 (s, 3 H), 1.76 (q, J = 7.60 Hz, 3H), 1.42 (t, J = 7.33 Hz, 3H), 0.86 (t, J = 7.57 Hz, 2H) ppm.

^{13}C-NMR: (300 MHz, DMSO-d$_6$): δ = 176.4, 137.7, 124.0, 122.4, 44.5, 36.1, 32.3, 15.6, 12.1 ppm.
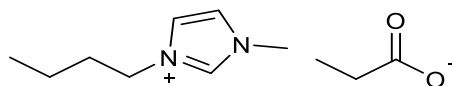
Synthesis of 3-butyl-1-methyl-1*H*-imidazol-3-ium propionate. From 3-Ethyl-1-methyl-imidazolium chloride (4.0 g, 22.9 mmol, 1.0 eq) and sodium propionate (2.2 g, 22.9 mmol, 1.0 eq).

Yellow oil. Yield: 2.42 g, 11.4 mmol, 50%. Spectroscopic data is consistent with literature values.[4]

^{1}H-NMR: (500 MHz, DMSO-d_6): δ = 9.54 (s, 1H), 7.80 (br s, 1H), 7.73 (br s, 1H), 4.18 (q, J = 7.31 Hz, 2H), 3.87 (s, 3 H), 1.77 (m, 4H), 1.27 (m, 2H), 0.86 (m, 6H) ppm.

[3]C-NMR: (300 MHz, DMSO-d_6): δ = 176.1, 137.6, 124.0, 122.7, 48.9, 36.1, 32.1, 31.8, 19.2, 13.7, 12.0 ppm.

5.3.4.   References

1.   L. Beyer and J. Angulo Cornejo, *Koordinationschemie*, Vieweg+Teubner Verlag, Wiesbaden, **2012**.
2.   S. Troppmann and B. König, *Chem. Eur. J.*, **2014**, *20*, 14570-14574.
3.   X. Chen, X. Li, H. Song, Y. Qian and F. Wang, *Tetrahedron Lett.*, **2011**, *52*, 3588-3591.
4.   Y. Zhang, Z. Wu, S. Chen, P. Yu and Y. Luo, *Chem. Eng. J.*, **2013**, *52*, 6069-6075.

List of Figures

List of Schemes

List of Tables

Danksagung

Ich danke Herrn Prof. Dr. *René Wilhelm* für die durchgehende Betreuung, das Vertrauen und die wissenschaftliche Freiheit, die mir gewährt wurde.

Ich danke Herrn Prof. *Dr. Jan Paradies* für sein Engagement im Rahmen des Zweitgutachtens.

Mein weiterer Dank gilt:

Herrn Prof. Dr. *Burkhard König*, für die Möglichkeit eine lehrreiche Zeit in Regensburg zu verbringen und die Unterstützung,

sowie allen *Mitarbeitern des Lehrstuhls König*. Insbesondere möchte ich *Malte* und *Stefan* danken, die durch ihre fachliche Unterstützung einen wichtigen Beitrag für diese Arbeit geleistet haben.

Der *Evonik Stiftung* für die finanzielle Unterstützung durch das Promotionsstipendium und die zahleichen Erfahrungen rund um meine Promotion, die mich für meinen weiteren beruflichen Weg vorbereitet haben.

Dem gesamten *Department für Chemie* der Universität Paderborn, für die zahlreichen analytischen Messungen und die fachliche Unterstützung,

sowie allen *Mitarbeitern des Arbeitskreises Wilhel*m, mit denen ich viele Stunden im Labor verbracht habe.

Magda und *Markus* für ihre Freundschaft.

Dr. *Heinz Weber*, für seine fachliche und moralische Unterstützung, den zahlreichen Aufmunterungen und jegliche Art von Hilfe, die ich immer in Anspruch nehmen konnte.

Dennis, der mich zu meinem Glück überhaupt erst gezwungen hat.

Eidesstattliche Erklärung

Hiermit versichere ich, dass ich die vorliegende Arbeit selbstständig verfasst und keine anderen als die angegebenen Quellen und Hilfsmittel benutzt habe. Alle Ausführungen, die anderen veröffentlichten oder nicht veröffentlichten Schriften wörtlich oder sinngemäß entnommen wurden, habe ich kenntlich gemacht.

Ich versichere außerdem, dass ich die beigefügte Dissertation nur in diesem und keinem anderen Promotionsverfahren eingereicht habe und, dass diesem Promotionsverfahren keine endgültig gescheiterten Promotionsverfahren vorausgegangen sind.

Dagny Konieczna